Laser Excitation and Detection of Magnetic Resonance

DIETER SUTER
INSTITUTE OF QUANTUM ELECTRONICS
SWISS FEDERAL INSTITUTE OF TECHNOLOGY (ETH) ZÜRICH
CH-8093 ZÜRICH, SWITZERLAND

JÜRGEN MLYNEK
DEPARTMENT OF PHYSICS
UNIVERSITY OF CONSTANCE
D-7750 CONSTANCE. GERMANY

ADVANCES IN MAGNETIC AND OPTICAL RESONANCE, VOL. 16

I. Introduction

Magnetic resonance spectroscopy basically measures tbe interaction of electronic or nuclear angular momenta witb each other and with external magnetic fields (Abragam, 1961). The interaction energies are retatively small ($< 10^{-22}$ J), so that the corresponding frequencies are in the radiowave-microwave regime ($< 10^{11}$ Hz). While the first magnetic resonance experintents were performed in the frequency domain using continuous wave (cw) methods, it was soon recognized that time domain spectroscopy offers, in many cases, better sensitivity as well as additional possibilities (Hahn,1950). In this technique, one applies a sequence (in many cases consisting of a single pulse) of short, intense pulses of narrowband radio frequency (rf) radiation and records the response of the system in the time domain. If desired, the frequency domain spectrum can be recovered by Fourier transformation of the free induction decay (FID), i.e., the response of the system to a single pulse. In addition to the possibilities offered by the frequency-domain or cw spectroscopy, the time domain experiments allow the observation of time-dependent phenomena, where the system is not in internal equilibrium. Examples of such phenomena are nutation, free induction decay, and spin echoes.

These possibilities have made magnetic resonance an indispensable tool in many areas of research, such as chemistry, medicine, and solid state physics. Today, the biggest remaining weakness of the technique is its relatively low sensitivity, compared, for example, to optical experiments. In the area where magnetic resonance has become most popular, that of nuclear magnetic resonance (NMR) of liquids, the minimum number of atoms that Can be detected is of tbe order of 10^{18}, while optical spectroscopy of individual atomic ions has become rather popular (Dehmelt, 1990). Several reasons contribute to this low Sensitivity. The small size of interaction energy leads to small thermal population differences between the energy levels participating in a particular transition and to Small detector efficiency and high thermal noise levels. While population differences in thermal equilibrium, $e^{-h\nu/kT}$, for optical transitions ($\nu \approx 10^{15}$ Hz) are of the order of unity, those associated with rf transitions ($\nu \approx 10^{8}$ Hz) are of the order of 10^{-5}. Similarly, optical photons can be detected with an efficiency near unity, while a large number of rf photons are required to exceed the noise level.

In cases where the sensitivity provided by classic& magnetic resonance is not sufficient, it is often possible to increase the population difference be_ tween the different magnetic sublevels or the detection efficiency. Among other methods, optical pumping of the system has been used to increase the population difference (see, e.g., Balling, 1975; Bernheim, 1965). Like the population difference between ground and electronically excited states, the

population difference between levels differing only in their spin state can then reach values near unity. Conversely, the population difference and coherence between the magnetic substates can change the optical properties of the system; it is therefore possible to detect the magnetization optically, with a sensitivity much greater than if the radio frequency photons are detected (Kastler, 1967; Brossel and Kastler, 1949; Bitter, 1949). This gain in sensitivity can be understood as an amplification of the radiation by transferring the angular momenta from the internal degrees of freedom of the system to photons with optical energies instead of rf energies. In classical terms, this transfer of angular momentum basically leads to a (circularly) polarized radiation field.

Instead of transferring the angular momentum to an optical transition to gain sensitivity, it is also possible to use a resonance line that corresponds to a transition between states that differ in their electronic, vibrational, or rotational states, as well as their magnetic quantum numbers. The transition frequency is then given by the sum of the optical and magnetic energy. It has been applied successfully in the far infrared region of the spectrum (Davies, 1981), but is not likely to provide sufficient resolution in the visible region of the spectrum, since there the broadening mechanisms of the optical transitions, such as Doppler broadening and spontaneous emission from the excited state, make it impossible to obtain sufficient resolution of magnetic resonance transitions with this method.

Apart from the gain in sensitivity, the use of optical radiation also provides the option to perform magnetic resonance spectroscopy of electronically excited states. Since these states are not populated in thermal equilibrium, the atoms or molecules that are to be studied must be brought into the excited state before magnetic resonance can be performed. If the excitation can be achieved with light, it is often advantageous to use selective excitation of the magnetic substates to obtain a polarized system. This is also necessary since the population that can be achieved may be substantially smaller than in the ground state so that sensitivity again becomes an important issue. The fluorescence, which is emitted by these systems, is often polarized and can be used directly to measure the excited state magnetization.

Early experiments on optical excitation and detection of magnetic resonance used conventional light sources such as discharge lamps. Due to the limited intensity of these light sources, the optical pumping rates that could be achieved were relatively low, and appreciable polarization of the sample was possible only if the relaxation that tended to counteract the optical pumping could be kept slow, for example, by adding buffer gas and coatings, which are applied to the walls of the sample cell and reduce the relaxation via wall collisions. Light was used mainly in order to polarize the spin system and to observe the precessing magnetization, while rf irradiation was used to change

the dynamics of the spin system. Nevertheless, it was realized in 1962 (Cohen-Tannoudji, 1962, 1972) that optical radiation cannot only polarize the spin system, but also leads to shifts and broadening of the magnetic resonance transitions.

With the introduction of the laser, the available light intensity and the coherence properties of the radiation field have changed in such a way that many experiments that were not feasible before have become routine (Demtröder, 1982; Levenson and Kano, 1988; Shen, 1984; Brewer, 1977b). One important example is the generation of ultrashort pulses to obtain a very high time-resolution (Lehmitz and Harde, 1986). On the theoretical side, many concepts and descriptions of physical processes had to be revised. The high spectral intensity of the laser light leads, in general, to a nonlinear response of the system to the optical field. The high spectral purity of a cw laser leads to additional phenomena, such as velocity-selective excitation. With incoherent light sources, the spectral width of the light had generally been much broader than the inherent line width of the optical transition, and the process of absorption could be described with rate equations for the populations. With narrow band lasers, the situation is reversed; in many cases, the optical coherences have to be taken into account, and the dynamics must be formulated in terms of the density operator (Decomps *et al.*, 1976).

Other effects, which were discovered with discharge lamps, but were too small to be of practical significance, were increased by many orders of magnitude when laser radiation became available. For example, the light-shift effect, an apparent shift of energy levels due to optical irradiation of an adjacent transition, does not exceed a few hertz when discharge lamps are used (Cohen-Tannoudji, 1962). Using lasers, light shifts of the order of kilohertz to megahertz can be achieved readily and can therefore have a strong effect on the spin dynamics. Under appropriate experimental conditions, these shifts have the same effect on the spin dynamics as magnetic fields. By selectively irradiating certain optical transitions, these virtual magnetic fields can be used as an additional degree of freedom for the modification of spin dynamics. It is therefore possible to perform many experiments by purely optical methods; the usage of the optical radiation field is then threefold: it polarizes the spin system by transferring angular momentum from the photons to the spin system, it modifies the dynamics of the system via an effective Hamiltonian, and it is used to detect the resulting time-dependent magnetization.

Although the system is studied via its interaction with optical photons, the resolution that can be achieved is not limited by the coherence properties of the radiation field. This is best demonstrated by the early experiments with discharge lamps, which already reached resolutions in the hertz range—many orders of magnitude below the line width of the radiation used in the experiments. This can be understood qualitatively by considering that no net

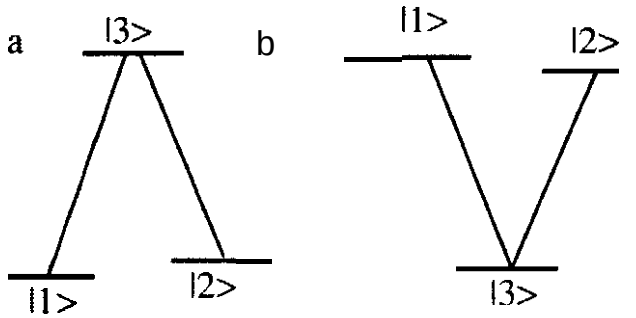

FIG. 1. Λ- (a) and V-type (b) three-level systems; the solid lines indicate optical transitions; the magnetic resonance transition couples |1⟩ and |2⟩.

absorption of photons occurs during the detection process. instead, the magnetic interaction leads to a modulation of the intensity of the pump or probe beam and can be measured with the same absolute resolution as in purely magnetic resonance experiments.

While the systems under study can have very different energy level schemes, the basics of the techniques can often be explained in terms of a simple three-level scheme (Fig. 1). The transition of interest is the $|1> \leftrightarrow |2>$ transition, and the two optical transitions involved in the Raman-type resonance are indicated with a full line. In the case of a A-type level system (left side of Fig. I), the rf-transition therefore couples the two sublevels of the atomic ground state, while in the case of the V-type system, the rf-transition lies within the electronically excited state. In many actual cases, both types of transitions occur in the same atomic system, so that resonances in both the ground and excited states can be excited.

This chapter covers the following topics: Section II gives an overview of the development of magnetic resonance, coherent optical spectroscopy, and the more traditional optically detected magnetic resonance (ODMR). The general theoretical framework of this is developed in Section III, with an overview of magnetic resonance and coherent optical experiments. The topic of this chapter necessarily deals with optics as well as magnetic resonance. While such a cross-disciplinary field can be fruitful for researchers in both disciplines, it also creates problems due to the different languages that have evolved in different fields. In order to introduce the notation used throughout this chapter and establish a common theoretical framework for readers with either a magnetic resonance background or a background in quantum electronics, a brief theoretical treatment of the properties of optical and magnetic two-level systems from a very basic point of view is given. The main emphasis lies on the development of a notation that should be understandable for readers with a background either in optics or magnetic resonance. Apart from the purely

static Hamiltonians for the various systems, the basic processes that are discussed include the absorption and emission of radiation and the associated changes in the state of the systems. After establishing the basic notation. the most important phenomena occurring in laser magnetic resonance are treated in an example of some simple prototype systems. This theoretical framework is used in Section IV to give a summary of some experiments performed in this field. In Section V, we discuss possible trends for the future and make some concluding remarks.

II. Historical Overview

A. Magnetic Resonance Spectroscopy

The first experiments probing transitions between different spin states were performed with atomic beams (Rabi *et* al., 1938). In these experiments, nuclei with different spin states were spatially separated in an inhomogeneous magnetic field and recombined by a second field gradient of opposite sign. Between the two inhomogeneous regions, a region of homogeneous field was used to perform the resonance experiment. If an rf field induced transitions between the spin states in this region, the nuclei affected by the irradiation would no longer recombine on the detector, thereby leading to a decrease of the count rate. If the frequency of the rf field was scanned, a drop in the detected count rate would therefore indicate a resonance. In this experiment, every nucleus participated in the resonance process, and only very few nuclei were needed for the detection of a resonance.

Only several Years later were magnetic resonance transitions measured in bulk material (Purcell *et al.*, 1946; Bloch, 1946; Bloch *et al.*, 1946). Instead of a few atoms, these experiments were done on samples of some 10^{24} atoms, indicating that their sensitivity was considerably lower than that in the beam experiments. The difference can be traced back to two major causes: only the small fraction of spins that corresponds to the population difference between the two stationary spin states actually participates in the experiment, and the resonance is detected via the rf-photons absorbed by the resonating spins; these photons are much harder to detect than atoms.

In these early experiments, the strength of the static magnetic field was adjusted such that the energy difference between the different Zeeman states became equal to the energy of the monochromatic photons used to irradiate the system. These slow-passage or cw experiments, where the system is studied as a function of frequency, were to a large degree superseded by experiments where a time-dependent perturbation is applied to the system under study, and the response of the system is measured as a function of time. The initial Preparation of the system has the objective of converting population

differences present in the spin system in thermal equilibrium into off-diagonal density operator components that do not commute with the internal Hamiltonian of the system and therefore evolve when the perturbation is removed. These time-domain experiments have the advantage of providing higher sensitivity, since the whole system is excited simultaneously, and allowing more flexibility in the design of the experiment.

B. Optical Spectroscopy

Spectroscopy uses electromagnetic radiation to measure properties as a function of wavelength or frequency of the radiation. The most frequently measured properties are the absorption of radiation and the dispersion, i.e., the velocity of the radiation as it propagates through the material, Changes in either property usually indicate that the frequency of the radiation matches, via the relation $AE = h\nu$, an energy difference in the system under investigation. In the visible region of the spectrum, spectroscopic light sources were traditionally thermal sources, such as light bulbs or discharge lamps. The power, within the desired frequency band, that was available from these light sources was relatively low; the number of absorbed photons was therefore too small to excite an appreciable percentage of the atoms. The process of interaction between the radiation field and the atomic systems was usually described with perturbation theory, which is useful when the rate of absorption is small compared to the spontaneous emission rate.

With the introduction of coherent radiation sources, such as lasers, the situation changed qualitatively. Although the total output power of the new radiation sources is often lower than that of thermal sources, it is concentrated within a narrow spatial direction and a narrow frequency range. The absorption rate is therefore increased by many orders of magnitude to values near or higher than the spontaneous emission rate. This has consequences not only for the experimentalist, but also for the theory, since additional processes, such as induced emission, have to he taken into account. This situation had been encountered before in magnetic resonance spectroscopy. Although the transition probabilities are small, the number of photons is large, and the spontaneous emission rate is negligibly small. The theoretical analysis treats the system, therefore, as an ensemble of identical spins interacting primarily with the applied field, while relaxation processes are considered only as perturbations,

Time-resolved experiments had been performed also in the optical domain for some time, but became widely used only after the invention of the laser. Laser radiation not only provided very intense radiation in a spatially well-defined direction, but the emitted radiation is also coherent, i.e., very monochromatic, In most cases, the uncertainty of the laser frequency is small

compared to the frequency uncertainty of the transitions being irradiated. With the advent of these sources of coherent radiation, many experiments invented in the domain of magnetic resonance spectroscopy, such as coherent transients and echoes, became feasible in the optic domain as well (Abella *et al.*, 1966; Brewer and Shoemaker, 1971; Brewer, 1977b; Golub *et al.*, 1988; Allen and Eberly, 1987). While similarities and analogies exist between the two fields, there are of course also many differences, either of a technological or a fundamental physical nature. The common features allow one to take advantage of the experiences created in one domain and use them in the other domain, while the differences limit the applicability of these analogies, but at the same time, may help to give a deeper understanding of the phenomena by distinguishing them from related phenomena.

One major distinction between magnetic resonance and coherent optics is the ratio between the wavelength of the radiation used and the typical dimensions of the sample. For magnetic resonance spectroscopy, the sample size d is always small compared to the wavelength λ ($d \ll \lambda$), while the opposite is usually true in optics ($\lambda \ll d$). *One consequence* is that in optics the radiation field is never homogeneous throughout the sample. The whole concept of coherence is therefore different in optical spectroscopy compared to magnetic resonance spectroscopy. Two spins that are oriented in the same direction in space at the same instant contribute to the overall signal with the same amplitude and phase; if an ensemble of spins is excited with an rf pulse, the spins evolve coherently, always pointing in the same (time-dependent) direction. In optical spectroscopy, atoms at different locations "see" fields with different phases, and their induced electric dipole moment points in different directions. However, they may still lead to a coherent radiation field, if the phase of their radiation differs just by the amount that the field accumulates when it travels from one atom to the other, Averaged over the whole sample, this results in a preferred direction in which the emitted radiation interferes constructively, and in which most of the radiative power of the sample is emitted. If a single laser beam is used to prepare the sample, this direction usually coincides with the direction of propagation of the laser beam. Since the phase accumulated by the radiation field depends on the index of refraction Of the sample, the direction in which the radiation is emitted may depend on the wavelength of the radiation. This leads to the so-called phase matching problem, which is important in frequency-conversion experiments, such as coherent Raman scattering and three- and four-wave mixing (Shen, 1984; Levenson and Kano, 1988).

In linear spectroscopy, the frequency of the radiation field behind the sample is always the same as the frequency of the radiation entering the sample. Until the introduction of the laser, deviations from this behavior could be seen only under relatively rare circumstances, With the availability of intense monochromatic radiation sources, this situation has changed com-

pletely. The systems under study can be excited in a nonlinear way so that the radiation emitted differs in frequency from the absorbed radiation. The first experiment of this kind was Raman scattering, where the frequency of the light is changed only slightly. Today, frequency conversion experiments have come up in a wide variety, including frequency doubling, tripling, or down-conversion, In all these cases, the new frequency differs from the old frequency by an amount that is of the same order of magnitude as the original frequency, In many optically detected magnetic resonance experiments, the light behind the sample contains a frequency component that differs from the original frequency by an amount in the rf range. These experiments may therefore be considered as Raman-type experiments.

C. Optical Pumping

One important limitation to the sensitivity of magnetic resonance experiments is the small population difference across magnetic resonance transitions under normal experimental conditions. A typical transition frequency of 100 MHz corresponds to a Boltzmann temperature, $7 = k/h\nu$ of 4.8 mK, so that spin systems at typical experimental temperatures are almost completely disordered: the Boltzmann factor $e^{-h\nu/kT}$ deviates from I by less than $2\,10^{-5}$. This factor, and therefore the sensitivity of the experiment, can be increased by several orders of magnitude if the population difference from a different system is transferred to the spin system, thereby lowering the spin temperature. The source of polarization can be either a different nuclear spin (Pines et *al.*, 1973), an electronic spin, as in dynamic nuclear orientation (Jeffries, 1963), or an electronic transition, as in optical pumping experiments (Balling, 1975; Bernheim, 1965).

Optical pumping of spin systems relies on the fact that photons carry angular momentum, which is transferred to the spin system during absorption and emission of photons (Kastler, 1967; Happer, 1972). Accordingly the spin state of the system changes during such an event, The nature of this change depends on the polarization of the photons and their direction of propagation. In the case of circularly polarized photons propagating along the quantization axis, the magnetic quantum number of the atomic system changes by ± 1, depending on the sense of polarization. While the photon absorbed by the atom is reemitted after a time that is of the order of the life time of the electronically excited state, it carries away some angular momentum. If the radiation that is incident on the atom differs from the reemitted radiation, the difference in angular momentum remains on the atom, thereby polarizing the spin system.

In order to optically pump a spin species, it needs to have an electronic transition for which intense light sources exist. Obviously not all spin species satisfy this requirement, an important exception being the nuclear spins of rare

gases. In many cases, however, it is possible to transfer spin polarization between different types of spins. The first demonstration of population transfer from an optically pumped species to an optically inactive species was done by Dehmelt (1958), who transferred polarization from optically pumped Na atoms to free electrons.

While the optical pumping has an effect primarily on the electron spin, the coupling between the electron and the nuclear spin (i.e., the hyperfine interaction) also leads to a Polarization of the nuclear spin. In this way, it is even possible to polarize nuclear spins if the ground state of the atom is diamagnetic (Lehmann, 1964).

D. Spin Systems Driven by Optical Fields

Apart from the presence of some sort of order in the system, the second ingredient required for a successful spectroscopic experiment is a means to manipulate this order. Magnetic resonance has accumulated a huge arsenal of such methods, most of them consisting of applying a sequence of resonant rf pulses with specific phases and durations to the spin system. The main purpose of these pulse sequences is the conversion of energy level Population differences into coherences, the transfer of coherences between different transitions! and the conversion of coherences into population differences. To perform these operations, it is necessary to change the Hamiltonian of the system in such a way that the new Hamiltonian no longer commutes with the old one. The most direct way to achieve this goal by optical means is to apply intense laser pulses, which have the same effect on the optical transitions as rf pulses on spin transitions. By applying an appropriate sequence of optical pulses, it is possible to manipulate the system in such a way that an overall effect on the spin system results.

If the optical Rabi frequency is smaller than the decay rate of the optical coherences, such pulse sequences are no longer possible. It then becomes inappropriate to describe the system in terms of a Hamiltonian evolution, but rate equations for the density operator elements become more meaningful. Nevertheless, it is still possible to change the dynamics of the spin system by applying strong off-resonant radiation to an adjacent optical transition. As was first suggested by Barrat and Cohen-Tannoudji (1961a,b,c) and confirmed experimentally by Arditi and Carver (1961) and Cohen-Tannoudji (1961, 1962; Cohen-Tannoudji and Dupont-Roc, 1972; Dupont-Roc et *al.*, 1967), such radiation causes an apparent shift of the energy levels associated with the optical transition. This so-called light shift is proportional to the intensity of the light and has a dispersion-like dependence on the optical detuning. By choosing the proper light polarization, it is not only possible to change the energy of the individual levels. but it is also possible to change the quantization axis of the Hamiltonian.

E. Optically Detected Magnetic Resonance

The third part of a spectroscopic experiment is the observation of the order present in the system. As discussed previously, traditional magnetic resonance spectroscopy relies for this purpose on the detection of the radiation emitted by the precessing magnetization. Since the energy of the photons associated with magnetic resonance transitions is relatively low, a large number of photons is required for a signal that is larger than the noise signal. If it is possible to transfer the order present in the system to a higher frequency mode of the radiation field, the energy per quantum of angular momentum, and therefore the detection sensitivity, is increased. This scheme may be considered a "quantum amplifier."

Different realizations exist of this method of enhancing sensitivity by upconverting the photon energy; they rely on a transfer to transitions of different nuclear spins (Hartmann and Hahn, 1962), electron spins [electron nuclear double resonance (ENDOR) (Feher, 1956)], to optical energies (Kastler, 1967), or even to nuclear radiation (Burns *et al.*, 1977; Brewer, 1982). In many cases, the schemes involve a direct (one-to-one) conversion of rf photons into higher energy photons, but in some cases it is also possible to convert each rf photon into several higher-energy photons, The detection process sometimes involves a transfer of coherence or population from the magnetic resonance transition of interest to the transition that is actually observed (Hartmann and Hahn, 1962). At other times, the polarization state of the system influences the spontaneous decay properties of the system, as in quantum beat experiments (Haroche, 1976; Dodd and Series, 1978) or detection via nuclear radiation (Brewer, 1982).

The first experiment involving detection of magnetic resonance transitions via an optical transition measured the influence of an rf field on optical radiation (Fermi and Rasetti, 1925). Subsequent experiments investigated changes in the polarization of the fluorescence intensity that occurred when a magnetic resonance transition was excited. These experiments used discharge lamps to optically pump the system, then the spontaneously emitted fluorescence was analyzed with a polarization selective detector used to measure the degree of polarization of the sample. When a resonant rf field is applied to the sample, it can induce transitions between Zeeman substates, and thereby decreases the polarization (Brossel and Kastler, 1949). The high sensitivity of this method and the fact that spontaneous emission is observed makes it especially useful for observing magnetic resonance in electronically excited atomic and molecular states (Breiland *et al.*, 1973).

Instead of observing the fluorescence emitted by the sample, it is possible to use the modification of the optical properties of a spin-polarized sample to detect atomic polarization. This method was proposed by Dehmelt (1957b) and observed by Bloembergen *et al.* (1960). In general, the optical properties, such as the absorption and dispersion coefficients, depend on the polarization

state of the light. As an example, the z component of the magnetization can be measured by sending a beam of light parallel to the z direction through the sample and then measuring either the absorption or dispersion of right versus left circularly polarized light.

Alternatively, if pulsed excitation is used and the magnetic field is applied perpendicular to the direction of propagation of the light, the energy difference between the excited state sublevels can be detected as the frequency of the fluorescence modulation of the sample (Kastler, 1967). This experimental setup, using a magnetic field perpendicular to the direction of the light, is usually referred to as transverse pumping, It also allows a steady-state measurement when intensity-modulated light is used (Bell and Bloom, 1961a). Resonances occur when the modulation frequency between two different spin states becomes equal to the transition frequency, Resonances are detected as maxima in the system's response to the optical pumping when either the modulation frequency or the magnetic held strength is scanned.

As in the case of optical pumping, the methods outlined here require that the magnetic resonance transition has an energy level in common with an accessible optical transition. If this is not the case, polarization transfer between different atoms can be used to indirectly detect magnetization of optically inaccessible spins (Dehmelt, 1958).

III. Theoretical Framework

Magnetic Resonance is a general spectroscopic method for measuring the interaction of atomic and molecular systems with external magnetic fields. The angular momentum of these systems is coupled to a magnetic momentum, which interacts with the external field as weil as with other magnetic moments in the system. States with different angular momentums interact differently with the magnetic field, and their energies arc therefore shifted relative to each other. In most cases, the experimentalist tries to isolate the magnetic interaction from other interactions by using states that differ only in their angular momentum, while all other quantum numbers arc identical. In atomic and molecular spectroscopy, such states are usually referred to as substates, and the coherences between them arc referred to as atomic or sublevel coherences. Magnetic resonance experiments can therefore be considered as special cases of sublevel spectroscopy, and many of the methods discussed here actually have a much wider range of applications.

The strength of the coupling between the angular momentum and external magnetic fields is measured by the gyromagnetic ratio. The size of this coupling constant depends on the type of angular momentum. For orbital angular momentum of electrons and electron spin angular momentum, it is of

the same order of magnitude; it exceeds that of nuclear spins by roughly 3 orders of magnitude. If direct excitation of the magnetic resonance transitions is used, the different orders of magnitude result in different frequency ranges and, therefore, different requirements on the experimental apparatus. Accordingly, a clear distinction exists between the fields of electron paramagnetic resonance (EPR), used to investigate mainly electron spin transitions, and nuclear magnetic resonance (NMR), which deals with nuclear spins.

In contrast, if optical radiation is used to excite the system, the distinction between the various types of angular momentum is less important and often impossible to make when more than one source of angular momentum is present in the system of interest. In low magnetic fields, the different angular momenta are strongly coupled to each other and the individual angular momentum operators are no longer constants of motion; only the total angular momentum can be specified for a given eigenstate of the Hamiltonian. In the examples discussed in the experimental section of this chapter, the angular momentum to which the magnetic field couples can lx either one of the three types just discussed or a mixture of these. In order to make the theoretical treatment as general as possible, we will not specify the type of angular momentum here, but will discuss it only in the experimental section. In order to keep the language simple, we will call the system of interest a spin system with the understanding that the angular momentum involved may also be of the orbital type.

The main purpose of this chapter is to introduce the notation and discuss the basic dynamics occuring in optically pumped spin systems. For this purpose we will discuss magnetic and optical two-level systems and the combination of both in a four-level system. We will use frequency units for energy differences; this convention not only allows a more compact notation, but provides a closer connection between theory and experiment, where energy differences are always measured in the form of frequencies. Alternatively, it is possible to assume that the units used are defined such that $\hbar = 1$.

The systems of interest can usually be treated in good approximation as an ensemble of identical subsystems, each of which consists of a single atom or molecule. As long as they are sufficiently isolated from each other and their environment, the evolution of the total system can be described by the Hamiltonian for an individual system and a density operator of the same dimension evolving under the Hamiltonian. The most important deviations from this idealization are relaxation effects and inhomogeneities. Relaxation effects are due to interactions between the various subsystems and imperfect isolation from the environment, mainly electromagnetic fields: they are discussed in the corresponding section. The only inhomogeneous effects that are important in our case are Doppler broadening of the optical transitions and inhomogeneous magnetic fields.

A. Magnetic Two-Level Systems

1. *Static Hamiltonian*

In order to introduce the notation, it is sufficient to consider the simplest magnetic resonance system, a single spin $S = \frac{1}{2}$. In a static magnetic field, $\mathbf{B} = (0, 0, B_0)$ oriented along the z-axis, the interaction of the spin with the magnetic field is described by the Hamiltonian

$$\mathscr{H} = -\gamma_S \mathbf{B} \cdot \mathbf{S} = -\omega_H S_z \tag{1}$$

where $\mathbf{S} = (S_x, S_y, S_z)$ represents the spin angular momentum operator, γ_S the gyromagnetic ratio (Abragam, 1961) and $\omega_H = \gamma_S B_0$ the Larmor frequency. A complete description of the system can be obtained in terms of its density operator ρ (Fano, 1957). The system has three degrees of freedom, i.e., the system can be expanded in terms of a basis set of three operators in addition to the unity operator, It is usually convenient to choose the spin operators S_x, S_y, and S_z as the basis. If we write the corresponding expansion coefficients as x, y, and z, the density operator becomes

$$\rho' = 1 + xS_x + yS_y + zS_z \tag{2}$$

The unity operator does not depend on time and does not contribute to any observable quantity; as an abbreviation it is therefore simpler to use the traceless part of the density operator

$$\rho = xS_x + yS_y + zS_z \tag{3}$$

which is often referred to as the reduced density operator. Since the magnetization M of the system is related to the spin, $\mathbf{M} = n_S \gamma_S \mathbf{S}$, the coefficients x, y, and z can be regarded not only as coefficients of the density operator in the chosen basis, but simultaneously as the components of the magnetization vector in real, three-dimensional space.

In many cases, spin systems are well isolated from the environment and the dynamics are determined mainly by the coupling to the magnetic field. The equation of motion is then determined by the Schrödinger equation,

$$\dot{\rho} = -i[\mathscr{H}, \rho] \tag{4}$$

We use the Schrödinger picture and include the time dependence of the density operator in the coefficients

$$\rho(t) = e^{-i\mathscr{H}t}\rho(0)e^{i\mathscr{H}t} = x(t)S_x + y(t)S_y + z(t)S_z \tag{5}$$

With the Hamiltonian in Eq. (1), the coefficients become

$$\begin{aligned} x(t) &= x(0)\cos(\omega_H t) + y(0)\sin(\omega_H t) \\ y(t) &= y(0)\cos(\omega_H t) - x(0)\sin(\omega_H t) \\ z(t) &= z(0) \end{aligned} \tag{6}$$

corresponding to a precession of the spin vector around the direction of the magnetic field.

2. Rotating *Frame* and *Nutation*

An alternating magnetic field with a frequency ω near the Larmor frequency ω_H of the two-level system and orientation perpendicular to the static magnetic field leads in a quantum mechanical picture to an exchange of photons between the spin system and the radiation field and simultaneous transitions between the two spin states. In a semiclassical picture, the rf field causes a notation of the magnetization vector, thereby changing the angle between the direction of the magnetization vector and the static magnetic field. If we choose x axis of the coordinate system along the direction of the alternating field, the Hamiltonian becomes

$$\mathscr{H} = -\omega_H S_z - 2\omega_1 \cos(\omega t) S_x \tag{7}$$

where $\omega_1 = \gamma_S B_1/2$ represents the Rabi frequency, and B_1 represents the amplitude of the alternating magnetic field. The analysis of the process can be simplified by transforming the system into a rotating frame of reference, This transformation, a special kind of interaction representation, is a time-dependent unitary transformation defined as

$$\begin{aligned} \mathscr{H}^r &= U(t)\mathscr{H}U^{-1}(t) + i\dot{U}(t)U^{-1}(t) \\ \rho^r(t) &= U^{-1}(t)\rho(t)U(t) \\ U(t) &= e^{-i\omega t S_z} \end{aligned} \tag{8}$$

The equation of motion in this frame of reference is the usual Schrödinger equation, with $\mathscr{H}$ replaced by $\mathscr{H}^r$ and $\rho(t)$ by $\rho^r(t)$. The Hamiltonian in the rotating frame is

$$\mathscr{H}^r = -\Delta\omega_H S_z - \omega_1 S_x + h(2\omega) \tag{9}$$

with $\Delta\omega_H = \omega_H - \omega$. The term $h(2\omega)$ comprises terms oscillating at twice the rf frequency; perturbation theory shows that this component can be ignored in lowest order, i.e., if the alternating field is small compared to the static field. In this rotating reference frame, the static magnetic field appears reduced to the difference between the Larmor frequency and the rf frequency, while the rf field is now static.

Mathematically, the transformation into the rotating frame, as defined here, is somewhat ambiguous, since the frequency ω can be chosen with positive or negative sign. Physically, however, the only meaningful choice is such that the remaining longitudinal component $\Delta\omega_H$ is minimized. This implies that the reference frame rotates with respect to the laboratory frame with the same sense of rotation and approximately the same angular velocity as the spins due to Larmor precession. The decomposition of the rf field into

a static part and a component rotating at twice the Larmor frequency Provides then a natural decomposition of the linearly polarized rf field into the two circularly polarized components. Only the component rotating with the Larmor precession leads to actual resonance with the spin system. This is a manifestation of the conservation of total angular momentum: the resonance process can be considered as an interaction between an atom in the $m_z = -\frac{1}{2}$ spin state and a circularly polarized photon with $m_z = 1$. If the photon is absorbed by the atom, the angular momentum is transferred to the atom, which changes into the $m_z = +\frac{1}{2}$ spin state. The opposite component of Circular polarization cannot interact with the spin system, since conservation of energy and conservation of angular momentum allow only the absorption of photons with $m_z = 1$.

In general, the equation of motion for the rotating-frame density operator also includes, in addition to the Hamiltonian part, a relaxation term. For our purposes, it is sufficient to assume that the relaxation behavior of the system during rf irradiation can be calculated from the phenomenological relaxation times T_1 and T_2 of the freely precessing system Under these conditions, the general solution of this equation has been given by Torrey (1949). Since this general solution is too complicated for analytical use, we consider here only some limiting cases that are of interest under our conditions. For infinitely long relaxation times, the motion of the spin vector corresponds to a precession of the magnetization around the total field. This is an important case for magnetic resonance experiments, where the Rabi frequency is usually large compared to the transverse relaxation rate. The general solution to the equation of motion is then analogous to the case of free precession:

$$\begin{aligned} x'(t) &= x'(0)\cos(\Omega t) + y'(0)\sin(\Omega t) \\ \mathrm{Y}'(\mathrm{r}) &= y'(0)\cos(\Omega t) - x'(0)\sin(\Omega t) \\ z'(t) &= z'(0) \end{aligned} \tag{10}$$

where

$$\Omega = \sqrt{\Delta\omega_{\mathrm{H}}^2 + \omega_1^2} \tag{11}$$

represents the strength of the effective field. The coefficients x', y', and z' refer to a tilted coordinate system whose z' axis is parallel to the effective field

$$\begin{aligned} x' &= x\cos(\theta) - z\sin(\theta) \\ \mathrm{Y}' &= y, \\ z' &= x\sin(\theta) + z\cos(\theta) \end{aligned} \tag{12}$$

and θ represents the tilt angle of the effective field

$$\theta = \tan^{-1}(\omega_1/\Delta\omega_{\mathrm{H}}) \tag{13}$$

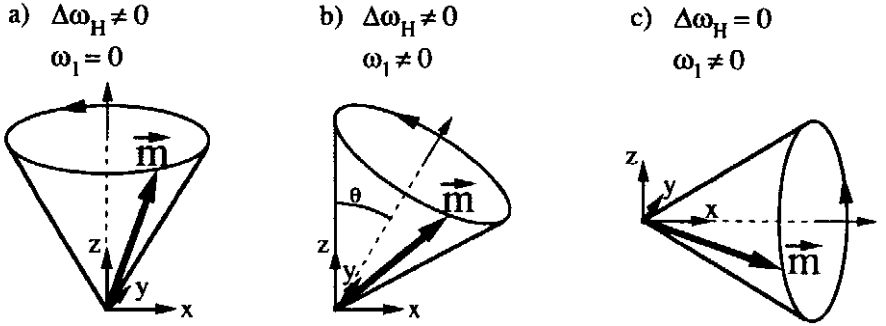

FIG. 2. (a), Evolution of a spin-$\frac{1}{2}$ in the rotating frame for the case of free precession; (b), off-resonance irradiation; and (c), on-resonance irradiation.

Some common situations are shown in Fig. 2. In the absence of rf irradiation [$\omega_1 = 0$, Fig. 2(a)] the spins precess around the z axis. We recover, therefore, the case of free precession, this time in the rotating frame of reference. The precession frequency is therefore reduced to $\Delta\omega_H$. Generally, all frequencies calculated in the rotating reference frame are frequency shifted with respect to calculations done in the laboratory frame. The signals calculated via this method are therefore directly those measured in a heterodyne experiment, where the reference frequency is equal to the rf. This is the usual situation in magnetic resonance experiments, where phase-sensitive detection at the frequency of the rf irradiation is used. Another important case is that of on-resonance irradiation [$\Delta\omega_H = 0$ and $\omega_1 \neq 0$, Fig. 2(c)]. In this case, the precession occurs around the x axis. The general case of off-resonance irradiation, where the effective field lies in the xz plane is shown in Fig. 2(b).

B. OPTICAL TWO-LEVEL SYSTEMS

In order to describe the interaction of an atomic system with optical radiation, we use a simple model system consisting of two energy levels connected by an electric dipole-allowed optical transition (Allen and Eberly, 1987; Brewer, 1977b). Although atoms with only two energy levels do not exist in nature, they are a convenient fiction and often a good approximation to reality if the frequency of the radiation field is close to an atomic transition. As a result, the model of a two-level atom is widely used and serves to introduce the notation used for optical experiments throughout this chapter. Quantum effects of the radiation field are not important for our purpose; we therefore use a semiclassical description. Furthermore, we assume that the two eigenstates $|g\rangle$ (groundstate) and $|e\rangle$ (excited state) of the atomic Hamiltonian are simultaneous eigenstates of the angular momentum

operator **J** and its z component J_z. The transition connecting the two states should be electric-dipole allowed, so that the states are of opposite parity.

Following the usual Feynman–Vernon–Hellwarth (Feynman *et al.*, 1957) parametrization, we expand the two-level system in terms of the three operators I_x, I_y, and I_z, which obey the usual commutation relations for angular momentum operators, although their physical significance is not that of actual spin operators. We define them via their matrix representation

$$\begin{aligned} \langle g|I_x|g\rangle &= 0 & \langle g|I_x|e\rangle &= \tfrac{1}{2} & \langle e|I_x|e\rangle &= 0 \\ \langle g|I_y|g\rangle &= 0 & \langle g|I_y|e\rangle &= -\tfrac{i}{2} & \langle e|I_y|e\rangle &= 0 \\ \langle g|I_z|g\rangle &= \tfrac{1}{2} & \langle g|I_z|e\rangle &= 0 & \langle e|I_z|e\rangle &= -\tfrac{1}{2} \end{aligned} \tag{14}$$

With these definitions, it is clear that the system is formally equivalent to the magnetic two-level system if the operators $I_\alpha(\alpha = x, y, z)$ are replaced by S_α. The Hamiltonian for the atom interacting with the radiation field can now be written as

$$\mathscr{H} = -\omega_0 I_z + \omega_x(t) I_x + \omega_y(t) I_y \tag{15}$$

where ω_0 represents the electronic excitation energy and the coupling constants

$$\omega_x = \mathrm{Re}\{\mu_E \cdot \mathbf{E}\}$$

and

$$\omega_y = \mathrm{Im}\{\mu_E \cdot \mathbf{E}\} \tag{16}$$

describe the interaction between the atomic dipole moment and the electric field. As in the magnetic resonance case, we may now transform the Hamiltonian into the rotating frame of reference, with the rotation frequency ω now in the range of $5 \cdot 10^{14}$ Hz. The sense of rotation should again be chosen such that the longitudinal component $A = \omega_0 - \omega$ is minimized.

Mathematically, the equation of motion for this system and therefore the evolution of the optical system is determined by the Torrey solutions for the Bloch equations of the driven hvo-level system, as in the case of the magnetic two-level system. However, the parameters that determine its behavior can be quite different from the typical parameters in magnetic resonance experiments. One major difference is that the width of the optical resonance line is often considerably larger than the optical Rabi frequency. In these cases, the evolution of the system does not correspond to a rotation around the effective field, but is strongly damped. It is then more appropriate to use a rate equation for the description of the system. Before discussing these effects, however, we would like to extend the two-level model to give a more realistic description of atomic systems.

C. Multilevel Systems

When the magnetic level system is coupled to an optical transition, as is the case in all systems of interest here, the interaction between the atomic level system and the radiation field depends on the magnetic quantum numbers of the levels involved as well as on the polarization of the light. Therefore., we first give a short summary of the usual semiclassical description of electromagnetic fields as it is used in optical spectroscopy.

1. *Radiation Field*

The optical radiation fields of interest to us are always harmonic plane waves. We use a coordinate system where the z axis is parallel to the direction of propagation of the laser beam. The electric field component at the (fixed) location of the atomic system can then be written as

$$\mathbf{E} = (E_x, E_y, 0) = [A_x \cos(\omega t + \phi_x), A_y \cos(\omega t + \phi_y), 0] \tag{17}$$

where E_x and E_y are the amplitudes along the respective coordinate axes, and ϕ_x and ϕ_y are the corresponding phases. The longitudinal component E_z vanishes in all systems of interest. Instead of the Cartesian basis, it is often more useful to use a spherical basis (d'Yakonov, 1965) with

$$\mathrm{E} = (0, E_+, E_-) = [0, A_+ \cos(\omega t + \phi_+), A_- \cos(\omega t + \phi_-)] \tag{18}$$

and the usual transformation relations

$$E_\pm = \frac{1}{\sqrt{2}}(E_x \pm iE_y) \tag{19}$$

and

$$E_x = \frac{1}{\sqrt{2}}(E_+ + E_-)$$

$$E_y = \frac{-i}{\sqrt{2}}(E_+ - iE_-) \tag{20}$$

For all cases of interest to us, it will be sufficient to consider the coupling between atom and radiation field as an interaction between the atomic dipole element $\boldsymbol{\mu}_E = (\mu_{Ex}, \mu_{Ey}, \mu_{Ez})$ and the semiclassical external field E.

The three possible spin states of the photon, $J_z = 0, \pm 1$, correspond to three orthogonal polarization states of the radiation field. These polarization states are usually labelled as π, σ_+, and σ_-, respectively. If the quantization axis coincides with the direction of propagation of the photon, only the σ_+ and σ_- states are allowed, which is the quantum mechanical analog of the transversality condition for electromagnetic waves. The σ polarization

indicates circularly polarized light, while linearly polarized light can be written as a superposition of two circularly polarized components with equal amplitudes. If the quantization axis is perpendicular to the direction of Propagation, π light is also allowed. It represents linearly polarized light whose electrical field vector is parallel to the quantization axis.

2. *Angular Momentum and Selection Rules*

A transfer of polarization between different quantum mechanical systems corresponds to an equilibration of populations in one system and a simultaneous increase of the population differences in the other. The changes in each subsystem are accompanied by changes in energy and momentum, quantities that must be conserved in the total system. In the context discussed here, the most important conservation laws are those for energy and angular momentum. Since states with different angular momentum correspond to different energies, transfer of population differences affects both quantities simultaneously. If the additional polarization of the spin system is obtained from another spin system, angular momentum is simply exchanged between the spin system?., while energy is conserved by exchange of photons with the radiation fields, which are usually applied to the spin systems. In the case of optical pumping, the additional order is obtained from the radiation field. It provides, therefore, not only the energy for the population transfer but also the angular momentum. On the other hand, the population difference across the electronic transition often remains unchanged during the process; it can be considered as a means to couple the spin system to the radiation field.

The optical radiation applied in the experiments we want to discuss here interacts, in genera4 with a single atomic transition. Since only the electronic ground state is appreciably populated at normal laboratory temperatures, the only states of interest to us are the ground state and theelectronically excited state connected by the optical transition. Both states consist, in general, of a number of substates with a different angular momentum. This angular momentum can be attributed to different sources: orbital angular momentum of the electron, conventionally designated by the letter **L**, spin angular momentum of the electron, designated as **S**, and the spin of the nucleus. designated I. These angular momenta couple to a total angular momentum $\mathbf{F} = \mathbf{J} + \mathbf{I} = \mathbf{L} + \mathbf{S} + \mathbf{I}$.

In quantum mechanical terminology, the transfer of angular momentum between the radiation field and the atomic system relies on the fact that the photon is a particle with spin-I; the different spin states of the photon correspond classically to different polarizations of the light. If an atom is irradiated with polarized light, it can absorb the photons only if the angular momentum of the combined-system atom-radiation field is conserved: $\mathbf{F}' = \mathbf{F} + \mathbf{I}_{\text{photon}}$, where $\mathbf{F}$ represents the angular momentum of the lower state, $\mathbf{F}'$ that of the upper state, and $\mathbf{I}_{\text{photon}}$ that of the photon.

The conservation of angular momentum determines, therefore, the coupling constants with which optical radiation couples individual substates of the electronic ground state to substates of the electronically excited state. The calculation of transition matrix elements is described elsewhere in great detail (see e.g., Weissbluth). As an example Fig. 3 shows the relative intensities (i.e., $|\mu_E \cdot E|^2$) of the allowed transitions within the Na D_1 line for σ_+, σ_-, and I light. Since the only valence electron in the ground state occupies an s-orbital, the total electronic angular momentum is $J = \frac{1}{2}$. In the excited state, the orbital angular momentum of the valence electron is L = 1, resulting in two fine structure states $^2P_{1/2}$ and $^2P_{3/2}$. The D_1 line connects the ground state to the $^2P_{1/2}$ excited state, so that the ground and excited states have identical angular momentum. The nuclear spin of ^{23}Na is $I = \frac{3}{2}$, so that the ground and excited states split into two hyperfine multiplets with $F = 1$ and $F = 2$.

If the atom decays spontaneously into the ground state, it can emit a photon in any direction in space. Since the angular momentum of the photon is always parallel or antiparallel to its direction of propagation, the selection rules for this process are different from those for the stimulated absorption process. The orientation of the angular momentum carried by the photon, and therefore the ground state into which the atom decays, is determined by the spontaneous decay rate. Since the polarization states σ_+, σ_-, and π are orthonormal, the spontaneous decay rates within a single optical line are equal to the sum of the intensities for the individual polarizations.

3. *Optical Pumping*

We turn now to a description of the process by which optical radiation can induce nonthermal populations of atomic substates. The optical pumping process can be understood qualitatively from the difference in induced and spontaneous transition strengths when the optical field is polarized. If the level system depicted schematically in Fig. 4 is initially in thermal equilibrium, both ground state sublevels are equally populated, while the excited state is not populated. If the atom interacts with σ_+ light, the atoms in the $m_F = -\frac{1}{2}$ ground state can absorb a photon while simultaneously making a transition to the $m_{F'} = \frac{1}{2}$ excited state. As a result, both the ground and excited states are polarized, i.e., they have a nonvanishing angular momentum. This polarization process is obviously determined by the selection rules due to the polarized radiation field and the conservation of angular momentum.

In contrast to the stimulated absorption process, spontaneous emission has no preferred direction in space so that the excited states in Fig. 4 can decay into either ground state. If a finite probability exists that the atom falls into state $|2\rangle$, repeated cycles of absorption and spontaneous emission events can change the average angular momentum of the atoms. If the atoms reach the state of maximum angular momentum, they no longer absorb any radiation. As an example, consider the level scheme of the Na ground state shown in

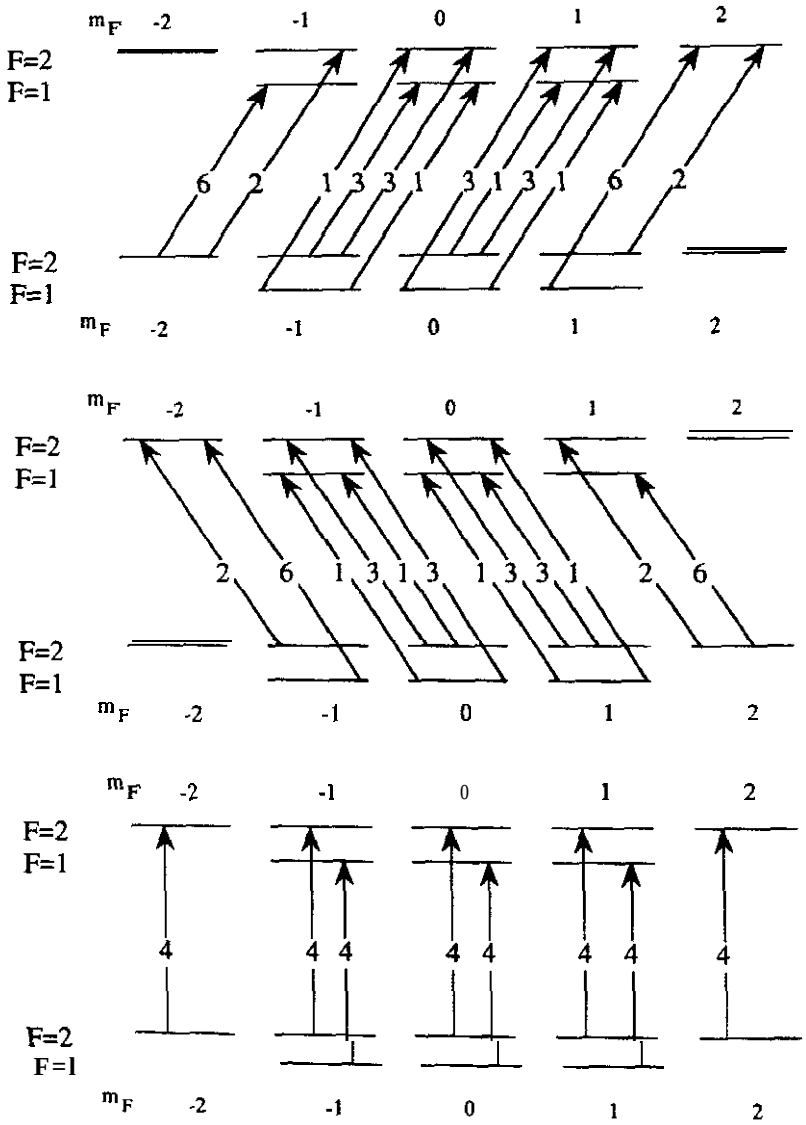

FIG. 3. Level scheme of the Na D_1-transition. The ground state is the $^2S_{1/2}$ state and the excited state is $^2P_{1/2}$; the nuclear spin of ^{23}Na is $I = \frac{3}{2}$, so that the total angular momentum is $F = 1$ or $F = 2$ for both ground and excited states. Also indicated are the transition strengths for σ_+ light (top), σ_- light (center), and π light (bottom).

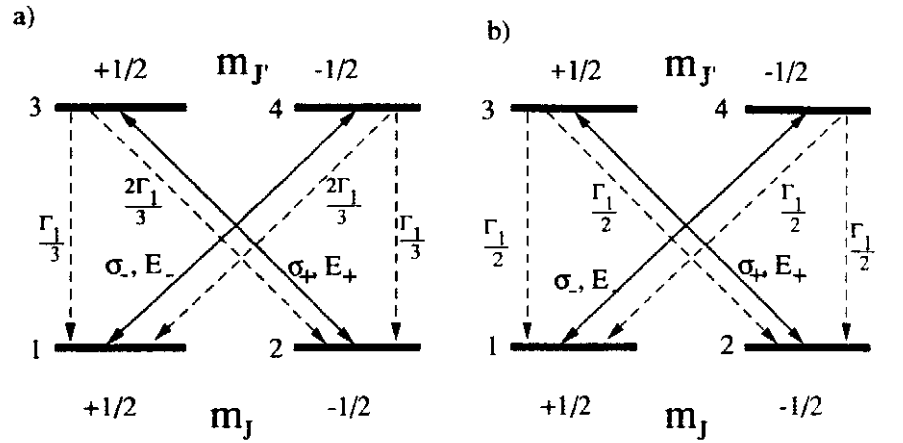

FIG. 4. Schematic representation of the $J = \frac{1}{2} \leftrightarrow J' = \frac{1}{2}$ system. The solid line represents the interaction with the laser field, while the dashed lines indicate allowed transitions. The number indicates the relative relaxation rates: (a), no relaxation in the excited state; (b), complete reorientation of the excited state.

Fig. 3. Atoms in state $F = 2, m_F = 2$ do not interact with σ_+ light. If the atomic system is irradiated with σ_+ light of sufficient intensity, the atoms will eventually accumulate in this state, and absorption will stop. The atomic system is then completely polarized, i.e., the atoms are all in the same angular momentum state. As such, this system represents au ideal starting point for magnetic resonance experiments.

The discussion of the spontaneous emission rates given here applies only to an isolated atomic system. If the optical pumping experiment includes buffer gas, the effect of collisions also has to be taken into account. One of the major effects is a randomization of the angular momentum of the excited state. This randomization corresponds to a mixing of the excited state sublevels. For the spontaneous emission process, it has the effect of averaging the transition probabilities. Figure 4 summarizes the effect for a $J = \frac{1}{2} \leftrightarrow J' = \frac{1}{2}$ transition. Figure 4(a) gives the spontaneous decay rates for the isolated system where no excited state reorientation occurs, while Fig. 4(b) gives the relative rates for complete excited-state reorientation.

The four-level system shown here is of course equivalent to two coupled spins-$\frac{1}{2}$, such as a $^1H-^{13}C$ two-spin system in which the ratio of the Larmor frequencies is about 10^7. Accordingly, it is possible to transfer polarization between the two coupled transitions by applying strong selective pulses to one of the electronic transitions, which is similar to selective inversion in NMR of coupled spin systems (Sørensen et *al.*, 1974). The selectivity can, in this case, be achieved by appropriate polarization of the light, so the pulse

does not have to be selective in frequency. Such a polarization transfer scheme assumes that the optical Rabi frequency exceeds the decay rate of the optical coherences; the excitation of the system then proceeds coherently, very much like in a pulsed NMR experiment, These are the typical conditions when sublevel transitions of the excited state are investigated, since they allow the transfer of a large proportion of the population into the excited state. The less familiar (for NMR spectroscopists), but still rather common case is the limit where the optical Rabi frequency is small compared to the optical dephasing rate. In this limit, the system shows no coherent evolution, and most of the population remains in the ground state. Since this process can be driven with considerably lower laser intensities while still achieving polarization of the ground state, we will discuss it here in more detail.

Under these conditions, the optical coherences are always relatively small, and if the laser intensity is well below the saturation level, the population of the excited state also becomes negligible. Most observable quantities are then determined only by the ground state populations and the atomic sublevel coherences, i.e., by the ground state multipole moments. It is then often desirable to eliminate the excited state altogether and derive an equation of motion for the ground state sublevels alone. This reduction of the state space should occur in such a way that the influence of the radiation field on the ground state dynamics is included correctly in the resulting equations of motion. The most important effects are (i) optical pumping, i.e., a redistribution of the populations among the ground state levels, (ii) an apparent shift of energy levels, usually called the light shift, and (iii) a damping of the ground state coherences.

For a mathematical derivation of the optical pumping process, we can further simplify the level system of Fig. 4. If the atom is irradiated with σ_+ light, the excited state sublevel $|4\rangle$ is not coupled to the rest of the system. Therefore, it is possible to calculate the full dynamics of the system from a reduced three-level system. We therefore consider two electronic ground state sublevels, one of which couples via the radiation field to an electronically excited state (see Fig. 5). This three-level system is described by a 3×3 density operator. We use the abbreviations

$$x_{ij} = \rho_{ij} + \rho_{ji}, \quad y_{ij} = i(\rho_{ij} - \rho_{ji}) \tag{21}$$

to describe the dynamics of the system in terms of a set of real parameters, in an obvious extension of Eq. (5). The x_{ij} represent the real part of the coherence, while y_{ij} correspond to the imaginary part. Physically, they both correspond to an induced electric or magnetic dipole moment. Writing $\Gamma_1^{3\to1}$ for the spontaneous decay rate from level 3 to level 1, the equations of motion for the density operator elements in a frame of reference rotating at the fre-

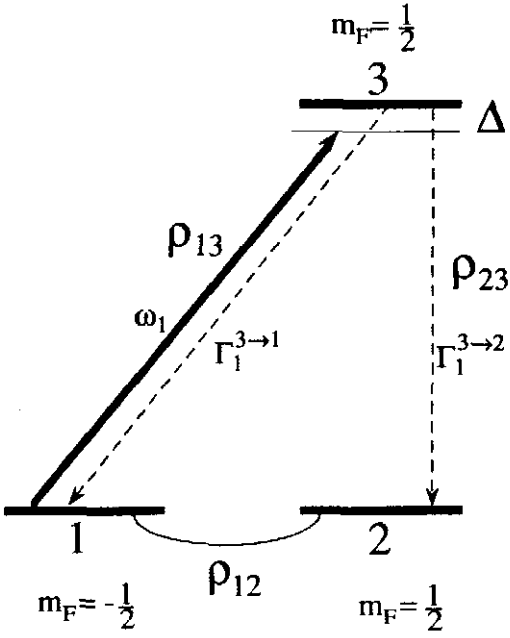

FIG. 5. Relevant level scheme for the perturbation analysis of optical pumping. Levels 1 and 2 are substates of the electronic ground state; level 3 is an electronically excited state. ω_1 represents the optical Rabi frequency. The solid arrow indicates the allowed optical transition for σ_+ light and the dashed arrows indicate spontaneous decay channels.

quency of the optical field are

$$\begin{aligned}
\dot{\rho}_{11} &= (\omega_1/2)y_{13} + \Gamma_1^{3\to1}\rho_{33} \\
\dot{x}_{12} &= (\omega_1/2)y_{23} \\
\dot{y}_{12} &= (\omega_1/2)x_{23} \\
\dot{\rho}_{22} &= \Gamma_1^{3\to2}\rho_{33} \\
\dot{x}_{13} &= \Delta y_{13} - \Gamma_2 x_{13} \\
\dot{y}_{13} &= -\Delta x_{13} - \omega_1(\rho_{11} - \rho_{33}) - \Gamma_2 y_{13} \\
\dot{\rho}_{33} &= -(\omega_1/2)y_{13} - \Gamma_1\rho_{33} \\
\dot{x}_{23} &= -(\omega_1/2)y_{12} + \Delta y_{23} - \Gamma_2 x_{23} \\
\dot{y}_{23} &= -(\omega_1/2)x_{12} - \Delta x_{23} - \Gamma_2 y_{23}
\end{aligned} \tag{22}$$

where Δ represents the offset of the laser frequency from optical resonance and ω_1 represents the optical Rabi frequency. $\Gamma_1 = \Gamma_1^{3\to1} + \Gamma_1^{3\to2}$ is the total

decay rate of the excited state and Γ_2 is the dephasing rate of the optical coherences. When the radiation field is initially switched on, the system is in a state of thermal equilibrium. The thermal equilibrium density operator does not commute with the Hamiltonian of the combined system atom plus radiation field. It is therefore forced into a precession and relaxes on a time scale of tbe order of the optical dephasing time Γ_2^{-1} to a quasistationary state in which the optical coherences are

$$x_{13} = \rho_{11} \frac{\omega_1 \Delta}{\Delta^2 + \Gamma_2^2}, \qquad y_{13} = \rho_{11} \frac{-\omega_1 \Gamma_2}{\Delta^2 + \Gamma_2^2} \tag{23}$$

and the population of the excited state is

$$\rho_{33}(t) = \rho_{11} \frac{\omega_1^2}{2(\Delta^2 + \Gamma_2^2)} \frac{\Gamma_2}{\Gamma_1} \tag{24}$$

As explained previously, the finite probability of the excited state to decay to level 2 leads to the optical pumping effect. With the decay rate $\Gamma_1^{3\to 2}$ and the result for ρ_{33} valid for the quasistationary state, we can therefore write an equation of motion for the populations of the ground state sublevels:

$$\frac{d}{dt}\rho_{11}(t) = -k\rho_{11}(t) = -\frac{d}{dt}\rho_{22}(t) \tag{25}$$

with the rate constant

$$k = \Gamma_2 \frac{\Gamma_1^{3\to 2}}{\Gamma_1^{3\to 1} + \Gamma_1^{3\to 2}} \frac{\omega_1^2}{2(\Delta^2 + \Gamma_2^2)} \tag{26}$$

or in terms of the population difference $z_{12} = \rho_{22} - \rho_{11}$

$$\dot{z}_{12} = \frac{d}{dt}(\rho_{22} - \rho_{11}) = 2\dot{\rho}_{11} = 2k\rho_{11}(t) = k[(1 - z_{12}(t)] \tag{27}$$

Under the assumptions made here, the ground state population is therefore pumped completely into the second level. This is of course only valid as long as the relaxation of the ground state can be neglected and no magnetic field is present.

4. *Light Shift and Damping of Sublevel Coherence*

In addition to the optical pumping, which describes the effect of the optical irradiation on the ground state populations, the light also affects the ground State coherences x_{12} and y_{12}. As seen from Eq. (22), the optical field couples them to the optical coherences x_{23} and y_{23}. As a result, the distinction between ground-state coherences and optical coherences is no longer exact, and this partial mixing affects the precession and decay of the ground state coherences.

In order to simplify the system's equation of motion, we make the assumption that the dynamics of the ground-state coherence is slow compared to the decay rate of the optical coherences. In all cases of practical importance in this context, this assumption is well justified. On the time scale of the ground-state dynamics, the optical coherences are in a quasistationary state. The situation is therefore very similar to that of the Born-Oppenheimer approximation for the separation of electronic and nuclear degrees of freedom Since the relaxation rate of the optical coherences is extremely fast compared to that of the ground-state coherences, even a small mixing between the ground-state coherences and the optical coherences leads to a damping of the ground-state coherences. In addition, the optical resonance offset, which leads to a precession of the optical coherences, also causes a precession of the ground-state coherences. This effect was first predicted by Barrat and Cohen-Tannoudji (1961a,b,c) and observed by Arditi and Carver (1961) and Cohen-Tannoudji (1961, 1962; Cohen-Tannoudji and Dupont-Roc, 1972; Dupont-Roc et al., 1967) with conventional light sources. Its observation presented conceptual difficulties, and several authors therefore worked on different formulations of the process (Happer, 1972; Happer and Mathur, 1967; Pancharatnam, 1966).

In order to discuss the effect, we again use the model system consisting of two degenerate ground-state sublevels, one of which is coupled to the excited state by a weak laser field (see Fig. 5). We are now interested in the dynamics of the ground-state coherences x_{12} and y_{12}. As is evident from the equations of motion [Eq. (22)], the coherence between the degenerate ground-state sublevels is time-independent if the optical field is absent. As an initial step for the solution of these equations, we put

$$x_{12} = \cos(\delta t)\, e^{-\gamma t} \qquad y_{12} = -\sin(\delta t)\, e^{-\gamma t} \tag{28}$$

for the ground state coherences and

$$\begin{aligned} x_{23} &= [-c_1 \cos(\delta t) + c_2 \sin(\&)]\, e^{-\gamma t} \\ y_{23} &= [-c_1 \sin(\&) - c_2 \cos(\delta t)]\, e^{-\gamma t} \end{aligned} \tag{29}$$

where δ represents the light shift, i.e., the frequency of the precession caused by the optical field and γ is the associated relaxation rate. Inserting these into the equations of motion, we find the coefficients in the quasistationary regime

$$c_1 = 2\delta/\omega_1, \qquad c_2 = 2\gamma/\omega_1 \tag{30}$$

and the frequency and damping rates are

$$\delta = \Delta \frac{\omega_1^2}{4(\Delta^2 + \Gamma_2^2)} \qquad \gamma = \Gamma_2 \frac{\omega_1^2}{4(\Delta^2 + \Gamma_2^2)} \tag{31}$$

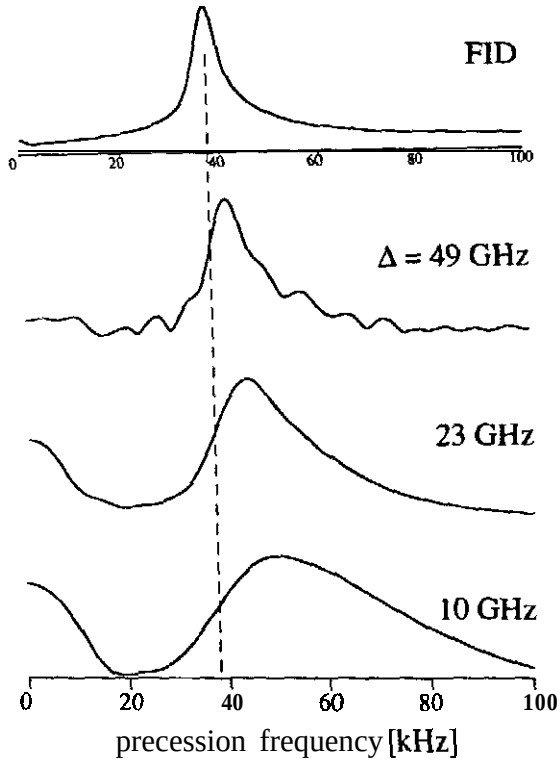

FIG. 6. Effect of optical irradiation on ground state coherences. The top trace represents the Fourier transform of an FID signal, while the lower traces were obtained from precessing magnetization in the presence of the pump beam at constant intensity and variable laser detunings. The dashed vertical line indicates the Larmor frequency.

An experimental demonstration of this effect is shown in Fig. 6. The top trace shows the Fourier transform of the FID signal from the ground state of atomic Na. This is equivalent to the laser being tuned infinitely far away from resonance. The precession frequency marked by the dashed line is therefore equal to the Larmor frequency. The subsequent traces represent the Fourier transforms of precessing magnetization in the presence of a laser field of constant intensity and variable frequency. According to Eq. (31), the light shift as well as the damping rate should both increase as the laser frequency is moved closer to resonance. The light shift has a dispersive dependence on the laser detuning, while the damping has an absorption-like dependence. The precession frequency observed in this experiment should be given by $\Omega = (\delta^2 + \Omega_L^2)^{1/2}$. While we cannot discuss the detailed dependence of the precession frequency on the laser detuning at this place, the qualitative agreement between Eq. (31) and the experimental data is evident.

Since the damping rate of the ground state coherences g does not depend on the spontaneous emission rates $\Gamma_1^{r\to s}$ it is in general different from the optical pumping rate k, as calculated in Eq. (26). For the isolated $J = \frac{1}{2} \leftrightarrow J' = \frac{1}{2}$ system shown in Fig. 4(a), the two rates differ by a factor 1.5; the relaxation of the ground-state magnetization is therefore anisotropic in this case. In the case of complete reorientation of excited-state magnetization by collisions, leading to equal decay rates as shown in Fig. 4(b), the damping rates for ground-state population difference and coherence become the same.

5. *Magnetic Interactions*

In the current context, the magnetic interactions between the various angular momenta and the external magnetic fields are not of primary interest, bat for the sake of completeness we will give a short summary. More details are found in the literature (Abragam, 1961; Balling, 1975; Weissbluth, 1978).

Three sources of angular momentum occur in our context: electron-orbital L, electron-spin S and nuclear-spin **I**. Each of these interacts with the external magnetic fields and with other angular momenta of equal or different types. The spin-orbit coupling of the electron is always the strongest interaction, while the interaction between the nuclear- and electron-spin is often the same order of magnitude as the Zeeman interaction of the electron; the Zeeman interaction of the nuclear spin is usually negligible compared to the other terms.

In the absence of an external magnetic field, the various angular momenta couple to each other via the spin-orbit interaction of the electron and the hyperfine interaction between electron and nucleus. For our purpose it is sufficient to write these interactions as

$$\mathcal{H}_i = \xi \mathbf{L} \cdot \mathbf{S} + A\mathbf{I} \cdot (\mathbf{L} + \mathbf{S}) \tag{32}$$

where the coupling constants ξ of the spin-orbit interaction and the hyperfine coupling constant A are functions of the spatial part of the electron wave function. For the Na ground state, the hyperfine coupling constant is 886 MHz, leading to a splitting of 1772 HMz. The spin-orbit interaction for the $3p$ orbital is 344 GHz, leading to a separation of the D_1 and D_2 transitions of 0.6 nm or 17.2 cm^{-1}. The interaction of the angular momenta with the external magnetic field is

$$\mathcal{H}_e = \beta \mathbf{B} \cdot (\mathbf{L} + 2\mathbf{S}) + \gamma_I \mathbf{B} \cdot \mathbf{I} \tag{33}$$

where β represents the Bohr magneton. Its numerical value is 14 GHz/T and for ^{23}Na, γ_I is 11.3 MHz/T, so that the Zeeman interaction of the nucleus is usually negligible.

Since the Zeeman interaction is often much smaller than the spin-orbit coupling, and the two interactions do not commute with each other, the Zeeman interaction can be truncated with respect to the spin-orbit interaction.

Spin- and orbital-angular momentum of the electron then remain coupled, and the resulting first-order energyis written as

$$\mathcal{H}_1 = \gamma_1 \mathbf{B} \cdot \mathbf{J} \tag{34}$$

where γ_1 describes the effect of the truncation. In the ground state of Na, the electron has no orbital angular momentumso the spin-orbit interaction vanishes and the electronZeeman interaction corresponds tothe spin Zeeman interaction; the Larmor frequency is therefore 28 MHz/mT. In the excited state, the orbital angular momentum is $L = 1$ and the γ_1 factors become 9.3 MHz/mT and 18.7 MHz/mT for the $^2P_{1/2}$ and $^2P_{3/2}$ states, respectively.

In actual experiments, magnetic field strengths can vary over a relatively wide range. Figure 7 shows the energy levels of the Na ground state as a function of the magnetic field strength, measured as the Larmor frequency ω_1 of an isolated electronic spin. The spectra (top) of the figure represent examples

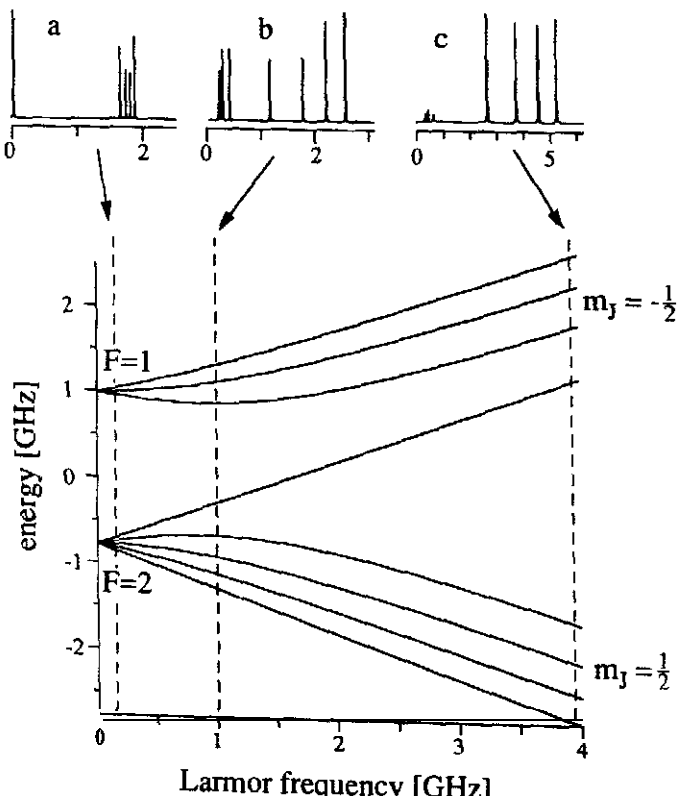

FIG. 7. Energy levels of the Na ground state as a function of magnetic field strength and corresponding spectra. (a), weak field region; (b), intermediate field; (c), strong field.

for weak ($\omega_J \ll A$), intermediate ($\omega_J \sim A$), and strong magnetic fields ($\omega_J \gg A$). As the magnetic field strength increases, the eigenstates of the system change from the fully coupled states, $F = 2$ and $F = 1$, into the uncoupled states where the individual angular momenta of electron and nucleus can be distinguished. In the low-field region (a), the spectrum consists of the low frequency lines, corresponding to Zeeman transitions within the $F = 1$ and $F = 2$ multiplets, and the lines near 1.8 GHz, corresponding to hyperfine transitions between the multiplets. At intermediate fields, these transitions can no longer be distinguished. In the high-field region (c), the high-frequency lines correspond to electron spin transitions near the Larmor frequency, while the low-frequency lines near a truncated hyperfine coupling correspond to nuclear-spin transitions,

The single low-frequency line of the spectrum in Fig. 7(a) indicates that the $F = 1$ and $F = 2$ multiplets in the low-field region can be considered as individual spins being subjected to a linear Zeeman effect. Accordingly, one defines a Hamiltonian for this spin as

$$\mathcal{H}_F = \gamma_F \mathbf{B} \cdot \mathbf{F} \tag{35}$$

with a coupling constant $\gamma_F = \gamma_J/(2I + 1)$ for an alkali atom. The apparent gyromagnetic ratio is therefore reduced by the multiplicity of the nuclear spin compared to a hypothetical atom with no nuclear spin. For the Na ground state, this results in a Larmor frequency of 7 MHz/mT, while the excited-state Larmor frequencies are 2.3 MHz/mT and 4.7 MHz/mT for the $^2P_{1/2}$ and $^2P_{3/2}$ states, respectively. Since the angular pseudo-spin F, appearing in Eq. (35), represents the vector sum of the electronic and nuclear spin, the resonances of Fig. 7 cannot be assigned transitions of the electron or nuclear spins,

6. *Relaxation Effects*

In addition to the coherent (Hamiltonian) evolution, it is necessary to take relaxation effects into account. Some relaxation mechanisms affect only optical transitions, others affect only magnetic transitions; some affect both. Some relaxation mechanisms affect only coherences (optical or magnetic), others influence populations as well as coherences. For the experiments we will discuss, the most important mechanisms are

(1) Lifetime broadening: The electronically excited state can decay to the ground state by spontaneous emission of a photon; it tends to depopulate the excited state and populate the ground state. It affects the lifetime of optical population differences and coherences, as well as magnetic transitions in the excited state. Under certain conditions, the polarization of the excited state is partly retained during the decay. Another important source of lifetime broadening is the removal of atoms from the interaction region by free flight

(e.g., an atomic beam) or diffusion (e.g., in a gas cell in the presence of a buffer gas). This source of relaxation can be minimized by using a large interaction region (e.g., a glass cell with coated walls) or Ramsey spectroscopy in an atomic beam (Ramsey, 1980).

(2) Collision-induced relaxation: In a gas, collisions of the atoms with the walls of the sample cell or with other atoms and molecules present in the gas can lead to de-excitation and loss of phase of the coherence. Thii mechanism therefore affects both magnetic and optical transitions, although in different ways. It also has different effects on coherences and population differences. If the electronic ground state is spherically symmetric (i.e., an s-state), coherences between ground state sublevels are only weakly affected. However, if the electron wave function is not spherically symmetric, as in the excited States of alkali atoms, relaxation of the magnetization by collisions with buffer gas atoms can be very efficient and makes it often impossible to observe magnetic resonances in pressure-broadened systems.

(3) Time of flight: If the atom in a gas leaves the laser beam during the process, the information stored in it is lost, so that this appears as a relaxation mechanism. This affects coherences and populations of optical and magnetic transitions in exactly the same way.

(4) Inhomogeneous effects: In the calculations, we usually assume that all the parameters of the system are homogeneous throughout the sample volume. If this is not the case, the coherences of the different atoms precess out of Phase with respect to each other, leading to an inhomogeneous decay of the macroscopic observables. The most important examples of inhomogeneous effects are the velocity distribution of the atoms in a gas, which leads to the Doppler broadening of the optical transitions, strain broadening in crystals, which can affect optical as well as magnetic resonance transitions, and inhomogeneous magnetic fields.

(5) Fluctuating external fields: If external fields have a nonvanishing spectral density at one of the transition frequencies of the system, they can induce absorption or emission, thereby driving the population difference of the transition towards zero. This relaxation mechanism can always be neglected for optical transitions, but is important for magnetic transitions. The spectral densities have to be evaluated in the center of mass system of the atom, so that inhomogeneous static fields can lead to relaxation of moving atoms. Spectral densities near zero frequency can also lead to nonresonant (adiabatic) relaxation of coherences of any transition. If, as we have assumed, there is no static electric dipole moment, this mechanism affects only magnetic coherences.

(6) Coupling to other systems: If the interaction between various identical or different atoms is not negligible, our description of the total system as an ensemble of many individual subsystems is no longer valid. Since an exact

description of a system of $\geq 10^{12}$ atoms is not feasible, these effects are taken into account in a qualitative, phenomenological way. In many cases, a qualitatively correct description of the system is obtained by adding a homogeneous relaxation mechanism to the transitions. While these couplings can affect all transitions, their effect can differ widely, depending on the nature of the interaction. These mechanisms are usually of little importance in gaseous systems, but are usually quite important in solids. As in the case of fluctuating external fields, these intersystem couplings can lead to relaxation effects of populations and coherences if the power spectral density of their autocorrelation function does not vanish at the transition frequency. They can also lead to adiabatic relaxation of coherences if the power spectral density near zero frequency is appreciable.

D. Ground State Magnetization (Spin $\frac{1}{2}$)

1. *System*

In the preceding section, the derivation of the equation of motion for a reduced ground-state density operator under the influence of circularly polarized light was outlined. Here, we apply it to the generic case of a $J = \frac{1}{2}$ ground state and present an analytical solution. Figure 4 gives a simplified schematic representation of a possible system consisting of a $J = \frac{1}{2}$ ground state and a $J' = \frac{1}{2}$ excited state. This system is a model of the ground state of an alkali atom with nuclear spin $1 = 0$. While real alkali all have a nonvanishing nuclear spin, the treatment of this hypothetical system yields many of the features of real systems, and since it can be solved analytically, it gives much better insight into the actual physics than numerical solutions of the real systems.

The spin-$\frac{1}{2}$ system in which we are interested (see Fig. 4) consists of a $J = \frac{1}{2}$ atomic ground state and a $J' = \frac{1}{2}$ excited state. We choose the quantization axis parallel to the direction of the laser beam, so that the only allowed transitions are the ones indicated by the dashed lines. If the system is irradiated with left circularly polarized light, it couples to the transition $|1\rangle \leftrightarrow |4\rangle$. The three levels $|1\rangle, |2\rangle$, and $|4\rangle$ correspond then exactly to the three-level system used for the derivation of optical pumping and light-shift effect. In order to use the formulas derived there, we have to specify the spontaneous emission rates from level $|4\rangle$ to both ground-state sublevels. In a free atom, the spontaneous emission rate is proportional to the square of the electric dipole matrix element, which has relative values of 2 to 1 for the $J\text{-}J' = \pm 1$ vs. the $J\text{-}J' = 0$ transitions [see Fig. 4(a)]. However, if the atom of interest is located in a cell with a buffer gas, it undergoes many collisions with buffer gas atoms during the lifetime of the excited state. Since the valence electron is in a p-type orbital in the excited state, these collisions with buffer gas atoms

lead to a relatively efficient equilibration of the excited state population: although the optical radiation connects only to level $|4\rangle$, both excited-state sublevels actually get populated. This results, for example., in a dependence of the optical pumping on the buffer gas pressure (Franz and Franz, 1966). In our context, it is sufficient to model the excited state as shown in Fig 4(b) or with a single energy level with equal relaxation rates to both ground state sublevels.

The dynamics can be described in a relatively simple way if we parametrize the effects of optical pumping, damping, and light shift calculated previously. We define the optical pumping rate P+ as

$$P_+ = \frac{\omega_1^2}{4\Gamma_2(1+\bar{\Delta}^2)} \tag{36}$$

We consider two ground-state sublevels, as in the mode system just treated. Since this now represents Our total system of interest, we drop the indices 1 and 2 and use the spin operator S for the description of a two-level ground state system.

2. *Longitudinal* Pumping

We first consider the case where a magnetic field is applied parallel to the direction of propagation of the light. The system is then axially symmetric, and it is most convenient to choose the quantization axis (the z-axis) parallel to the symmetry axis so that the equation of motion for the ground-state subsystem becomes

$$\dot{\rho} = -i[\mathscr{H}_L, \rho] + \hat{\Gamma}\rho + P_+ S_z \tag{37}$$

$$\mathscr{H}_L = (\bar{\Delta} P_+ + \Omega_L) S_z \tag{38}$$

where $\bar{\Delta} = \Delta/\Gamma_2$ represents the resonance offset A of the laser frequency. normalized to the dephasing rate Γ_2 of the optical coherence. $\hat{\Gamma}$ represents the relaxation superoperator that includes all the damping mechanisms summa&ad previously. As we have seen, the relaxation rate of the populations and coherences depend in general on the strength of the optical transitions coupled to the sublevels. In order to simplify the theoretical analysis, we assume here that Population differences and coherences decay with the same rate $\gamma_{eff} = \gamma_0 + P_+$, where γ_0 summarizes the terms that do not depend on the optical irradiation, such as diffusion processes. This isotropic relaxation occurs in a system where collisions of the excited atoms with buffer gas atoms lead to a reorientation of the excited-state magnetization. The equation of motion can then be rewritten as

$$\dot{\rho} = -i[\mathscr{H}_L, \rho] - \gamma_{eff}\rho + P_+ S_z \tag{39}$$

The general solution of the equation of motion is

$$\rho(t) = S_z[z_{eq} - (z_{eq} - z(0))\, e^{-\gamma_{eff}t}] + [xS_x \cos(\Omega t) + yS_y \sin(\Omega t)]\, e^{-\gamma_{eff}t} \quad (40)$$

where x, y, and z are expansion coefficients determined by the initial conditions x(O), y(O), and $z(0)$, and the equilibrium magnetization is $z_{eq} = P_+/\gamma_{eff} = P_+/(\gamma_0 + P_+)$. $\Omega = \bar{\Delta} P_+ + \Omega_L$ represents the total precession frequency determined by the sum of the light shift contribution and the Larmor precession. The motion of the longitudinal component parallel to the symmetry axis is thus decoupled from the motion of the transverse component perpendicular to it. Magnetization is created by the optical pumping process along the z axis, and this component approaches the stationary value exponentially at a rate γ_{eff}. Transverse components decay at the same rate, while simultaneously precessing around the symmetry axis. The dynamics of this system therefore closely resemble those of a freely precessing spin, with the magnetic field augmented by the light-shift effect and the equilibrium magnetization depending on the light intensity, As discussed earlier, the expansion coefficients of the density operator in terms of the angular momentum operators are proportional to the magnetization components. We emphasize this fact by writing them as $\mathbf{m} = m_x, m_y$, and m_z. For the typical case where the system is in thermal equilibrium when the laser is turned on, the magnetization of the system evolves as

$$\mathbf{m}(t) = [0,\ 0,\ z_{eq}(1 - e^{-\gamma_{eff}t})] \quad (41)$$

This is the typical situation of optical pumping where transfer of polarization from the light field to the spin system is used to enhance the magnetic resonance signal.

3. *Transverse Pumping*

Another possible experimental setup uses a magnetic field B perpendicular to the laser beam. The system is now no longer axially symmetric; we choose the coordinate system such that the z axis remains parallel to the laser beam, and we orient the x axis in the direction of the magnetic field. The equation of motion is the same as for the case of longitudinal pumping, but the Hamiltonian changes to

$$\mathcal{H}_T = \bar{\Delta} P_+ S_z + \Omega_L S_x \quad (42)$$

Since the magnetic field is no longer parallel to the laser beam, the overall effective field now forces a precession of the magnetic moment around the axis $\boldsymbol{\Omega} = (\Omega_L, 0, \bar{\Delta} P_+)$, whose x component, Ω_L, is given by the strength of the magnetic field B, and whose z component results from the light-shift term

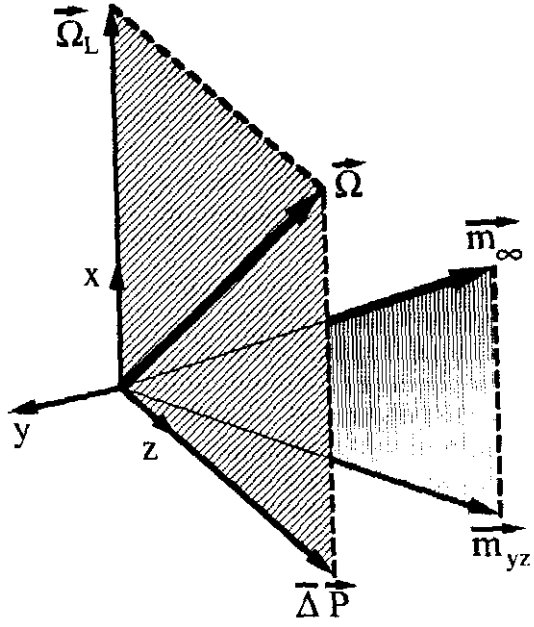

FIG. 8. The true and effective fields appearing in the dynamics of the ground state pumping.

$\tilde{\Delta}P_+$ (see Fig. 8). With our choice of coordinate system, the effective field is thus always in the xz plane. The second and third terms of Eq. (37) remain the same.

It is instructive to rewrite the equation of motion in terms of the magnetization vector $\mathbf{m}$ (Mitschke *et al.*, 1986).

$$\dot{\mathbf{m}} = \boldsymbol{\Omega} \times \mathbf{m} - \gamma_{\text{eff}}\mathbf{m} + \mathbf{P} \tag{43}$$

with

$$\boldsymbol{\Omega} = (\Omega_L, 0, \tilde{\Delta}P_+) \tag{44}$$

representing the effective field whose z component is equal to the light-shift, and whose x component is equal to the Larmor contribution, This equation is quite analogous to the Bloch equation with a magnetic field in the xz-plane, except that the magnetization that is generated by the inhomogeneous third term in Eq. (43) is not aligned with the effective field.

The general solution of this equation of motion is

$$\mathbf{m}(t) = \sum_{i=-1}^{1} c_i \boldsymbol{\xi}_i e^{\lambda_i t} + \mathbf{m}_\infty \tag{45}$$

where the eigenvectors ξ_i and eigenvalues λ_i are given as

$$\begin{aligned} \xi_0 &= (\Omega_L, 0, \bar{\Delta}P_+), & \lambda_0 &= -\gamma_{eff} \\ \xi_{\pm 1} &= (\bar{\Delta}P_+, \pm i\Omega, -\Omega_L), & \lambda_{\pm 1} &= \pm i\Omega - \gamma_{eff} \end{aligned} \tag{46}$$

with

$$\Omega = \sqrt{\Omega_L^2 + \bar{\Delta}^2 P_+^2} \tag{47}$$

and the stationary value is

$$\mathbf{m}_\infty = \frac{P_+}{\gamma_{eff}(\Omega_L^2 + \bar{\Delta}^2 P_+^2 + \gamma_{eff}^2)} (\bar{\Delta}P_+\Omega_L, -\gamma_{eff}\Omega_L, \bar{\Delta}^2 P_+^2 + \gamma_{eff}^2) \tag{48}$$

It has been shown that this stationary magnetization can be calculated exactly for arbitrary laser intensities (Adonts *et* al., 1989). Since the magnetization is generated along a direction that does not coincide with the effective field, the equilibrium magnetization $\mathbf{m}_\infty$ is in general not parallel to either of the two directions. A typical example is shown in Fig. 8. Note that the eigenvectors $\xi_0, \xi_{\pm 1}$ given by Eq. (46) are not normalized to unit length.

The eigenvector ξ_0 is parallel to the effective field and thus corresponds to longitudinal magnetization, while $\xi_{\pm 1}$ describes the transverse component precessing around the effective field. The precession frequency Ω is determined by the Larmor frequency Ω_L and the light-shift term $\bar{\Delta}P_+$. The deviation from the Larmor frequency is always positive and largest if the optical detuning is equal to the homogeneous line width ($\bar{\Delta} = 1$).

The expansion coefficients c_i are determined by the initial condition. For a sample in thermal equilibrium, the ground state orientation vanishes, i.e., $m(O) = 0$. The coefficients are then

$$c_0 = -\frac{\bar{\Delta}P_+^2}{\Omega^2 \gamma_{eff}}, \qquad c_{\pm 1} = \frac{P_+ \omega_H (\pm i\Omega + \gamma_{eff})}{2\Omega^2(\Omega^2 + \gamma_{eff}^2)} \tag{49}$$

The evolution of the magnetization is shown graphically in Fig. 9 for the parameters $P+ = 5 \cdot 10^4\ \mathrm{sec}^{-1}$, $\gamma_0 = 10^4\ \mathrm{sec}^{-1}$, $\Omega_L/2\pi = -1.5$ MHz, $\bar{\Delta} = -0.1$ [Fig. 9(a)], and $\bar{\Delta} = 0$ [Fig. 9(b)]. The curved line represents the tip of the magnetization vector tracing out a curve in three-dimensional space. Also shown is the separation of the initial magnetization [$\mathbf{m}(O) = 0$] into the eigenvectors. The component $\mathbf{m}_\infty$ represents the stationary magnetization, and $c_0\xi_0$ is the longitudinal magnetization, i.e., the component of the time-dependent magnetization $\mathbf{m}(t) - \mathbf{m}_\infty$ that is parallel to the effective field, and $c_1\xi_1 + c_{-1}\xi_{-1}$ is the transverse component perpendicular to the effective field.

For $\bar{\Delta} \neq 0$, the evolution of the time-dependent components leads to a precession of the magnetization vector whose tip traces out the dashed curve

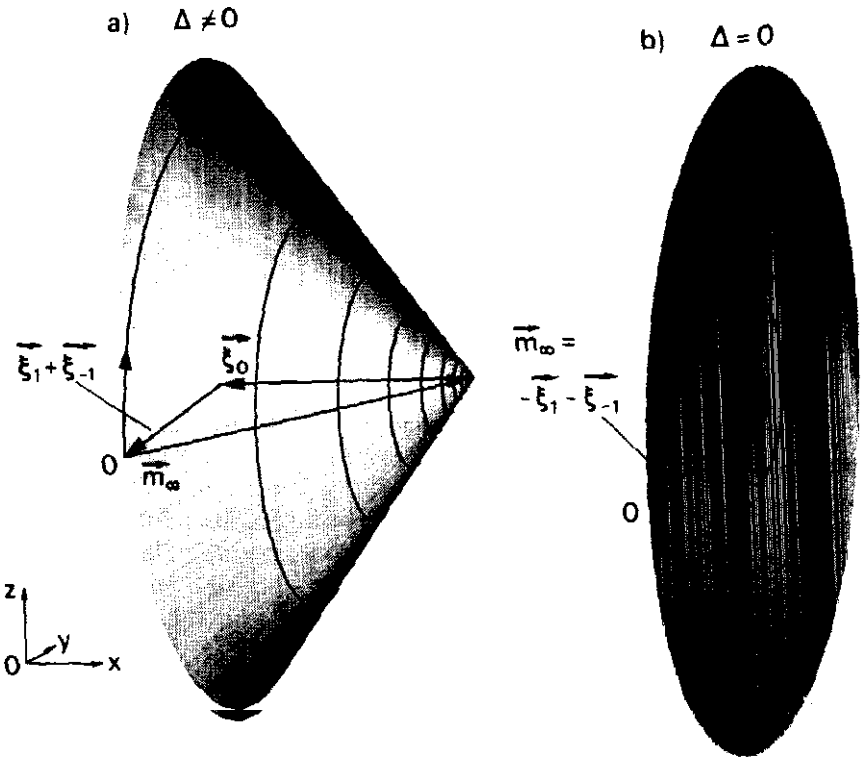

FIG. 9. Motion of the magnetization vector in space.

on the surface of the shaded cone. The tip of this cone is the stationary magnetization; its location is determined by the system parameters [see Eq. (48)]. The symmetry axis of the cone is parallel to the direction of the effective. field Ω, and the opening angle is determined by the initial condition (in our case the origin O), which must lie on the surface of the cone. If the optical field is applied at exact resonance ($\bar{\Delta} = 0$), the virtual field due to the light shift vanishes; as shown in Fig. 9(b), the cone collapses in this case to a circle lying in the *yz* plane.

The motion of the magnetization vector can be compared to the precession of magnetization around the effective field in the rotating frame during rf irradiation. Since the optical pulse generates a dc effective field, the spin precession occurs here in the (static) laboratory frame of reference. A similar case is known from zero-field magnetic resonance, where dc magnetic field pulses can be used for excitation and detection (Kreis *et al.*, 1985; Millar *et al.*, 1985). The main difference between the two cases is the optical pumping effect, which basically drives the equilibrium magnetization, i.e., the tip of the cone, away from the origin.

It is interesting to compare polarization enhancement of magnetic resonance transitions by optical pumping to the more familiar example of Hartmann-Hahn cross-polarization (Hartmann and Hahn, 1962; Levitt *et al.*, 1986) from the point of view of thermodynamics. In both cases, the transfer of polarization leads to an entropy decrease in the system of interest; however, since the process occurs spontaneously under the appropriate conditions, the overall entropy must increase. In the Hartmann–Hahn case, this is achieved by a decrease of the population difference of the second spin species. In the case of optical pumping, the entropy is transferred into the radiation field: polarization of the spin system is only possible by scattering photons from the laser mode into different modes (different spatial modes as well as different polarization states), which were not populated before the interaction.

Apart from the entropy increase, thermodynamics also requires the conservation of energy. In the case of longitudinal pumping, the energy levels are nondegenerate, so the spin system also needs to exchange energy with the radiation field, thereby shifting the frequency of the scattered photons. The scattered light is therefore slightly red-shifted with respect to the pump wavelength. In the case of transverse pumping, the levels are degenerate, and the transfer of population between them is energy preserving. Frequency shifts of the scattered photons are still possible, but the upper and lower frequency sidebands have the same intensity, so there is no overall transfer of energy from the spin system to the radiation field.

E. Optical Detection

1. *Principle*

Magnetization in an atomic system can be detected in several ways. At this point we are not interested in detecting the radiation associated with the precessing magnetic dipole, but we do want to consider those methods where light incident on the system is modified by the presence of the Zeeman polarization. The methods that have been used for this purpose use either the light scattered by the sample or light transmitted through the sample. Observation of the polarization of scattered light (Kastler, 1967) primarily provides information on the excited state: the polarization is uniquely determined by the population of the excited state and the decay rates for the individual transitions to the ground state. However, since the polarization of the radiation that optically pumps the system is known, indirect information about the ground state is also available. Transmitted light, on the other hand, is modified by the polarization in the ground state as well as in the excited state, The order present in the system can change the absorption probability or the index of refraction of the medium.

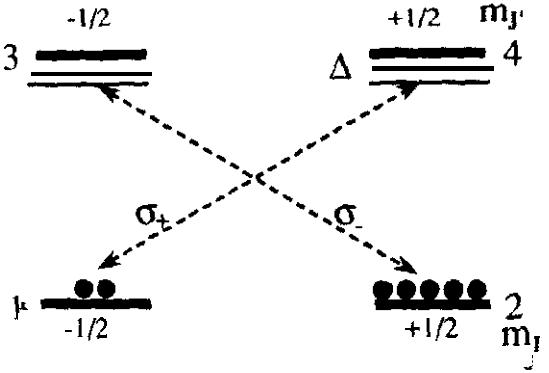

FIG. 10. Principle of the optical detection of magnetization

The observation of fluorescent light has the advantage that all the photons detected were scattered by the sample and therefore carry information on the resonance under investigation. It is therefore background-free in the sense that radiation that does not interact with the atoms is not detected and does not interfere with the measurement. However, the sensitivity of this methed is limited in other respects: only a small fraction of the photons scattered by the sample can actually be detected in this way. If the radiation transmitted through the sample is detected instead, it is possible in principle to detect all of the radiation that interacted with the sample simply by focussing the transmitted laser beam on a photodiode.

How transmitted light is affected by the polarization in the sample can be easily visualized by considering Fig. 10. If the population of the excited state is negligible, only the atoms in state $|1\rangle$ interact with σ_+ light, while the atoms in state $|2\rangle$ interact with σ_- light. If circularly polarized light is transmitted through the sample, the absorption probability, as well as the dispersion, is proportional to the number of atoms in the corresponding substate and is therefore determined by the polarization of the sample. While such measurements are possible and actually have been used (Dehmelt, 1957a), they have the disadvantage that fluctuations of the laser amplitude are transformed directly into noise in the recorded signal. This problem can be largely eliminated by performing difference measurements. Conceptually, one compares the absorption of right circularly polarized light with the absorption of left circularly polarized light, thereby directly measuring the population difference, i.e., the z component of the magnetization.

The usual implementation of this method uses linearly polarized light, which represents a superposition of two circularly polarized beams of equal intensity. The two components are separated behind the sample via a beam splitter, and the intensities of the partial beams are measured separately, then

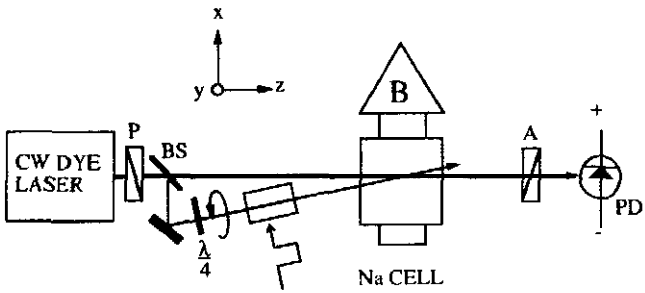

FIG. 11. Schematic representation of a simple experimental setup for the optical excitation and detection of magnetization.

the resulting signals are subtracted. Since the amplitude fluctuations of the two partial beams are correlated, they can be eliminated hy subtraction of the two photocurrents. The method is therefore, to first order, insensitive to fluctuations in the laser amplitude and has better sensitivity than fluorescence measurements, unless the absorption is only a small fraction of the transmitted light, In this case, shot noise from the large background amplitude can become the predominant noise source; if the two laser beams were derived from the same source, the shot noise is anticorrelated on the two detectors and therefore adds up if the photocurrents are subtracted.

A possible experimental setup for a purely optical magnetic resonance experiment is shown in Fig. 11. A circularly polarized pump beam excites the magnetization in the sample cell, which is placed in a magnetic field. A second, linearly polarized laser beam, which is derived from the same laser, is passed through the sample cell at a small angle with respect to the pump beam in order to achieve maximum overlap of the two beams. The second beam has an intensity that is much smaller than that of the pump beam and is used as a probe for the polarization state of the system. Since it is linearly polarized, it interacts with both transitions labelled σ_+ and σ_- in Fig. IO.

Since our interest lies in the rf transition, but we detect the optical transition, some kind of heterodyne detection scheme must be used when measurements are performed in the time domain. In an optical experiment, the nonlinear element that achieves the mixing between the signal and the local oscillator is the detector itself. If the signal and the local oscillator are both plane waves propagating in the same direction, the electric field amplitude A_d at the detector can be written as

$$A_d = A_{,,} + A \tag{50}$$

where A_0 represents the amplitude of the local oscillator and A is the signal amplitude. The detector yields a signal which is proportional to

$$A_d^2 = (A_{,,} + A)^* = A_0^2 + 2A_0A + A^2 \tag{51}$$

The optical frequencies are eliminated since the response time of the detector is much longer than an optical cycle. In most cases, the laser wed for detection also provides the local oscillator. If ω represents the signal frequency and ω_0 the frequency of the local oscillator, the interference term $A_0 A$ in Eq. (51) oscillates, therefore, at the difference frequency ω-ω_0. This detection scheme has several remarkable properties: the interference term can be considerably stronger than the signal term A*. This so-called heterodyne advantage can provide a sensitivity, which is considerably higher than if only the signal were detected (Levenson and Eesley, 1979). In addition. the subtraction of the laser frequency from the signal that was formed with the same laser beam eliminates laser frequency jitter as a possible line broadening mechanism. Although the detection uses optical radiation, the resolution is therefore not limited by the laser line width, but can actually be many orders of magnitudehigher.

2. *Propagation of Light in a Polarized Medium*

In a homogeneous medium, the propagation of light can be described with two parameters: the index of absorption α and the index of refraction n. Due to the optical pumping, the system considered here is anisotropic, and consequently the absorption coefficient and the index of refraction depend on the polarization of the light. In general, the polarization of light can be described as a point in a two-dimensional space with any two different states as basis states (Born and Wolf, 1980). The most frequently used basis states are either those of left and right circular polarization or those of linear polarization, e.g., along the x and y axis. Light with a given polarization entering such an anisotropic system is not only attenuated and delayed, but the polarization can also be changed; linearly polarized light, for example, can be converted into elliptically polarized light.

In the case of our $J = \frac{1}{2} \leftrightarrow J' = \frac{1}{2}$ model system, light entering the system with circular polarization remains circularly polarized; the circularly polarized states therefore represent polarization eigenstates. It is therefore advantageous to use them as basis states for the description of light propagating through the medium. We write $\alpha_+ (\alpha_-)$ for the absorption coefficient for right (or left) circularly polarized light, and n_+ (or n_-) for the index of refraction. As described previously, the index of absorption (orrefraction)is directly proportional to the population difference for that particular transition, We therefore have (Mitschke *et al.*, 1986)

$$\alpha_\pm = \alpha_0(1 \pm m_z) \tag{52}$$

$$n_\pm - 1 = (n_0 - 1)(1 \pm m_z) \tag{53}$$

where α_0 and n_0 represent the coefficients of the unpolarized medium,

We now have to calculate the complex amplitude of the probe laser beam as it passes through the test region. We write E+(O)($E_-(0)$) for the amplitude of the right (or left) circularly polarized light. After passing a distance I through the sample, the amplitude of the + component becomes

$$E_+ = E_+(0)\, e^{-\alpha_+ l/2}\, e^{-in_+ kl/2} \tag{54}$$

and for the − component accordingly, Phase and amplitude of the light behind the sample therefore contain information about the polarization of the sample, which can be extracted by an appropriate analysis of the transmitted light. With an appropriate experimental setup, it is possible to extract this information either from the absorption or the dispersion, i.e., either from the amplitude or the phase of the transmitted light.

3. *Absorptive Detection*

If the transmitted laser beam passes through the setup shown in Fig. 12, the retardation plate together with the beam splitter separate the light into two components whose intensity is equal to the intensity of the circularly polarized components, The intensity of each beam is proportional to the input intensity multiplied by the attenuation for the corresponding circular polarization by the sample. On the photodiodes, this intensity is converted into a photocurrent so that after subtracting the two photocurrents, the resulting signal is proportional to the difference of the two intensities.

From Eq. (54), we calculate the intensity difference ΔI between left and right circularly polarized light after the sample as

$$\Delta I = \frac{E_0 2}{c\varepsilon_0} e^{-\alpha_0 l} \sinh(m_z \alpha_0 l) \tag{55}$$

For small signals, i.e., $m_z \alpha_0 l \ll 1$, it it useful to expand this expression in a power series with respect to m_z. Since all even order terms vanish, the linear

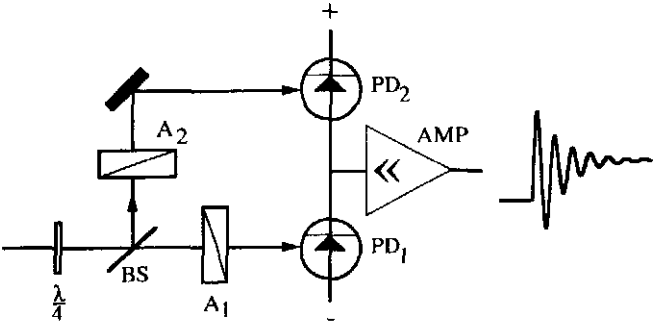

FIG. 12. Optical beam path for polarization selective absorption measurement. The retardation plate is rotated 45° with respect to the beam splitter.

term

$$\Delta I_1 = m_z\left(-\frac{E_0^2}{c\varepsilon_0}e^{-\alpha_0 l}\alpha_0 l\right) \tag{56}$$

is Often a good approximation for the exact signal. Apparently, this detection scheme allows a direct measurement of the polarization component m_z via the change in the differential absorption profile. It is background-free, and the resulting signal is directly proportional to the magnetization component m_z, weighted with the absorption coefficient α_0 multiplied by the interaction length l of the sample and attenuated by the absorption of the isotropic sample $e^{-\alpha_0 l}$.

4. Dispersive *Detection*

Instead of measuring the difference in absorption, it is also possible to measure the difference in dispersion between right and left circularly polarized light. The experimental setup remains almost the same as the One shown in Fig. 12, except that the retardation plate labelled $\lambda/4$ is removed. The difference of the two photocurrents becomes then

$$\Delta I = \frac{E_0^2}{2c\varepsilon_0}e^{-\alpha_0 l}\sinh(2m_z\delta_0) \tag{57}$$

where $\delta_0 = (n_0 - 1)l$. We can again make a linear expansion

$$\Delta I_1 = m_z\delta_0\frac{E_0^2}{c\varepsilon_0}e^{-\alpha_0 l} \tag{58}$$

The signal is now proportional to the dispersion δ_0 of the unpolarized medium,

Both detection schemes therefore have similar properties, except for the dependence on the optical detuning. The dispersive scheme is advantageous if measurements are to he performed far from resonance, since its sensitivity drops off more slowly as a function of optical detuning, while the absorptive scheme allow measurements near the center of the optical resonance line. Both detection schemes discussed here refer to spin-$\frac{1}{2}$ systems where the observable of interest is always a component Of the magnetization. In more complicated spin systems, other detection geometries can be used in order to detect different observables such as alignment (Mishina *et al.*, 1988).

IV. Phenomenological Overview

Of the many different experiments performed in the area of optically detected magnetic resonance, we are interested primarily in time-resolved experiments, where transient phenomena are investigated. The systems un-

der investigation are either atomic gases or solids. The simplest systems for the study of coherent spin transients are clearly atomic vapors where the coherences can be excited either between different Zeeman substates or between hyperfine substates. Most experiments have been performed on alkali or rare earth atoms (Mlynek and Lange, 1979; Mlynek et *al.*, 1981b; Fukuda *et al.*, 1981; Lehmitz *et al.*, 1986; Buhr and Mlynek, 1986).

Another group of experiments was performed on ionic solids, where transition metal ions exhibit a strong coupling between electronic (optical) transitions and nuclear spin substates. In these systems, it is therefore possible to excite nuclear spin transitions, often in combination with rf irradiation. (Mlynek *et al.*, 1983; Mitsunaga *et al.*, 1984, 1985; Shelby *et al.*, 1983; Szabo, 1986; Erickson, 1990). However, electron spin transitions have also been observed (Holliday *et al.*, 1990; Kohmoto *et al.*, 1983).

In this section, we give an overview of these experiments. Our main goal is to show how these signals arise and by which parameters the experimenter can control the dynamics of these systems. For the sake of clarity, we present only our own experimental data from Na vapor. In addition, we summarize other authors' experiments and refer to the literature for the details.

A. Experimental Arrangement

Atomic vapors of alkali, such as Na, or of rare earths with a single valence electron, such as Yb, provide systems that are simple enough to study in detail experimentally as well as theoretically, A typical experimental setup for the study of alkali vapors is shown in Fig 13. As a specific example, we discuss Na vapor. The metal is placed in a ceramic tube, which can be evacuated and filled with a buffer gas. The tube is heated until the vapor pressure of the metal is high enough that some 20% of a probe laser beam passing through the sample cell is absorbed. The purpose of the buffer gas is to broaden the

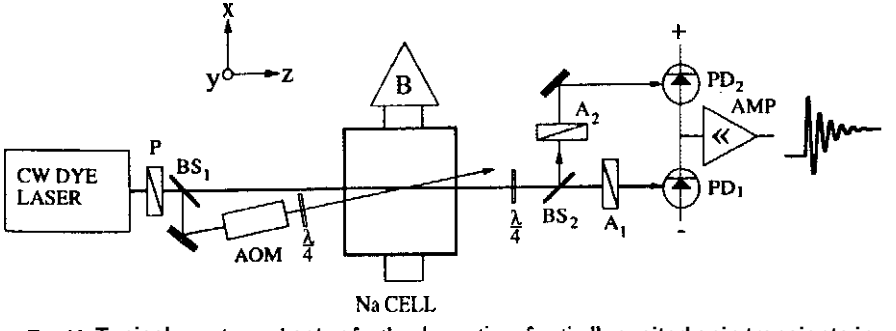

FIG. 13. Typical experimental setup for the observation of optically excited spin transients in an atomic vapor; BS = beam splitter, AOM = accoustooptic modulator, PD = photodiode, AMP = amplifier.

homogeneous optical line width by causing collisions between Na atoms and the buffer gas, thereby eliminating the inhomogeneous Doppler broadening If the pressure broadening exceeds the hyperfine interaction, the optical resonance line can be considered homogeneous. For many purposes, it is then possible to disregard the hyperfine interaction altogether and approximate the system by a $J = \frac{1}{2} \leftrightarrow J' = \frac{1}{2}$ system. It is then possible to compare the measurements directly with a simple theory. In addition. the motion of the Na atoms in the vapor cell becomes diffusive, and the average time that the atoms spend in the laser beam is increased by two orders of magnitude to about 100 μsec.

The laser beam, which is derived from a cw ring dye laser is split into two parts: a circularly polarized pump beam and a linearly polarized probe beam The pump beam is chopped by an accoustooptic modulator, which can provide pulses with rise times in the order of 100 ns. The two beams are Passed through the sample at a small angle of ~0.5' and overlap in the probe region. This allows one to separate the two beams behind the detector and block the pump beam, while the probe beam is split into the two circularly polarized components whose intensities are measured with fast photodiodes. As described in the previous section, the difference of the two photocurrents is then directly proportional to the z component of the magnetization. The external magnetic field is produced by Helmholtz coils in three orthogonal directions. The currents in the coils are adjusted to generate a field perpendicular to the direction of the laser beam; the experiment thus represents an example of transverse pumping

In a specific example, the experiments were performed on the D_1 line of atomic Na ($\lambda = 589.6$ nm) (Suter *et al.*, 1990; Rosatzin *et al.*, 1990a,b). Argon (210 mbar) was added as a buffer gas, which lead to a pressure broadening of $\Gamma_2 = 2.1$ GHz of the optical transition. The total power in the pump beam was ≤ 100 mW, and the beam diameter was of the order of 1 mm^2, so the intensity was of the order of 10^5 Wm^{-2}, well below the saturation intensity. The optical coherences and the population of the excited state are therefore negligible and the observed dynamics are due only to the ground state, The total power of the probe beam was $\sim 10\,\mu$W, low enough that the dynamics of the system were not affected. The magnetic field was of the order of some tens of μT; the Landé factor of the ground state of Na is $|g_F| = 0.5$, so that the Larmor frequency is 7 MHz/mT.

Figure 14 shows a typical response of the system to an optical pulse. The system is initially in thermal equilibrium so that the signal vanishes. When the laser is turned on, it creates magnetization in the sample, which starts to precess around the effective field. This nutation appears as an oscillation of the signal, which is damped by the optical pumping. On a timescale of a few tens of microseconds, the magnetization of the sample reaches a stationary

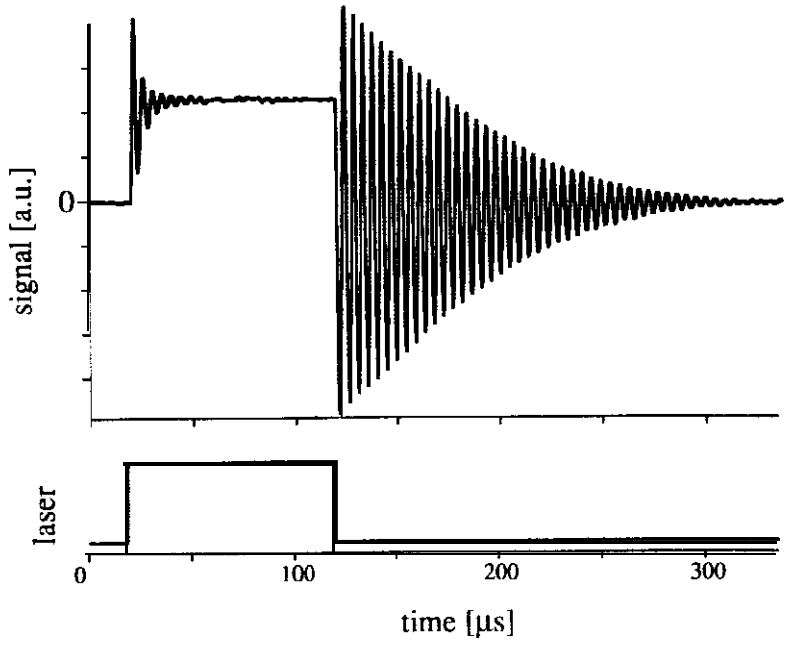

FIG. 14. Typical signal from Na when a pulse of circularly polarized light is applied to the system. Experimental parameters: pump laser power = 15 mW, laser detuning $\Delta/2\pi = -0.5$ GHz.

state. Since this stationary magnetization is not parallel to the direction of the magnetic field, it starts to precess after the end of the laser pulse; this precession appears as a free induction decay in the signal.

B. SPIN NUTATION

With the experimental arrangement described previously, the observable signal is proportional to the magnetization component parallel to the direction of the laser beam m_z. From the solution of the equation of motion derived in the theoretical section we find that immediately after the optical pulse is turned on, the time dependence of this component can be written as

$$m_z(t) = [A_1 \cos(\Omega t - \phi) + A_2]\, e^{-\gamma_{\text{eff}} t} + m_{z\infty} \tag{59}$$

where the amplitudes of the oscillatory and the background component are

$$A_1 = \frac{-P_+ \Omega_L^2}{\Omega^2 \sqrt{\Omega^2 + \gamma_{\text{eff}}^2}} \tag{60}$$

$$A_2 = -\frac{\bar{\Delta}^2 P_+^3}{\gamma_{\text{eff}} \Omega^2} \tag{61}$$

The phase of the oscillatory signal is

$$tg\phi = -\frac{\Omega}{\gamma_{eff}} \tag{62}$$

and the stationary magnetization becomes

$$m_{z\infty} = \frac{P_+}{\gamma_{eff}}\left(1 - \frac{\Omega_L^2}{\Omega_L^2 + \bar{\Delta}^2 P_+^2 + \gamma_{eff}^2}\right) \tag{63}$$

We can thus distinguish three terms via their Characteristic time dependence: the first term, originating from the magnetization orthogonal to the effective field, oscillates at the frequency Ω and is simultaneously attenuated at a rate γ_{eff}. The second term, corresponding to the magnetization component parallel to the effective field, does not oscillate, but decays at the same rate as the oscillating part. The third, time-independent term represents the stationary ground-state magnetization. The evolution of the component m_z as a function of time is shown graphically in Fig, 15(a). The relevant parameters used for the calculation are $\bar{\Delta} = 2$, $P_+ = 2.10^5\,\mathrm{sec}^{-1}$, $\Omega_L/2\pi = 318$ kHz, and $\gamma = 3.3 \cdot 10^4\,\mathrm{sec}^{-1}$. The solid line represents the magnetization component $m_z(t)$ as a function of time; the second term of Eq. (59), i.e., the contribution from the exponentially decaying longitudinal magnetization, is depicted separately by the dashed curve. The precession of the transverse magnetization is seen as an oscillation superimposed onto the exponential background, The final value is determined by the stationary term $m_{z\infty}$.

Figure 15(b) shows the Fourier transform of the baseline-corrected time domain signal displayed in Fig.15(a). In this representation, the longitudinal and transverse (with respect to the effective field) components of the magnetization appear as separate resonances at $\omega = 0$ and $\omega = \pm\Omega$, respectively. The longitudinal component appears as an absorption signal, while the transverse component has a mixed phase which is given by Eq. (62).

The stationary value of the ground state magnetization, $m_{z\infty}$, is determined by two Competing effects which are represented by two different terms in Eq. (63): the first term, P_+/γ_{eff}, is the ground state orientation as it would result from optical pumping in the absence of a magnetic field. The second term is the modification due to the precession around the tilted effective field. The presence of the magnetic field thus always leads to a decrease of the ground state orientation. In the limit of strong magnetic fields, $\Omega_L^2 \gg \bar{\Delta}^2 P_+^2, \gamma_{eff}^2$, the stationary value of the z magnetization vanishes. This can be understood as an off-resonance effect: the optical pumping as well as the light shift appear as dc effects in the ground-state dynamics and are therefore shifted away from the resonance by the Larmor frequency. At high Larmor frequencies, the excitation scheme described here can therefore provide only relatively small polarization of the system.

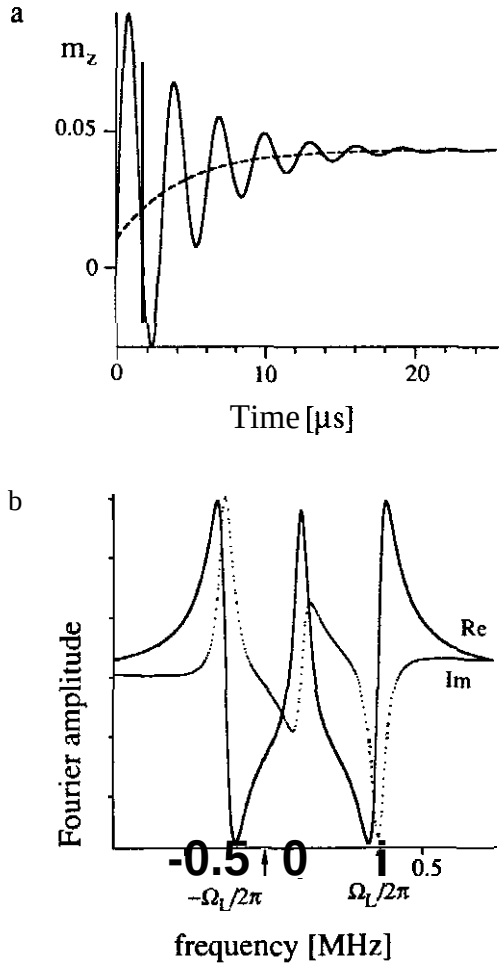

FIG. 15. (a), Nutation signal as a function of time; (b), Fourier transform of (a).

Equations (60)–(63) predict that amplitude, phase, and damping rate of the nutation signal should depend on the laser intensity. Some typical experimental results for the dynamic response of the sample at different pump powers are shown in Fig. 16. Since the beam diameter was 1.1 mm, the laser powers given in the figure in milliwatts correspond approximately to average. intensities measured in kilowatts per square meter. The corresponding Rabi frequencies are $< 10^8$ Hz, well below the optical saturation intensity. The signals were recorded with the laser frequency *tuned 1.5 GHz* below resonance, i.e., at $\bar{\Delta} = -0.7$. When the laser field is switched on, the sublevel

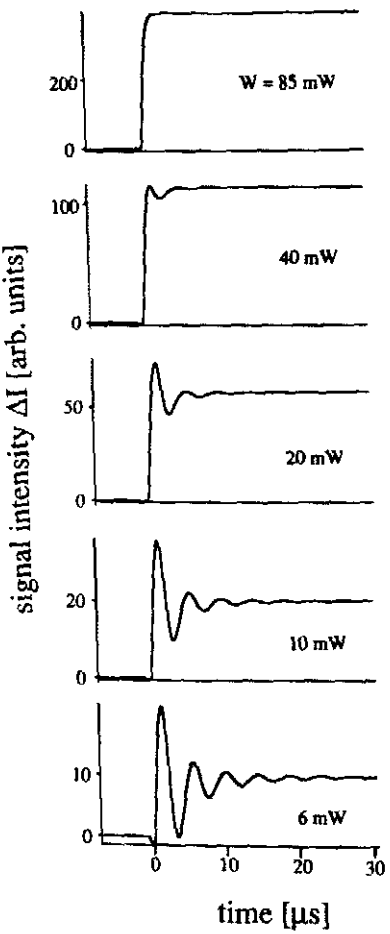

FIG. 16. Nutation signal as a function of laser power. The data were recorded at a resonance detuning of $\Delta/2\pi = -1.5$ GHz.

polarization starts to build up and at the same time precesses around the effective field. At low laser intensities, the resulting polarization is small, while higher laser intensities not only lead to a higher equilibrium polarization, but also to a faster damping of the transient nutations. At the same time, the increase in laser intensity should also lead to an increase in the precession frequency. Since this effect is relatively small with the experimental parameters chosen and is obscured by the associated damping, the increase in the precession frequency is not readily seen in these figures. All the measurements presented here were performed with Gaussian laser beams, so that the laser intensity was not homogeneous over the sample. As a result, the damping of

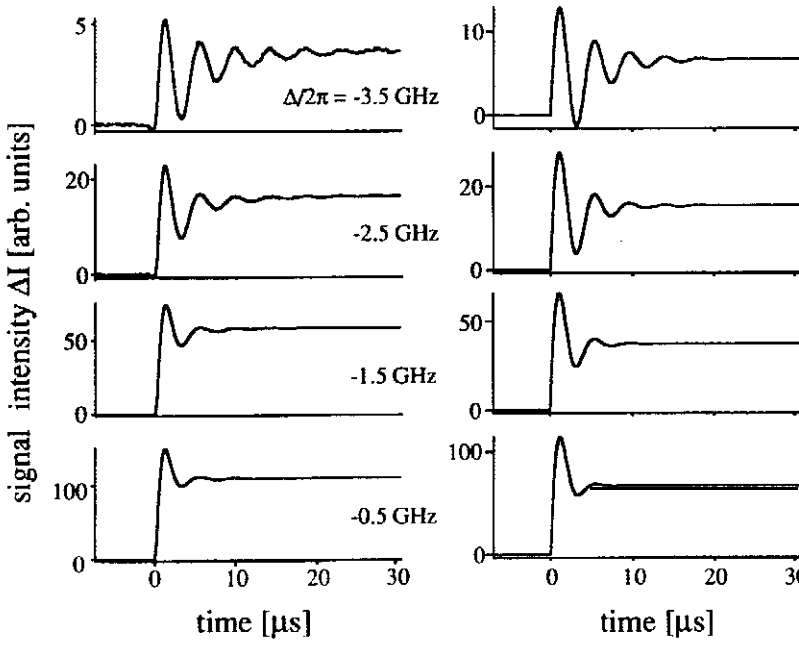

FIG. 17. Nutation signal as a function of optical detuning. The left column shows the experimental data which were recorded with a pump beam power of 20 mW. The right column represents theoretical calculations.

the oscillations by the optical pumping leads to a nonexponential decay of the signal, with the signal components from the center of the pump beam decaying faster than the signal contributions from the regions with lower intensities.

The dependence of the nutation signal on the optical detuning is shown in Fig. 17. The left column shows the experimental data, and the right column was calculated with Eqs. (59)–(63). The experimental signals were recorded with 20 mW pump power, and the same parameter values were used for the theoretical curves. Apart from the overall amplitude for all four spectra, no adjustable parameters have been used for this calculation. The agreement between the theoretical prediction and the experimental results is quite good, which is very satisfying in view of our rather simple model. From our theory, we expect that the observed signals should not depend on the sign of the optical detuning. Experimentally we observe a small asymmetry of the signal amplitude, which we tentatively assign to the unresolved hyperfine structure of the optical transition or to a misalignment of the laser beam with respect to the magnetic field.

In the theoretical as well as in the experimental data, we find that as the detuning is increased, the pump rate is reduced, and the signal intensity and

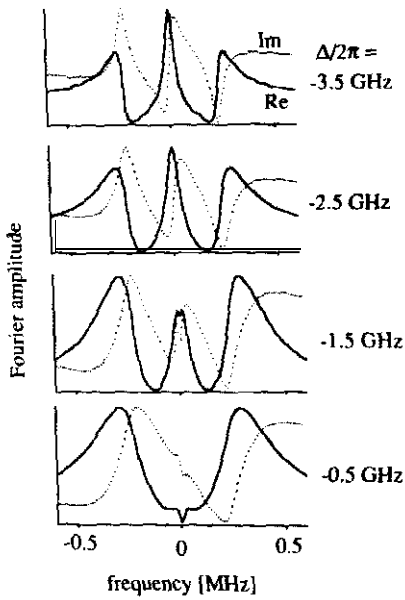

FIG. 18. Fourier transforms of the data shown in Fig. 17. (For details see Suter.)

the magnetization decay rate are decreased. In addition to the amplitude, the phase of the nutation signal also depends on laser intensity and laser detuning. These variations are not so easily observed in the time domain signals, but are readily seen in the corresponding Fourier transforms. Figure 18 shows an example of spectra, which are the Fourier transforms of the data shown in Fig. 17.

The theoretical model and the measurements give some guidelines for the experimentalist who wants to polarize the ground state by optical pumping to the largest extent possible. In the limit of low laser power, i.e., if the optical pump rate P_+ falls below the Larmor frequency Ω_L, the evolving magnetization show pronounced oscillations as a function of time (see Fig. 15). Since the amplitude of these oscillations is larger than the stationary value of the magnetization by a factor of or&r Ω_L/P_+, it is advantageous to sample the magnetization not in the steady state, but at the peak of the oscillation, which is reached after a time $\pi/(2\Omega_L)$. In the case of strong irradiation, on the other hand, the oscillatory component is small; the magnetization quickly reaches an equilibrium value and remains constant thereafter.

These observations can be related to rf experiments, where it is well known that if one suddenly applies an rf field to nuclear spins, it is possible to observe oscillations at the generalized Rabi frequency, including the resonance detuning from the sublevel splitting frequency (Abragam, 1961). I,, the optical case, the effective field is the combination of a magnetic field and a pseudo

magnetic field due to the light shift effect. The main differences are that in the rf case, the magnetization precesses around the effective field but stays constant in length (apart from relaxation effects). In the optical case, the magnetization is created during the irradiation and the stationary value is nonzero.

C. Free Induction Decay

The optical pulse generates a polarization that does not commute with the Hamiltonian of the free atom. If the laser field is turned off nonadiabatically, the polarization starts to precess around the magnetic field, which is oriented along the x axis. In the experiment described previously, the z component of the magnetization is observed; the part of the magnetization that contributes to the observed signal is therefore the projection into the yz plane $\mathbf{m}_{yz}$. After the end of the optical pulse, this component evolves as

$$\mathbf{m}_{yz}(t) = A[-\sin(\Omega_L t + \phi), \cos(\Omega_L t + \phi)]e^{-\gamma_0 t} \tag{64a}$$

$$A = \sqrt{m_y(0)^2 + m_z(0)^2} = \frac{P_+}{\gamma_{eff}} \frac{\sqrt{\gamma_{eff}^2 \Omega_L^2 + (\bar{\Delta}^2 P_+^2 + \gamma_{eff}^2)^2}}{\Omega_L^2 + \bar{\Delta}^2 P_+^2 + \gamma_{eff}^2} \tag{64b}$$

$$tg\phi = \frac{m_y(0)}{m_z(0)} = \frac{\gamma_{eff}\Omega_L}{\bar{\Delta}^2 P_+^2 + \gamma_{eff}^2} \tag{65}$$

As shown in Fig. 19, A and ϕ represent the polar coordinates of the magnetization vector in the yz plane (left side of Fig. 19); in the FID signal (right side of Fig. 19), they appear as amplitude and phase.

The dependence of amplitude and phase of the FID signal on laser intensity and laser detuning can be seen more easily in the limit where the optical pumping rate is large compared to the relaxation due to diffusion, $P+ \gg \gamma_0$. This condition is usually fulfilled as long as the irradiation frequency is near resonance. We have then

$$A = \frac{p\sqrt{1 + p^2}}{1 + p^2 + \bar{\Delta}^2} \tag{66}$$

$$tg\phi = \frac{1}{p} \tag{67}$$

where the dimensionless parameter

$$p = \frac{\omega_1^2}{4\Gamma_2 \Omega_L} \tag{68}$$

is the ratio of the on-resonance optical pumping rate to the Larmor frequency. In the limit considered here, the phase of the FID signal depends only on p, while the amplitude depends also on the normalized optical detuning.

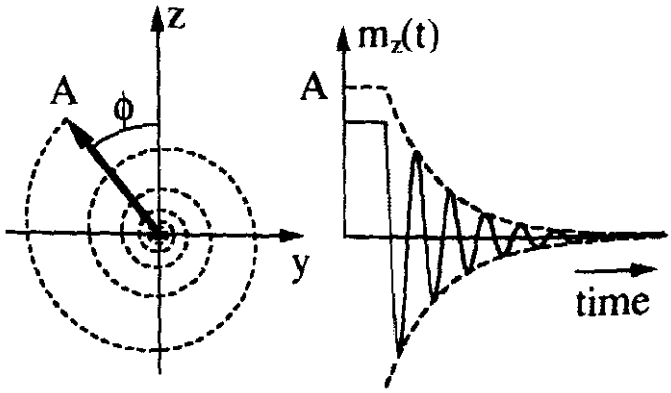

FIG. 19. Projection of the magnetization into the yz plane (left) and corresponding detector signal (right). The length A of the magnetization vector determines the envelope of the FID signal (dashed line), while the polar angle ϕ determines the phase.

Figure 20 shows two examples of experimental signals at different laser intensities, together with the time-dependent amplitude of the optical pump beam (Rosatzin *et al.*, 1990a). The variation of the signal amplitude with the laser intensity is evident from the different scale of the two signals. Also evident is the strong variation of the phase with the laser intensity. The insets show qualitatively the orientation of the magnetization in the yz plane at the end

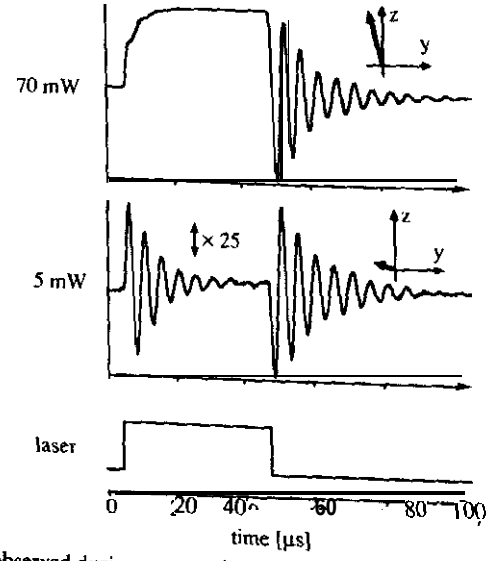

FIG. 20. Signal observed during a one-pulse experiment at two different laser intensities. The insets indicate the orientation and size of the equilibrium magnetization during the pulse.

of the optical pulse. At high laser intensity, the stationary magnetization is large and almost parallel to the laser beam. Accordingly, the measured signal evolves as $\cos(\Omega_L t)$, starting near its maximum; at low intensity the magnetization is oriented almost parallel to the y axis, and its amplitude is much smaller. The signal is correspondingly smaller and starts as $\sin(\Omega_L t)$, with oscillations that are much larger than the stationary signal during the pulse.

Systematic measurements of the variation of amplitude and phase as a function of the laser intensity are summarized in Fig. 21 together with the theoretical prediction. The three sets of data were taken at different magnetic

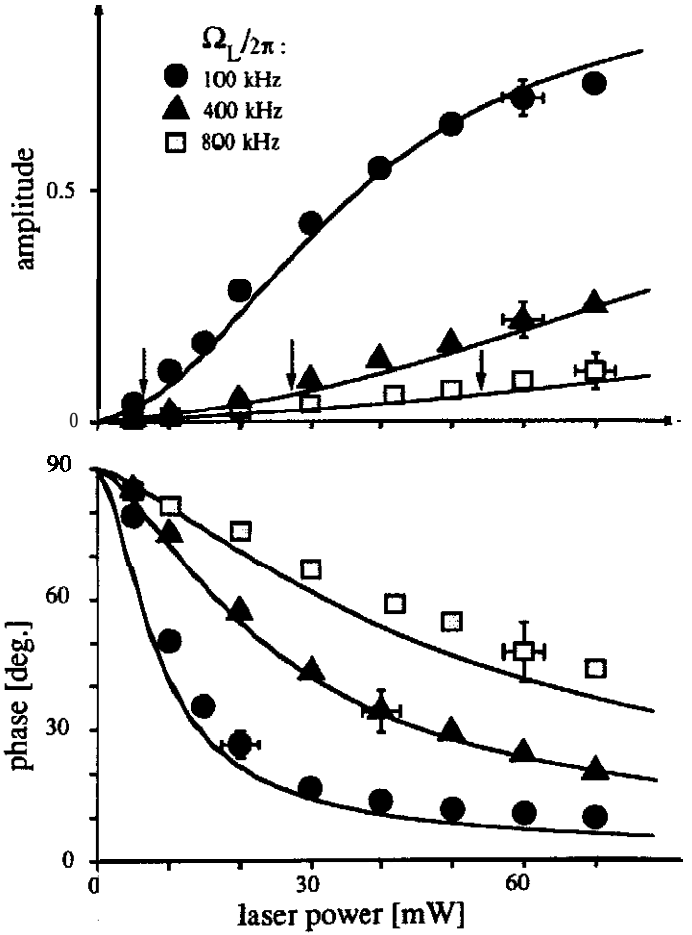

FIG. 21. Amplitude and phase of FID signal as a function of laser power for three magnetic field strengths.

field strengths. For high enough laser power, when the optical Pump rate P_s exceeds the Larmor frequency Ω_L, the equilibrium magnetization is oriented almost parallel to the z axis ($\phi \sim 0$), and the amplitude can reach values near unity. If the laser intensity is decreased, the amplitude of the ground-state polarization decreases and the projection of the magnetization vector into the yz plane tilts towards the y axis. For the observed signal, this corresponds to an increase of the phase towards 90°. The resonance detuning of the laser was set to $\Delta/2\pi = 9.5$ GHz in all measurements.

Amplitude and phase of the FID signal depend not only on the laser intensity, but also on tbe resonance offset of the laser and the strength of the magnetic field. From the simplified Eq. (66)–(68), it is evident that the dependence of the FID phase on the optical detuning should be very small, while the amplitude has a Lorentzian dependence. It reaches a maximum of $p/(1+p^2)^{1/2}$ on resonance and falls off to half this value at $\bar{\Delta} = \pm(1+p^2)^{1/2}$. This behavior is qualitatively analogous to the situation in magnetic resonance (Ernst *et al.*, 1987). In the case of rf spectroscopy, the reason for the variation is basically a change of the direction of the effective field $\boldsymbol{\Omega}$; one component of this field is the resonance detuning of the rf field, the other is the rf field strength. In the optical case discussed here the effective field also depends on the optical detuning, but amplitude and phase are determined not only by the effective field, hut also by the optical pumping, which is oriented along the z axis, independent of the optical frequency,

Experimental results of the dependence of the FID signal on the optical detuning are summarized in Fig, 22. These data were recorded with a dispersive detection scheme. According to Eq. (58), the measured signal is then proportional to the magnetization component m_z and the detection sensitivity, which in this case is proportional to $\bar{\Delta}/(1+\bar{\Delta}^2)$. This dependence of the expected signal on the laser detuning has been taken into account for the calculation of the theoretical curve in Fig. 22. As a consequence, the measured signal vanishes on resonance where the magnetization is largest.

A special case arises in zero magnetic field where the Hamiltonian commutes with the magnetization, which is created by the optical pumping, so that no precession occurs and the magnetization remains along the laser beam. The phase of the FID is therefore always zero under these conditions, independent of the laser intensity.

By measuring the frequency of the free precession the method described here can be used, for example, to measure zero-field splittings such as hyperfine splittings in ground states as well as electronically excited states, One example is the measurement of the hyperfine splittings in the ionic solid Pr^{3+}: yttrium aluminum garnet (YAG) at low temperature (Shelby *et al.*, 1983). Here the FID signal contained several frequency components which could be extracted from the time-resolved data by subsequent Fourier transformation of the signals.

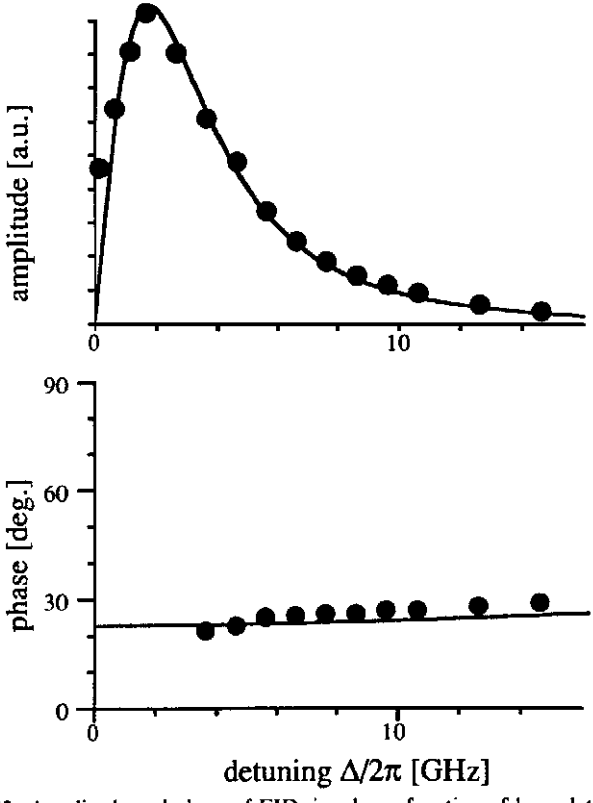

FIG. 22. Amplitude and phase of FID signal as a function of laser detuning.

As discussed previously, it is also possible to measure higher **multipole** moments like alignment instead of the magnetization, if different detection geometries are wed. It is therefore possible to use the technique to determine the relaxation rates of these **multipole** moments in ground **or** near-ground atomic levels. One example is the study of the depolarization of the $4f^6 6s^2\ ^7F_1$ near-ground level of samarium by collisions with rare-gas **perturbers** (Lowe *et al.*, 1987; McLean *et al.*, 1990). With an appropriate choice of polarization and geometry, **Zeeman** beat signals were obtained whose decay directly yields the relaxation rates of orientation and alignment. A striking result from those measurements was that **a** substantial **anisotropy** in the **collisional** relaxation in the $^7F_1$ level of **Sm** could be observed.

It is-also instructive to discuss the method in a different representation. **In** a reference frame with the **quantization** axis parallel to the direction of the static magnetic field, the ground-state orientation m_z (i.e., **along** the laser beam) appears as coherence between the ground-state sublevels that are induced by a

resonant two-photon transition of the Raman-type (see Fig. 1). In this picture, the relationship of the experiments to the well-known coherent Raman beats becomes obvious. In the latter case, the oscillations are observed in coherently prepared molecular samples when the level degeneracy is suddenly removed by Stark-pulse switching (Brewer and Shoemaker, 1971, 1972; Shoemaker and Brewer, 1972; Brewer, 1977b). The laser and the Raman light then propagate together and produce a coherent beat at a detector that corresponds to the level shift induced by the Stark-pulse switching. Coherent Raman beats have been observed, for example, in molecular systems such as $^{13}CH_3F$ (Shoemaker and Brewer, 1972) or $^{15}NH_3$ (Van Stryland and Shoemaker, 1979) and in ruby at liquid He temperature (Endo *et al.*, 1982). In the latter case, the Raman beats were associated with the superhyperfine structure due to the Cr–Al interaction in ruby.

In the method discussed so far, the time resolution of the experiment is determined by the speed of the accoustooptic modulator that generates the pulses and the optoelectronic detection system. If necessary, considerably higher time resolution can be obtained by using a pulsed laser system. The time-resolution that can be obtained is then determined only by the length of the optical pulses, which can be made as short as a few femtoseconds. Experimentally, the pulsed laser beam issplit into pump and probe beams. The probe beam is passed through an optical delay line and sent through the system to record the signal in a stroboscopic manner (Lange and Mlynek, 1978). By varying the delay time via the optical path length, one can then sample the evolution of the sublevel coherence (Harde *et al.*, 1981).

With the use of nanosecondpulses, this technique has been applied, for example, to measure electron spin resonance (ESR) free-induction decay signals in a magnetic field in the ground state of $Tm^{2+}:SrF_2$ (Kohmoto *et al.*, 1983). In this experiment, the Fourier transform of the observed signals gave the ESR spectrum, and the origin of the decay was attributed to the superhyperfine interaction between the Tm^{2+} ion and the neighboring fluorine nuclei. In the picosecond regime, this pump-probe scheme has been demonstrated using mode-locked dye lasers to study the hyperfine structure in the D-lines of Na (Harde et *al.*, 1981) and Cs (Lehmitz and Harde, 1986). With subpicosecond pulses, even fine structure beats in Na at 517 GHz could be clearly resolved (Burggraf *et al.*, 1986). This latter experiment is also an example of measuring sublevel coherence in an optically excited state, which can be studied with such a pump-probe scheme even if the lifetime of the excited state is very short.

Due to the widespread use of subpicosecond lasers, there is increasing interest in the possibility of Performing beat spectroscopy using pump-probe schemes as described here. Some studies, for example, of organic dyes using a transmission correlation technique (Rosker *et al.*, 1986; Walmsley et *al.*, 1988)

have revealed oscillatory behavior on a femtosecond time scale in the decay of photoexcited dye molecules. It was suggested that this behavior might be due to a teat phenomenon between coherently excited vibrational levels that are separated by several terahertz.

These examples make it clear that the technique described in this section is closely related to the well-known quantum-beat spectroscopy (Haroche, 1976; Dodd and Series, 1978). In a typical quantum beat experiment, a coherent superposition of atomic substates of an optically excited state is prepared by a light pulse. This superposition state is then allowed to precess freely, and the interference between the two probability amplitudes is observed as a time-dependent oscillation in the fluorescence signal. In contrast, our transmission technique relies on time-dependent changes of the absorption or dispersion of the sample induced by the pump pulse. Instead of using the term quantum beats, we prefer to call the observed transients "free induction decay" signals, in analogy to magnetic resonance experiments using rf fields.

D. Spin Echoes

An important prerequisite for many spectroscopic experiments is the ability to rearrange the order present in the system by converting populations into coherences, coherences from one transition into another and coherences into populations. As discussed in the theoretical section, this can be achieved in Purely optical experiments either by applying strong pulses of polarized light to the optical transitions or, in the low-power regime, by wing off-resonance Optical radiation to apply virtual magnetic fields to the spin system. In the following section we discuss one possible application of this method, the refocussing of spin coherence in an inhomogeneous magnetic field.

The virtual field induced *by* the laser pulse is oriented in the direction of the laser beam and acts like a pulsed magnetic field (Burschka and Mlynek, 1988; Rosatzin *et al.*, 1990b). In the arrangement discussed here, the direction of the laser beam is orthogonal to the direction of the magnetic field; the vector sum of the static magnetic field and the pseudo-field induced by the light shift add up to an effective field whose direction can be adjusted by variations Of the laser intensity and laser detuning. It is therefore possible to create effective fields in any direction in the upper half of the xz plane.

Figure 23 shows the experiment to be discussed; the atomic system is first prepared with a pulse of polarized light. After the end of the pulse, the spins dephase in an inhomogeneous magnetic field. A second, off-resonant laser pulse then creates an effective field that is not parallel to the static magnetic field and therefore leads to a partial inversion of the phases of the individual spin packets. In the subsequent second free evolution period, the newly acquired phase adds to the inverted phase and eventually cancels it. This

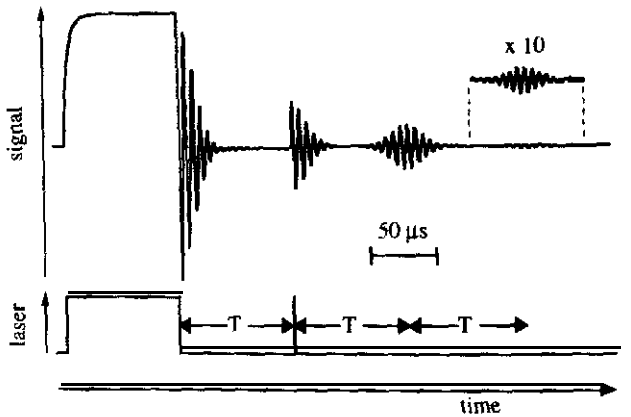

FIG. 23. Two-pulse experiment for the generation of spin echoes in an inhomogeneous magnetic field by an off-resonant optical pulse. The lower trace represents the amplitude of the pump beam, while the upper trace shows the evolving magnetization.

cancellation of the phases is independent of the strength of the magnetic field and is observed as a spin echo.

In order to calculate the evolution of the system during a two-pulse experiment, we assume that the spin system is prepared in a state of homogeneous polarization. Only the component perpendicular to the magnetic field is of interest in this context and the FID signal is described by Eq. (64a). The second pulse is applied at a time T after the end of the first pulse; immediately before this pulse, the spin system can be described by the density operator

$$\rho(T-) = e^{-\gamma 0 T}[I_z \cos(\Omega_L T + \phi) - I_y \sin(\Omega_L T + \phi)] \tag{69}$$

The second pulse of length τ rotates the magnetization around the effective field, and simultaneously drives it towards the equilibrium position

$$\rho(T+) = \rho_{eq} + e^{-\gamma_{eff}\tau} U_P[\rho(T-) - \rho_{eq}] U_P^{-1} \tag{70}$$

where

$$U_P = \exp[-i\tau(\Omega_L I_x + \bar{\Delta} P_+ I_z)] \tag{71}$$

represents the rotation induced by the effective field. The calculation of the echo amplitude can be simplified considerably if we neglect the effect of the inhomogeneous part of the magnetic field during the pulse. This is justified in most experimental situations, where the inhomogeneity of the magnetic field is small compared to the inverse of the pulse duration. A full refocussing is obtained if it is possible to Phase-invert the density operator, i.e., generate a density operator ρ_{inv} that is equal to the operator which is obtained by the

substitution $\Omega_L > -\Omega_L$ in $\rho(T-)$:

$$\rho_{inv} = e^{-\gamma_0 T}[I_z \cos(\Omega_L T + \phi) + I_y \sin(\Omega_L T + \phi)] \tag{72}$$

In general, it is only possible to approximate this process. We can measure the efficiency *E of* the echo pulse by calculating the projection of the resulting density operator onto this phase inverted part ρ_{inv}; it depends on the optical pump rate and the resonance offset as

$$E = \left(\frac{\bar{\Delta} P_+}{\Omega}\right)^2 \sin^2(\Omega\tau/2)\, e^{-\gamma_{eff}\tau} \tag{73}$$

The prefactor $(\bar{\Delta} P_+/\Omega_e)^2$ is the square of the sine of the angle between the direction of the effective field and the static magnetic field. It is a measure of the tilt of the effective field versus the static magnetic field. The second factor describes the rotation of the magnetization vector and the exponential term, the damping effect of the pulse. Unit efficiency, i.e., a perfect echo pulse is obtained for $\bar{\Delta} P_+ \gg (\Omega_L, \gamma_{eff})$, and $\Omega\tau = (2n+1)\pi$ with n integer. These conditions cannot be satisfied simultaneously, since a large optical pump rate required for $\bar{\Delta} P_+ \gg \Omega_L$ also implies a significant damping rate γ_{eff}. However, the different detuning dependence of the light shift term and the damping rate (Δ^{-1} vs. Δ^{-2}) makes it possible to reach unit efficiency asymptotically by using strong off-resonant radiation,

The calculated and measured refocussing efficiency as a function of the length of the second pulse is shown in Fig. 24. The upper part shows the theoretical time-dependence as given by Eq. (73). The lower trace shows the experimental data and a theoretical fit, which takes the inhomogeneous laser field into account (Rosatzin et *al.*, 1990b). The inhomogeneity of the laser field acts essentially like an inhomogeneous rf field and leads to a superposition of various traces with different periods; as a result, the echo amplitude never vanishes for pulse lengths > 0.

Equation (73) predicts a refocussing efficiency, which is determined by two effects; the rotation of the magnetization around the effective field and the damping due to the optical pumping. An important parameter for an efficient echo formation is the resonance detuning of the laser, which affects both terms in different ways. The precession angle can easily be maximized by adjusting the pulse length τ such that the flip angle of the pulse becomes an odd multiple of π, $\Omega\tau = (2n+1)\pi$. As seen in Fig. 24, a n-pulse ($n = 0$) provides the highest efficiency, since the damping effect associated with the laser pulse leads to *an* exponential loss of coherence.

In addition to the flip angle, the direction of the effective field, which determines the amplitude of the oscillation $(\bar{\Delta} P_+/\Omega)^2$, must be optimized. The upper half of Fig. 25 displays the dependence of this factor on the optical

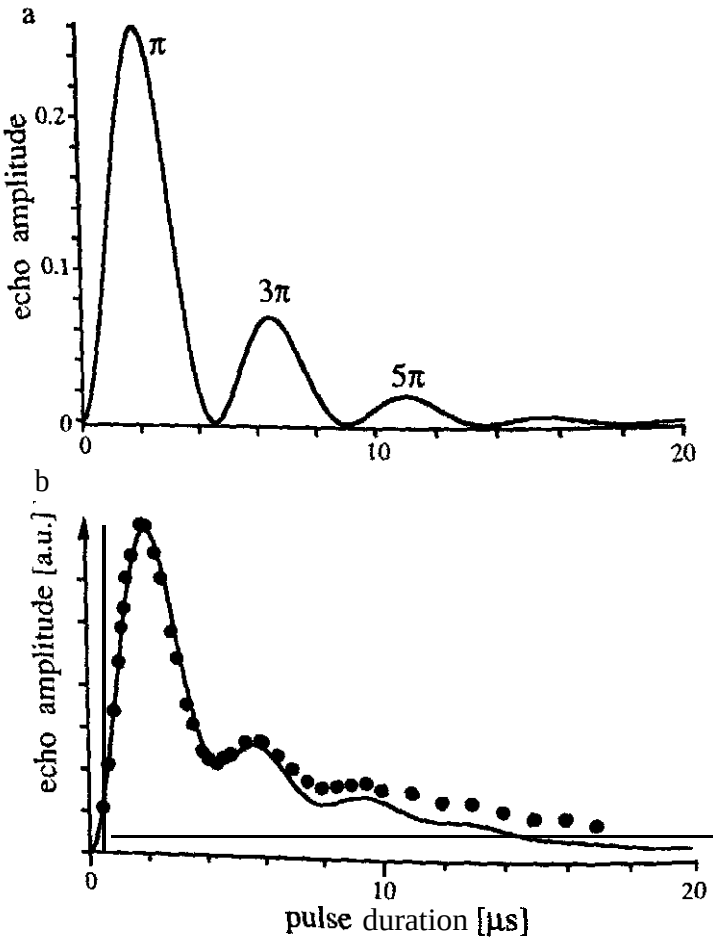

FIG. 24. Echo intensity as a function of the refocussing pulse length. (a), theoretical calculation for a homogeneous laser field. Parameters: $\Omega_L = 1$; $\gamma_0 = 0.1$; $\omega_1^2/\Gamma_2 = 5$; $\bar{\Delta} = 5$. (b), Experimental data and theoretical fit, taking the inhomogeneous laser field into account. Experimental parameters: $\Omega_L/2\pi = 91$ kHz, $\Delta/2\pi = 15$ GHz, pump beam power = 130 mW.

resonance detuning for constant laser power, together with the detuning-dependence of the damping factor $e^{-\gamma_0 \tau \bar{\Delta}^2}$ for a pulse length τ corresponding to a π pulse. The optimum tilt angle of the effective field is clearly reached at a detuning $\bar{\Delta} = 1$, i.e., where the light shift effect is strongest. However, the overall efficiency of the echo formation, as shown in Fig. 25(b), reaches its maximum at a different resonance offset, since the damping effect is too strong at small laser detunings. Due to the dispersion-like offset dependence of the light shift effect, no echo is formed at exact optical resonance. The refocussing

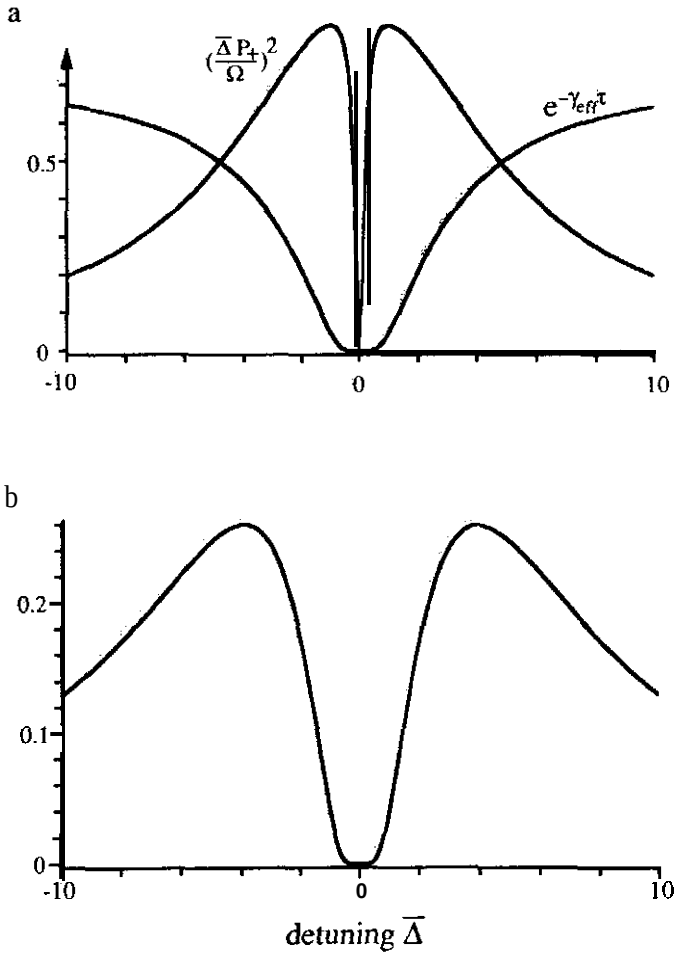

FIG. 25. Efficiency of refocussing pulse as a function of optical detuning. The parameters used were $P_+ = 5$; $\Omega_L = 1$; $\gamma_0 = 0.1$. (a), Maximum without attenuation and damping term plotted separately. (b), Efficiency including damping.

efficiency reaches a maximum at a finite detuning $\bar{\Delta} > 1$ and falls to zero at large offsets, where the light shift becomes too weak.

If the dependence of the echo intensity on the resonance detuning is measured experimentally, the measured echo amplitude depends not only cm the refocussing efficiency, but also on the degree of polarization established by the first pulse and the detection sensitivity. Figure 26 shows experimental data together with the theoretical curve which has been calculated taking the detuning dependence of the initial polarization and of the detection sensitivity into account. The experimental data clearly show the expected behavior with

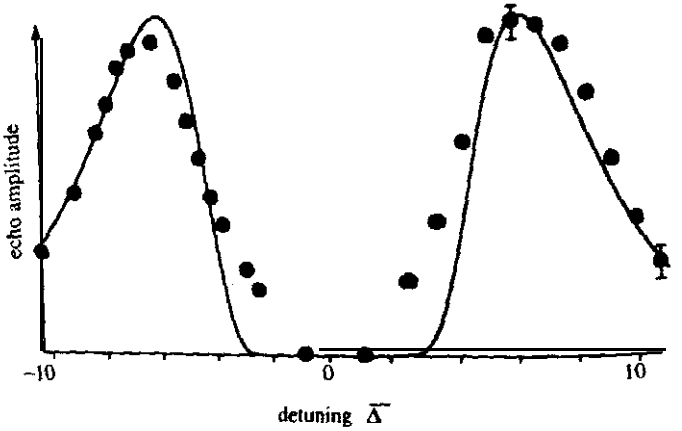

FIG. 26. Measured vs. calculated echo amplitude as a function of the optical detuning $\bar{\Delta}$. (For details see Rosatzin *et al.*, 1990b.)

vanishing echo on resonance, a maximum at $\bar{\Delta} \sim 6$ and a decrease at larger detunings.

Similar experiments have been performed in the nanosecond regime on Na using a pulsed laser and an optical delay line (Fukuda *et al.*, 1983). The generation Of echoes was observed, but the mechanism of the echo formation was not discussed.

If the experiments are performed on spin systems higher than the $J = \frac{1}{2}$ system assumed so far, the refocussing pulse can transfer coherences between various orders. One consequence is that more than one echo may appear, as seen in Fig. 23. The second echo is due to a transfer of coherence from $\Delta m = \pm 2$ transition into a $\Delta m = \mp 1$ transition. Since the precession of double quantum coherence is twice as fast as that of single quantum coherence, it takes twice the time between the pulses until the spin packets come back into phase. A more detailed discussion of this experiment is given in the next subsection. Such coherence transfer echoes have been observed in pulse NMR experiments (Maudsley *et al.*, 1978), but have never been reported in optically excited magnetic resonance experiments. Single- and double-quantum echoes were also observed in the $J = 1$ ground state of Sm, using the $^7F_1 \leftrightarrow {}^7F_0$ transition at $\lambda = 570.6$ nm (Rosatzin, 1990).

E. MODULATED EXCITATION

As we have shown, the system response to two optical pulses can be analyzed with a very simple theoretical model. If an infinite sequence of pulses is applied, the system evolves towards a steady state at approximately the

unperturbed damping rate γ_0. The equilibrium polarization is determined essentially by the average optical power of the pulse sequence, except if the pulse spacing is equal to the Larmor period or a multiple thereof (Mlynek *et al.*, 1981b; Fukuda *et al.*, 1981; Tanigawa *et* al., 1983). In this case, the precession of the spins becomes synchronized with the pulses, and their effect is increased in a resonant manner. This experiment can be understood much like a DANTE experiment (Morris and Freeman, 1978), where the pulse sequence has an effect similar to an extended low-power pulse.

The behavior of the spin system during irradiation with a sequence of optical pulses is shown in Fig. 27. The top trace shows the effect of a sequence

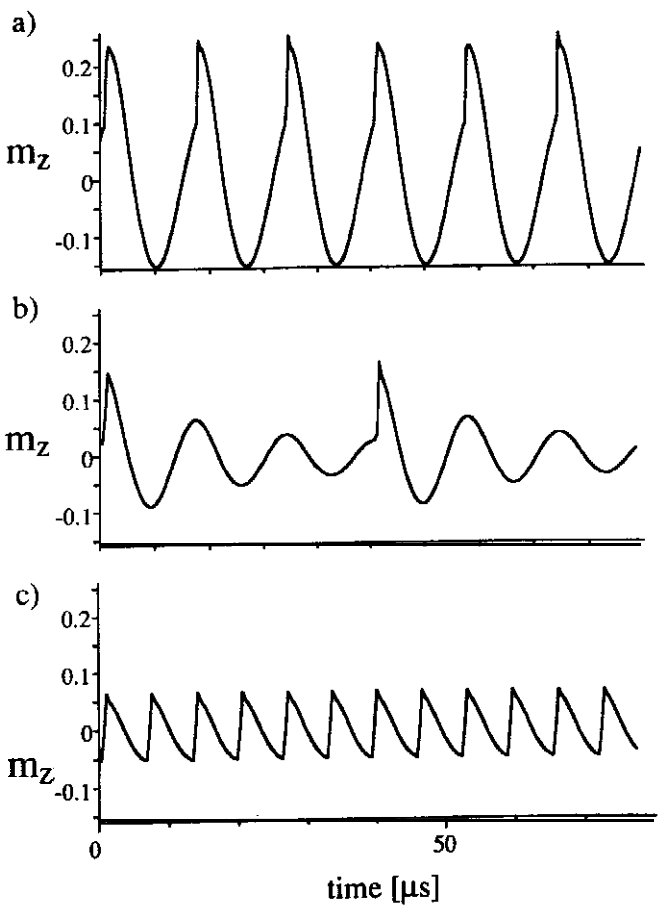

FIG. 27. Magnetization as a function of time for a continuous train of pulses. (a), Pulse spacing = Larmor period. (b), Pulse spacing = three times Larmor period. (c), Pulse spacing = Larmor period/2.

of pulses synchronized with the Larmor precession of the spins. The effect therefore accumulates and the signal reaches a maximum Trace (b) shows that a similar effect can also be obtained if the pulse spacing is adjusted to a multiple of the Larmor period. The resulting signal is clearly smaller in this case since a larger component of the magnetization decays before the next pulse is applied. Trace (c) shows the case where the pulse spacing is equal to half of one Larmor period. In this case, the effect of the pulses almost cad each other, since the magnetization generated by one pulse has precessed by 180° before the next pulse is applied. Exact cancellation is reached for vanishing damping rate.

The amplitude of the oscillating magnetization created by a "infinite pulse train is show" as a function of pulse spacing in Fig. 28. The resonances occuring where the pulse spacing is equal to a multiple of the Larmor period are clearly visible. The damping of higher order resonances is due to the decay of the coherence during the delay between the pubes, which in our case is determined by transit-time effects. For investigations of long-lived states such as ground states or metastable states and sufficiently long observation times, very high-order resonances in sublevel coherence can be used to measure gigahertz splitting frequencies with practical pulse rates in the megahertz range. A necessary condition for the coherent preparation of the atoms is that the optical pulses are short compared to the reciprocal of the splitting frequency. Therefore, picosecond pulses are required for measurements of gigahertz frequency splittings (Harde and Burggraf, 1982). Pulse trains are especially useful if the Larmor frequency is relatively large. As we have seen, excitation with an unmodulated laser pulse cannot excite the system efficiently if the Larmor frequency exceeds the optical pumping rate. The better

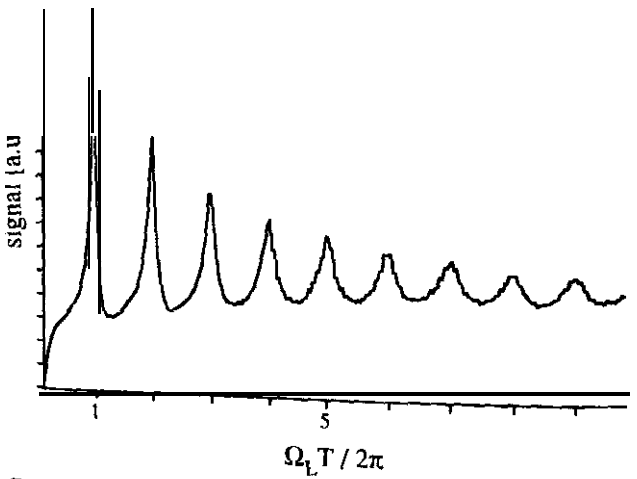

FIG. 28. Magnetization amplitude as a function of pulse spacing T.

excitation efficiency is due to the fact that the excitation frequency for the Zeeman system is equal to the modulation frequency; it can therefore be brought into resonance with the Zeeman transition frequency.

The resonances induced by periodic excitation can be observed either in fluorescence *or* again by an optical probe beam using a polarization selective technique. In the latter case, it is convenient to use a low-intensity fraction of the pump pulse train for this purpose With trains of ultrashort pulses from a synchronously pumped dye laser, this technique has been used to measure, for example, the hyperfine splitting of the Cs ground state (9.2 GHz) with an accuracy comparable to rf experiments (Lehmitz *et al.*, 1986). In this experiment, the coherence was driven and tuned through resonance by the 110th harmonic of the pulse rate (83 MHz). The resulting line width was only 30 Hz. Such trains of picosecond pulses can also be generated with semiconductor lasers, which have very low jitter and high stability in the pulse rate. Under appropriate conditions, this pulse train spectroscopy can be performed with cheap semiconductor lasers, which are directly modulated and supplied by electrical pulses from a comb generator (Lehmitz *et al.*, 1986; Mishina *et al.*, 1988).

Instead of using two single pulses to generate spin echoes, the echoes can also be induced by two finite length trains of pulses (Tanigawa et a/., 1983). In this case, the echoes are selectively generated for a sublevel pair whose frequency splitting is equal to an integral multiple of the repetition rate of the light pulses. This technique is of interest for situations in which many inhomogeneously broadened sublevels exist. So far it has been applied to the ground state of Na (Tanigawa *et al.*, 1983) and Cs (Mishina *et al.*, 1987); in the latter case, modulated light from diode lasers was used in the experiment.

Instead of using a pulse train, the laser radiation can also be modulated sinusoidally (Bell and Bloom, 1961a,b; Mlynek *et al.*, 1981a; Mishina *et al.*, 1988). Like pulse trains, this modulated excitation scheme is useful if the Larmor frequency is relatively large. Sinusoidal modulation of the light is easier to use if the light source is operated cw and the modulation is generated externally. If the available peak power is limited, it leads to higher average power and therefore often to a higher signal.

For a quantitative analysis of the situation, we start from the equation of motion for the ground-state spin $\frac{1}{2}$ system derived in Section III,D,3. We assume that the laser intensity is modulated sinusoidally so that the pump rate varies like $P(t) = 2P_0[1 + \cos(\omega t)]$. The effective Hamiltonian for the ground state system becomes then

$$\mathcal{H}(t) = \omega_0 I_x + 2\delta_0[1 + \cos(\omega t)]I_z \tag{74}$$

where $2\delta_0 = 2\bar{\Delta}P_0$ represents the average light shift, ω the modulation frequency and isotropic relaxation is assumed. In addition to the Hamiltonian,

the pump rate is also modulated so that the equation of motion is now

$$d\rho/dt = -i[\mathcal{H}(t), \rho] + \gamma_{\text{eff}}(t)\rho + P(t)I_z \tag{75}$$

We are now especially interested in the case of low power excitation, when the optical pumping rate is small compared to the sublevel splitting. In this case, it is useful to transform the time-dependent equation of motion into a frame of reference rotating at the modulation frequency ω:

$$d\rho'/dt = -i[\mathcal{H}', \rho'] + \gamma_{\text{eff}}(t)\rho' + P(t)I'_z \tag{76}$$

where the superscript indicates the rotating reference frame. The transformation can be accomplished by

$$\rho'(t) = U(t)\rho(t)U^{-1}(t) \tag{77}$$

$$U(t) = e^{i\omega t I_x} \tag{78}$$

$$\begin{aligned}\mathcal{H}'(t) &= U(t)\mathcal{H}(t)U^{-1}(t) - \dot{U}(t)U^{-1}(t) \\ &= \delta I_x + \delta_0[1 + 2\cos(\omega t) + \cos(2\omega t)]I_z \\ &\quad + \delta_0[2\sin(\omega t) + \sin(2\omega t)]I_y\end{aligned} \tag{79}$$

$\delta = (\omega_0 - \omega)$ represents the difference between the sublevel splitting and the modulation frequency. On a long time scale, compared to the precession frequency, the modulated terms can be neglected in first order. The Hamiltonian then becomes

$$\mathcal{H}'(t) = \delta I_x + \delta_0 I_z \tag{80}$$

This Hamiltonian is quite similar to the one describing the excitation of sublevel coherence with unmodulated light. The main difference is that the field, due to the sublevel splitting, is reduced by the modulation frequency and can therefore be made to vanish,

For the relaxation rate $\gamma_{\text{eff}}(t)$ we make the same approximation; the time-independent average becomes therefore $\gamma_{\text{eff}}(t) \approx \gamma_0 + 2P_0$. Finally, the pumping term has to be transformed as

$$P(t)I'_z = P_0[\{1 + 2\cos(\omega t) + \cos(2\omega t)\}I_z + \{2\sin(\omega t) + \sin(2\omega t)\}I_y] \tag{81}$$

and we may neglect the time-dependent terms so that

$$P(t)I'_z \approx P_0 I_z \tag{82}$$

The equation of motion for the system is therefore completely analogous to those obtained with unmodulated light, except that the dynamics occur in a frame of reference rotating at the modulation frequency. In this rotating frame of reference, we can therefore use Eqs. (45)–(48) to describe the evolution of the spin system.

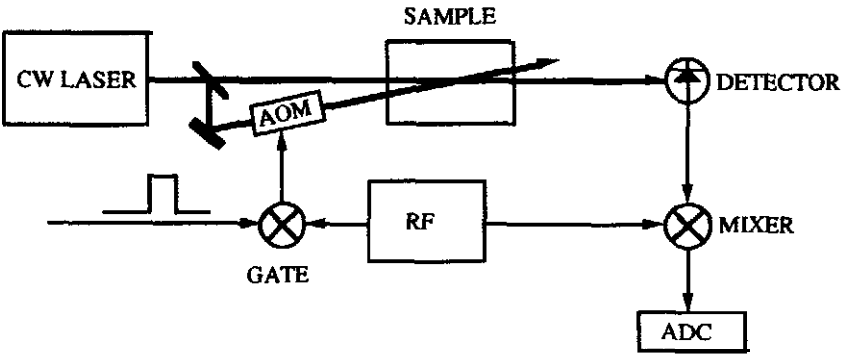

FIG. 29. Experimental scheme for modulated optical excitation.

A possible experimental setup for an experiment with modulated excitation of the spin system is shown schematically in Fig. 29. The modulated pump beam can be applied continuously or pulsed. The test beam is again cw. An experimental time-domain signal recorded with this method is shown in Fig. 30. Trace (a) represents the pump intensity: the laser beam is modulated and pulsed, The response of the signal is shown in trace (b). In response to the modulated pulse, the magnetization in the system builds up and starts to precess. As in the case of dc excitation, the system approaches a stationary state in which a precession at the modulation frequency occurs. The beat signal visible during the initial phase is due to interference between the eigenfrequency of the spins and the modulation frequency. This is seen more clearly in trace (c), which was obtained with phase-sensitive detection at the modulation frequency. The difference between the modulation frequency and the eigenfrequency of the system now appears as the nutation frequency, and the system settles into a stationary state. The full line represents the component of the magnetization that precesses in phase with the modulation; the dashed curve represents the out-of-phase component. When the pulse is turned off, a FID is observed. The oscillation frequency is given by the difference between the Larmor frequency and the modulation frequency.

As emphasized previously, the modulation of the laser intensity has the main effect of reducing the apparent magnetic field. All the experiments discussed previously can therefore also be performed with modulated light. In this context, the dependence of amplitude and phase of nutation and FID signal on the magnetic field strength now appear as off-resonance effects. This is evident from the equilibrium magnetization during the pulse plotted in Fig. 31 as a function of the modulation frequency. The upper part of the figure shows the data extracted from time-domain experiments as a function of the modulation frequency. The arrow indicates the data corresponding to

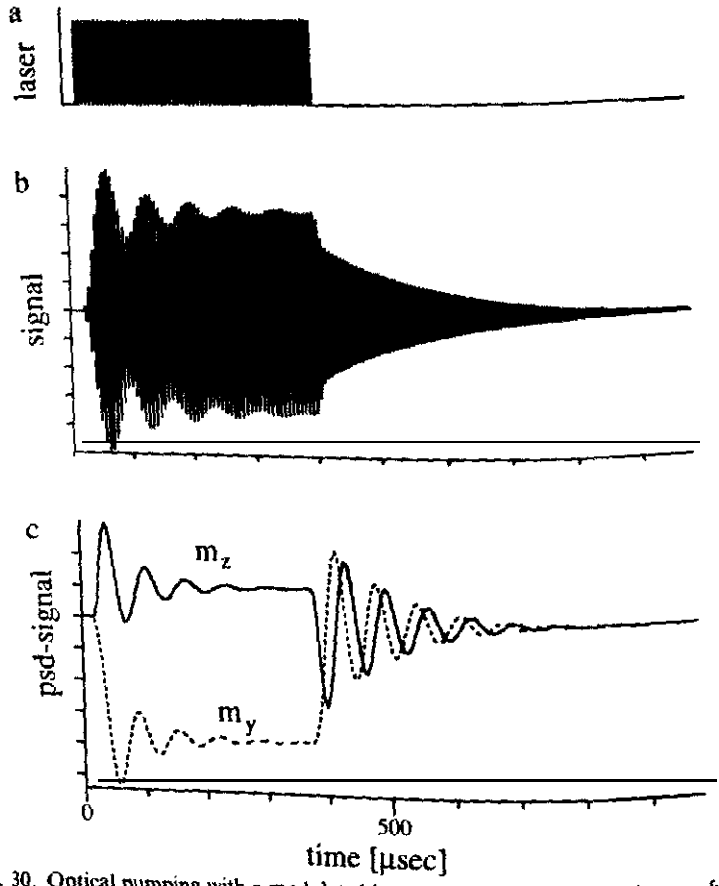

FIG. 30. Optical pumping with a modulated laser beam. (a), Laser intensity as a function of time; (b), measured signal; (c), signal after phase-sensitive detection at the modulation frequency.

Fig. 30. The data were obtained at the optical resonance, so that no light-shift effects occurred. While the dynamics described here appear very similar to those encountered during rf excitation of magnetic resonance transition, there are some subtle differences. As an example, since the transverse magnetization is generated by optical pumping and not by precession around an effective field, the in-phase component has an absorption-like dependence on the modulation frequency, while the out-of-phase component has a dispersion-like dependence.

In addition to allowing extension of experiments to higher Larmor frequencies, the modulation excitation scheme also introduces the frequency and the phase of the modulation as additional degrees of freedom into the experiment. The phase especially is a useful additional variable: it can, for

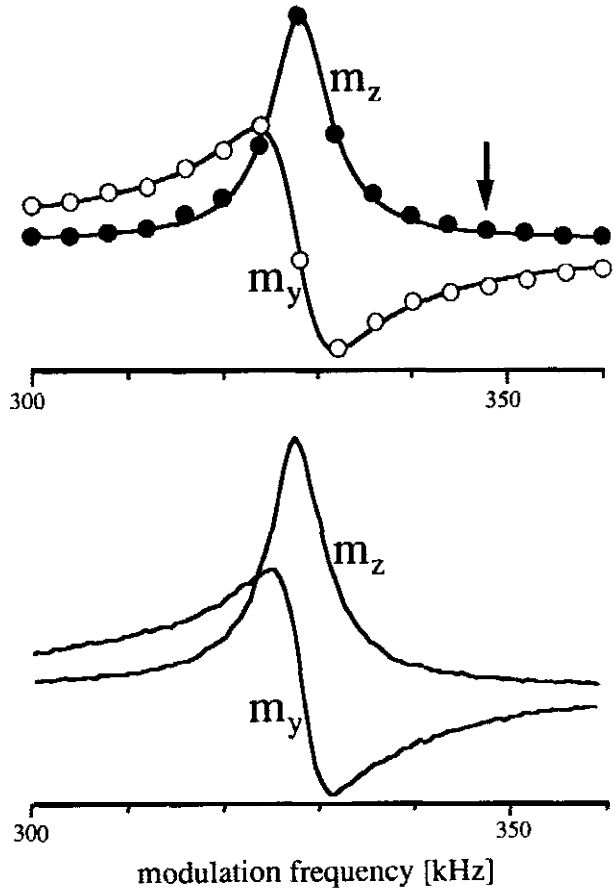

FIG. 31. Stationary magnetization during sine-modulated pump beam as a function of the modulation frequency; m_z and m_y denote the in-phase and out-of-phase components, respectively. The circles in the upper part represent the stationary value of the magnetization measured during a time-resolved experiment, and the full line is a least squares fit to a Lorentzian absorption/dispersion line. The lower part shows the signal measured in steady state with a phase-sensitive detector, while scanning the modulation frequency.

example, be used to "label" a coherence. This method has been exploited successfully to follow the transfer of coherence for the understanding of the multiple **echoes observed** in an two-pulse experiment (Rosatzin *et al.*, 1991). An example of such a signal is shown in the top part of Fig. 32. The measurement was performed on the ground state of atomic Na with a sequence of two modulated pulses. The first pulse excites the coherence as discussed previously. The second **pulse** excites a second FID and two spin echoes at times $t = 2T$ and $t = 3T$ after the end of the first pulse. In order to

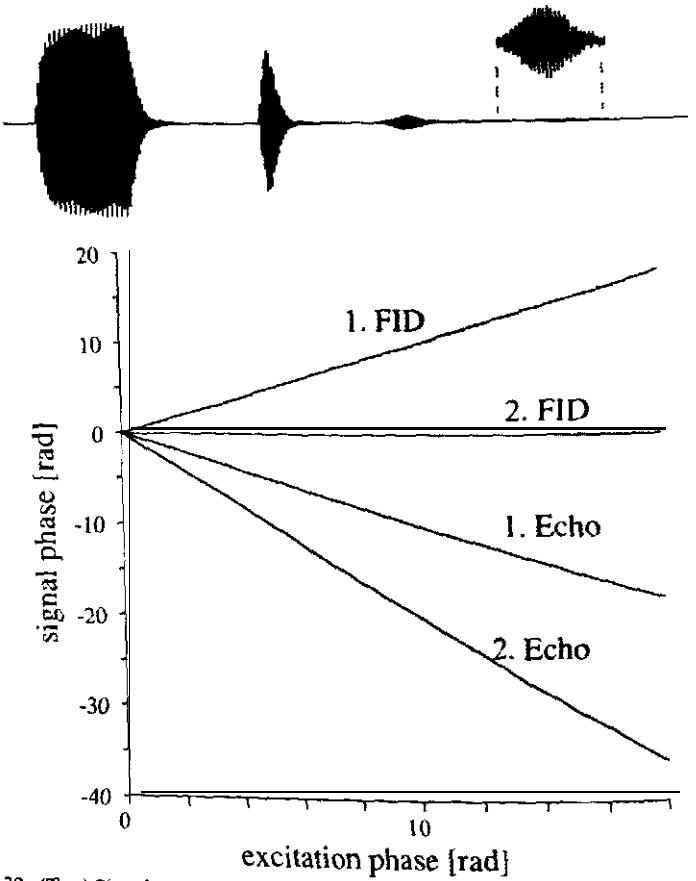

FIG. 32. (Top) Signal measured with a sequence of two modulated pulses showing two FID signals and two echoes at $t = 2T$ and $t = 3T$. (Bottom) Represents the phase of the four signal components measured as a function of the phase of the modulation of the first pulse.

confirm the hypothesis that the second echo is due to a transfer of coherence from double quantum into single quantum coherence we systematically changed the phase of the modulation of the first pulse. As shown in the lower half of the figure, the phase of the first FID was equal to the modulation phase; the second FID signal did not depend on the phase, since the magnetization giving rise to this signal is created during the second pulse. The first echo is a normal Hahn-echo, and its phase is therefore the inverse of the excitation phase. The magnetization giving rise to the second echo was created as double quantum coherence, which acquires twice the phase of single quantum coherence. The second echo therefore appears with twice the phase of the first echo,

F. Frequency-Domain Experiments

Optical pumping with modulated light can also be wed for frequency-domain experiments where the steady state signal is detected via a phase-sensitive detector (Mlynek *et al.*, 1981a). In- and out-of-phase components of the signal are then measured as a function of the modulation frequency. As shown in Fig. 31, the signal obtained in such an experiment is identical to the steady-state signal in time-domain experiments if the modulation frequency is changed. Similar experiments were performed as early as 1961 with discharge lamps (Bell and Bloom, 1961a,b). Since the apparent strength of the magnetic field is reduced by the modulation frequency, this method allows one to apply transverse pumping to systems with Larmor frequencies exceeding the optical pump rate. With a constant laser amplitude, the amount of polarization achieved is strongly reduced under such conditions.

Since this technique provides very high sensitivity, it is well suited for the detection of small numbers of spins. As an example, we studied a magnetic resonance signal from a very small probe volume near an interface (Aebersold *et* al., 1991). Figure 33 shows two different setups used for this experiment: the magnetization was measured with an optical probe beam that was incident on the interface at an angle larger than the critical angle for total internal reflection. The penetration depth of the probe beam into the absorbing medium was therefore only of the order of the optical wavelength, so that the probe volume was limited to about $1\text{mm} \times 1\text{mm} \times 1\,\mu\text{m}$. Under our experimental conditions, the number of interacting particles was therefore $< 10^5$. As in the other experiments, Ar at a pressure of 200 mbar was added as a buffer gas to obtain a homogeneous optical resonance line. In Fig. 34, the

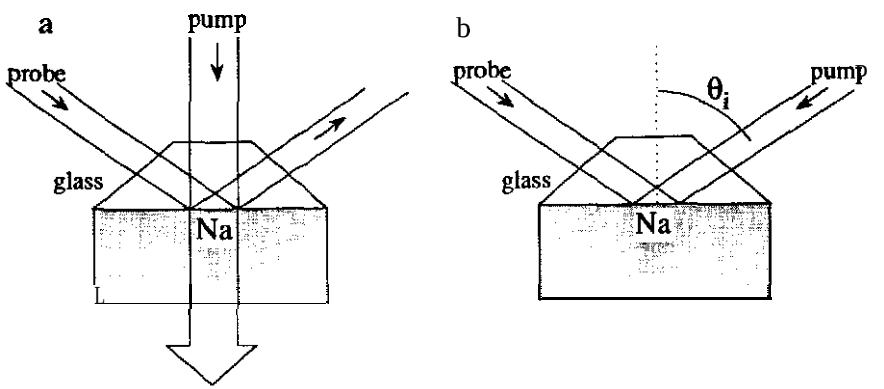

FIG. 33. Two possible experimental setups for spatially selective magnetic resonance experiments of atoms near a glass surface. (a), The pump beam propagates through the sampe volume, while the probe beam is totally reflected at the interface. (b), Both beams are totally reflected. θ_i represents the angle of incidence.

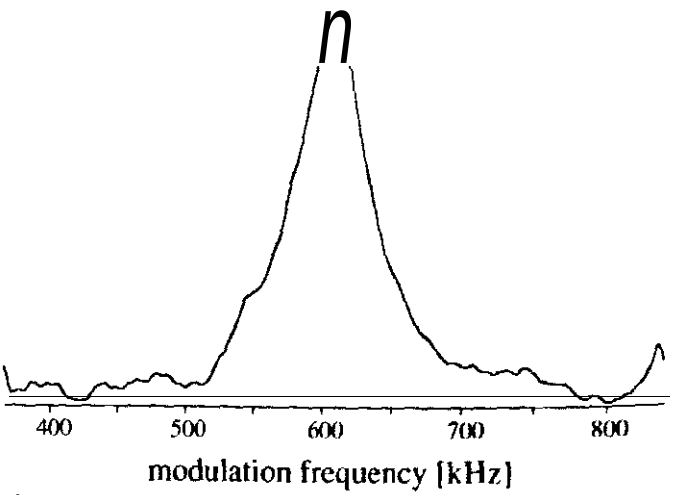

FIG. 34. Magnetic resonance signal from a glass–sodium vapor interface using the setup of Fig. 33(a). A magnetic field with a strength of 87 μT was applied parallel to the interface.

experimental signal obtain with phase-sensitive detection as a function of the modulation frequency is shown. For this measurement, the pump beam excited the full sample volume. Similar techniques can also be used for probing surface regions in solids. In one experiment, for example, nuclear quadrupole resonances were obtained in external reflection from a crystal surface by Stark-modulated optical pumping; the technique is sensitive to signals from a region that extends one optical wavelength into the crystal body (Lukac and Hahn, 1988).

So far, the optical transition was assumed to be homogeneously broadened; thus, signal features due to velocity-selective excitation of a Doppler-broadened line were of no importance. In the case of a Doppler-broadened optical transition and narrow-bandwidth laser excitation, the sublevel coherence is excited in a single atomic subgroup, whose width in velocity space is determined by the homogeneous optical linewidth. Thus, for a given laser frequency detuning with respect to the center of the Doppler profile, a sublevel coherence is created by the modulated pump field in atoms with a well-defined velocity v'. If the (""modulated) probe beam now has a different Doppler detuning, it interacts with a different velocity subgroup v''. Hence, the probe beam can detect the excited atoms only if they change their velocity from v' to v''. One well-known mechanism that provides velocity changes in a vapor are collisions that preserve the internal atomic state. Due to the time-delay corresponding to collisional diffusion between excitation and detection, the probe beam signal recorded in such an experiment displays Ramsey-type interference patterns (Buhr and Mlynek, 1986). In contrast to the conventional

Ramsey-type scheme in atomic beams (Ramsey, 1980), the Ramsey fringes in this experiment result from the "motion" of atoms with sublevel coherence between two interaction zones separated in "velocity space" rather than in "local" space. These collision-induced Ramsey resonances have been used to study the collisional velocity diffusion of samarium atoms within the Doppler-broadened $^7F_1 - {}^7F_0$ ^{154}Sm transition in the presence of rare-gas perturbers (Buhr and Mlynek, 1986).

In the case of cell experiments, the line widths that can be obtained are mainly determined by depolarizing collisions in the vapor or by transit time broadening of the atoms as they move through the laser beam. These limits of resolution can be circumvented by using an atomic or molecular beam and a technique similar to Ramsey's method of separating fields (Ramsey, 1980). This technique for observing narrow rf resonances is well known from atomic and molecular beam experiments. In general, these Ramsey fringes are induced by two spatially separated rf field?.. More recently, Ramsey resonances have also been observed for a resonance Raman transition in an atomic beam (Thomas *et al.*, 1982; Mlynek et *al.*, 1988). In one scheme (Thomas et *al.*, 1982), the two rf fields were simply replaced by two modulated laser fields, and the Ramsey fringes were detected via fluorescence from the optically excited state. This technique was applied to measure the 1.72 GHz hyperfine splitting in the ground state of Na in a beam. In another scheme (Mlynek et *al.*, 1988), the excitation of the sublevel coherence is again achieved with a modulated laser field. The required phase-sensitive detection of the atomic coherence, however, was performed in transmission with an unmodulated probe laser field in the second interaction region. This experiment, which was applied to Zeeman sublevels in the $^7F_1$ samarium ground state, represents a Raman analog of the gas-cell experiments described earlier.

G. RF–Optical Double Resonance

The techniques described so far all rely on purely optical means. For some applications, it can be advantageous to we rf-optical double resonance methods. Most rf-optical double resonance experiments use some sort of frequency-domain technique. The rf irradiation usually creates precessing magnetization in the sample, which leads to a phase or amplitude modulation of the detection beam. Resonances are obtained by changing either the magnetic field strength or the rf frequency.

The rf irradiation of the magnetic resonance transition can change the optical properties of the sample in different ways; saturation of the rf transition, for example, can be detected via changes in the optical absorption or dispersion. On the other hand, it is possible to use the rf irradiation to transfer coherence between optical transitions (Mlynek *et al.*, 1983, 1984;

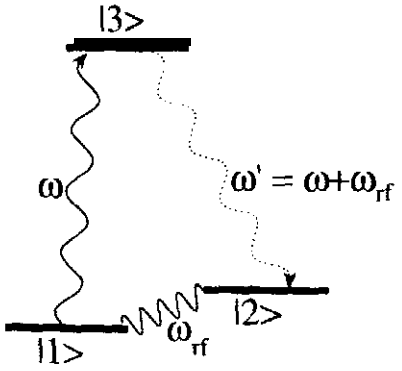

FIG. 35. Transfer of optical coherence by rf irradiation. The driving fields are the laser field ω and the rf field ω_{rf}.

Wong *et al.*, 1983). Figure 35 shows a basic example, The laser excites transition $1 \leftrightarrow 3$ and the rf irradiation transfers this coherence into the second optical transition $2 \leftrightarrow 3$. This coherence represents an optical polarization that radiates along the same direction as that of transition $1 \leftrightarrow 3$. After Passing through the sample (see Fig. 36), the laser beam contains additional frequency components. On the quadratic detector, these additionalfrequency components beat against the originalfrequency, leading to a signaloscillating at the rf frequency. The technique therefore employs heterodyne detection and is capable of monitoring coherent spin transients or nuclear magnetic

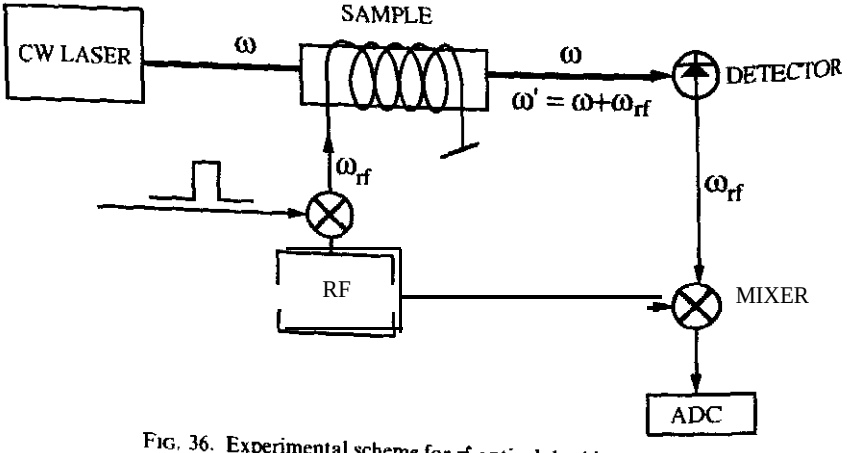

FIG. 36. Experimental scheme for rf-optical double resonance.

resonances under pulsed or cw conditions in both ground and excited electronic states.

The method can also be interpreted as a coherent Raman process being stimulated by a resonant rf field and a laser field. It differs from earlier studies of the stimulated Raman effect, where two optical fields drive two coupled electric dipole transitions, and the remaining third transition is radiatively inactive or is not monitored. Here all three fields appear, driving the three possible transitions, as in a three-wave mixing effect, The technique can be generalized to any three-level system where all three transitions are active, allowing detection of NMR, ESR, or even infrared transitions. So far this Raman heterodyne technique has been applied to various systems in the gas phase and to dilute solids. In a similar experiment, a forbidden double-quantum NMR transition was detected in a Raman-type process, using allowed single quantum NMR transitions (Yannoni *et al.*, 1987).

In the gas phase, the Raman heterodyne method was used to study velocity diffusion effects in rf-optical double resonance (Mlynek et *al.*, 1984; Tamm *et al.*, 1986). In these experiments, interesting new aspects due to the v&c-ity selective laser excitation within a Doppler-broadened line appeared. If the optical pumping process and the optical detection of the rf resonance are both applied to one velocity subgroup of the Doppler-broadened atomic ensemble, the time between subsequent collisional velocity changes limits the time interval of experimental observation of the rf-driven atoms. Thus, the resulting rf resonance line widths can be directly related to the rate of velocity-changing collisions, Experiments along these lines were performed on the $^7F_1 - {}^7F_0$ transition ($A = 570.6$ nm) in samarium vapor in the presence of rare gas perturbers such as He and Ne. The measurements showed that velocity-changing collisions can determine the characteristics of rf-laser double resonance signals by strongly affecting their line widths and line shapes (Tamm *et al.*, 1986).

More recently, Raman heterodyne spectroscopy was also applied to rubidium vapor (Scheufler *et al.*, 1990). In this experiment, the light source was a stabilized infrared laser diode that was tuned to the Rb resonance line near 795 nm. Raman-beat signals of the Rb ground state with different polarizations of the detecting light were obtained after pulsed rf excitation resulting in highly resolved spectra after Fourier transformation.

Raman heterodyne detection has also proven to be a powerful tool to study sublevel resonances in dilute solids at low temperature. Here the technique was first demonstrated in the impurity-ion solid $Pr^{3+}:LaF_3$ at 1.6 K using the Pr^{3+} optical transition, $^3H_4(\Gamma_1) - {}^1D_2(\Gamma_1)$ (Mlynek *et al.*, 1983; Wong *et al.*, 1983). Detailed theoretical predictions on the Raman process were confirmed by cw measurements of the $Pr^{3+}:LaF_3$ hyperfine splittings, where the optical

heterodyne signals were shot-noise limited. The Pr^{3+} nuclear quadrupole parameters were obtained for the $^3H_4$ and $^1D_2$ states. where the line centers were determined with kilohertz precision. Moreover, Pr^{3+} spin echoes of nuclear quadrupole transitions were detected not only in the $^3H_4$ ground state, but also for the first time in the $^1D_2$ excited state. which allowed a critical test of the line broadening theory of this system (Wong et al., 1983).

In these first experiments on ionic solids, two fundamental characteristics of the Raman heterodyne signals were puzzling for some time: first, the signals only appeared in the presence of an external magnetic field, and second, the line shapes were anomalous, resembling the second derivative of a Gaussian. Subsequent experiments identified that both phenomena were a manifestation of inequivalent nuclear sites that generate Raman signals of opposite sign, and thus can interfere when their frequencies match. as they do at low magnetic fields (Mitsunaga *et al.*, 1984.1985; Kintzer *et al.*, 1985). The reason is that the Raman heterodyne signal depends on the triple product of the three transition matrix elements connecting states 1, 2, and 3. Each matrix element is complex and appears linearly so that interference can occur. These interferences were observed from two inequivalent nuclear sites in the solid $Pr^{3+}:YAlO_3$ at 1.7 K (Mitsunaga t-r *al.*, 1984). For other experimental conditions, interference could be observed also in a single nuclear site among Zeeman-split hyperfine transitions (Mitsunaga *et al.*, 1985). From a more general point of view, the interferences in the Raman heterodyne signals offer a new way of identifying the crystal symmetry (Kintzer *et al.*, 1985; Taylor, 1984).

The Raman heterodyne technique was also extended to detect superhyperfine spectra (Szabo *et al.*, 1990). In this experiment, NMR of the four nearest neighboring sets of ^{27}Al surrounding Cr^{3+} in ruby were observed with high sensitivity using optical excitation of the R_1 line at 693.4 nm. Either excited- or ground-state resonances could be selectively measured by setting the sample temperature to 2 or 7.5 K respectively, In this case, all 40 expected NMR resonances were observed. More recently, optical pumping effects were studied in an rf-multiple pulse experiment (Erickson, 1990). In this work, optically detected multiple pulse spin-locked echoes in $Pr^{3+}:YAlO_3$, at low temperature were observed to decay at rates much faster than would be expected in the absence of the optical fields. This effect is due to loss of nuclei from the coherence because of the optical pumping. As in the purely optical experiments, the optical field slowly removes ions from the rf resonant levels to another ground-state level via weak optical transitions. Finally, Raman heterodyne signals of electron paramagnetic resonance from color centers in diamond were observed with transition frequencies of up to 1 GHz (Holliday *et al.*, 1990).

V. Conclusion and Outlook

We have reported various techniques for the optical creation and detection of magnetic resonance phenomena. The example of a spin-+ system was treated in detail, and the main processes were demonstrated by time- and frequency-domain experiments performed in the ground state of atomic sodium, The main advantage of these techniques is the superior sensitivity offered by the use of optical methods. The gain in sensitivity of optical and optical-rf double resonance methods over the traditional rf methods can be traced back to different sources. The two major contributions are due to the different Boltzmann factors and the different sensitivity in the detection of optical photons compared to the detection of rf photons. Each factor contributes some five orders of magnitude to the overall sensitivity. However, apart from considerations of excitation and detection efficiencies, additional aspects have to be taken into account in order to get a realistic comparison of signal-to-noise ratios in actual experiments.

In a more general sense, we have discussed the interaction of multilevel atomic systems with multiple resonant radiation fields. In the language of quantum optics, multiphoton processes are often grouped into various levels of "wave mixing," The processes considered here belong in two classes: resonant three-wave mixing (rf-optical double resonance) and four-wave mixing (optical-optical double resonance). In the context of this article, we were mainly concerned with the second class. Since our interest lies in the rf transition, but we detect the optical transition, some kind of heterodyne-detection scheme must be used when measurements are performed in the time domain. In most cases, the laser that probes the system also provides the local oscillator, thereby eliminating laser frequency jitter as a possible line broadening mechanism. In the time-domain, the magnetic resonance transition leads to a modulation of the laser amplitude; in the frequency domain the same effect leads to the appearance of additional frequency components, which appear as sidebands, spaced by the splitting frequency. On a quadratic detector, these sidebands appear as oscillations in the signal amplitude.

Magnetic resonance experiments using optical excitation or detection have seen a rapid progress in the past; it is likely that this will continue in the future. Applications for these experiments will be found mainly in areas where high sensitivity is crucial and cannot be obtained with conventional methods. Examples of such systems are mainly dilute systems, such as gases, and dilute solids. Another possible candidate is the study of processes on interfaces, where the number of available atoms is often quite small. In addition, the use of optical excitation may be useful in selectively exciting only atoms near the interface, if other atoms are also present. In most cases, it is therefore necessary

to have an optical transition available that can be used for excitation and detection. It may, however, be possible to use high-power pulsed laser systems that can excite transitions, even if their frequency is far away from the resonance. In other cases, the optical transition may actually provide important information for the analysis of the magnetic resonance data, and the magnetic resonance spectrum may be useful for the interpretation of optical data. Furthermore, the combination of optical and magnetic resonance methods may be especially useful in cases where optical excitation must be used to "create" the object of interest, such as atoms and molecules in optically excited states. The continuing development in the area of semiconductor lasers and diode-pumped solid-state lasers is likely to provide cheaper and more powerful tunable lasers in the near future, thereby enhancing the experimental possibilities.

ACKNOWLEDGMENTS

We gratefully acknowledge stimulating discussions with M. Rosatzin, who also contributed to most of the experiments described here. Moreover, we thank M. Ammann and J. Äbersold for technical assistance. Finally, this work would not have been possible without the financial support from the Schweizerischer Nationalfonds.

REFERENCES

Abella, I. D., Kurnit, N. A., and Hartmann, S. R. (1966). *Phys. Rev.* **141**, 391.
Abragam, A. (1961). "The Principles of Nuclear Magnetism." Oxford Univ. Press, London.
Adonts, G. G., Arutunyan, V. M., Akopyan, D. G., Arutunyan, K. V., and Slobodskoy, M. V. (1989). *J. Phys. B* **22**, 1103.
Aebersold, J., Suter, D., and Mlynek, J. (1991). To be published.
Allen, L., and Eberly, J. H. (1987). "Optical Resonance and Two-Level Atoms." Dover, New York.
Arditi, M., and Carver, T. R. (1961). *Phys. Rev.* **124**, 800.
Balling, L. C. (1975). *Adv. Quantum Electron.* **3**, 2.
Barrat, J. P., and Cohen-Tannoudji, C. (1961a). *C. R. Hebd. Seances Acad. Sci.* **252**, 255.
Barrat, J. P., and Cohen-Tannoudji, C. (1961b). *J. Phys. Radium* **22**, 329.
Barrat, J. P., and Cohen-Tannoudji, C. (1961c). *J. Phys. Radium* **22**, 443.
Bell, W. E., and Bloom, A. L. (1961a). *Phys. Rev. Lett.* **6**, 280.
Bell, W. E., and Bloom, A. L. (1961b). *Phys. Rev. Lett.* **6**, 623.
Bernheim, R. (1965). "Optical Pumping." Benjamin, New York.
Bitter, F. (1949). *Phys. Rev.* **76**, 833.
Bloch, F. (1946). *Phys. Rev.* **70**, 460.
Bloch, F. Hansen, W. W., and Packard, M. (1946). *Phys. Rev.* **70**, 474.
Bloembergen, N., Pershan, P., and Wilcox L. (1960). *Phys. Rev.* **120**, 2014.
Born, M., and Wolf, E. (1980). "Optics." Pergamon, Oxford.
Breiland, W. G., Harris, C. B., and Pines, A. (1973). *Phys. Rev. Lett.* **30**, 158.
Brewer, R. G. (1977a). *Phys. Today* **30**, 50.
Brewer, R. G. (1977b). *In* "Frontiers in Laser Spectroscopy" (R. Balian, S. Haroche, and S. Liberman eds.), p. 343. North-Holland Publ., Amsterdam.

Brewer, R. G., and Shoemaker. R. L. (1971). *Phys. Rev. Lett.* **27**, 631.
Brewer, R. G., and Shoemaker, R. L. (1972). *Phys. Rev. A* **6**, 2001.
Brewer. W. D. (1982). *Hyperfine Interact.* **12**, 173.
Brossel, J., and Kastler, A. (1949). *C. R. Hebd. Seances Acad. Sci.* 229, 1213.
Buhr, E., and Mlynek, J. (1986). *Phys. Rev. Lett.* **57**, 1300.
Burggraf, H., Kuckartz, M., and Harde, H. (1986). *In* "Methods of Laser Spectroscopy" (Y. Prior, A. Ben-Reuven, and M. Rosenbluh, eds.), p. 105. Plenum, New York.
Burns, M., Pappas. P., Feld, M. S., and Murnick, D. E. (1977). *Nucl. Instrum. Methods* 141,429.
Burschka, S., and Mlynek J. (1988). Opt. *Commun.* 66.59.
Cohen-Tannoudji, C. (1961). C. *R. Hebd. Seances Acad. Sci.* **252**, 394.
Cohen-Tannoudji, C. (1962). Ann. *Phys.* **7**, 423.
Cohen-Tannoudji, C., and Dupont-Roc, (1972). *Phys. Rev. A 5,968.*
Davies, P. B. (1981). *J. Phys. Chem.* **85**, 2599.
Decomps, B., Dumont, M., and Ducloy, M. (1976). *In* "Laser Spectroscopy of Atoms and Molecules" (H. Walther, ed.), p. 283, Springer-Verlag, Berlin.
Dehmelt, H. G. (1957a). *Phys. Rev.* **105**, 1487.
Dehmelt, H. G. (1957b). *Phys. Rev.* **105**, 1924.
Dehmelt, H. G. (1958). *Phys. Rev.* **109**, 381.
Dehmelt, H. G. (1990). *Rev. Mod. Phys. 62.* 525.
Demtröder, W. (1982). "Laser Spectroscopy.'" Springer-Verlag, Berlin.
Dodd, J. N., and Series, G. W. (1978). "Progress in Atomic Spectroscopy," Part A (W. Hanle and H. Kleinpoppen, eds.) p. 639. Plenum, New York.
Dupont-Roc, J., Polonsky, N., Cohen-Tannoudji, C., and Kastler, A. (1967). *Phys. Lett.* A **25A**, 87.
d'Yakonov, M. I. (1965). *Sov. Phys.—JETP* (*Engl. Tram,., 20. ,484.*
Endo, T., Nakanishi, S., Muramoto, T., and Hashi, T. (1982). *Opt. Commun.* **43**, 359.
Erickson, E. L. (1990). *Phys. Rev. B* 42.3789.
Ernst, R. R., Bodenhausen, G., and Wokaun, A. (1987). "Principles of Nuclear Magnetic Resonance in One and Two Dimensions." Oxford Univ. Press, London.
Fano, U. (1957). *Rev. Mod. Phys.* **29**, 74.
Feher, G. (1956). *Phys. Rev. 103,834.*
Fermi, E., and Rasetti, F. (1925). *Nature (London)* **115**, 764.
Feynman. R. P., Vernon, F. L., and Helwarth R. W. (1957). *J. Appl. Phys.* **28**, 49.
Franz, F. A., and Franz, J. R. (1966). *Phys. Rev.* **148**, 82.
Fukuda, Y., Hayashi, J., Kondo, K., and Hashi, T. (1981). *Opt. Commun.* **38**, 357.
Fukuda, Y., Yamada, K., and Hashi, T. (1983). *Opt. Commun.* 44,297.
Golub, J. E., Bai, Y. S., and Mossberg, T. W. (1988). Phys. *Rev. A* 37, 119.
Hahn, E. L. (1950). *Phys. Rev. 77,297.*
Happer, W. (1972). *Rev. Mod. Phys.* **44**, 169.
Happer, W., and Mathur, B. S. (1967). *Phys. Rev.* **163**, 12.
Harde, H., and Burggraf, H. (1982). Opt. *Commun.* **40**, 441.
Harde, H., Burggraf, H., Mlynek, J., and Lange W. (1981). *Opt. Lett.* **6**, 290.
Haroche, S. (1976). *In* "High Resolution Laser Spectroscopy" (K. Shimoda, ed.), p. 253. Springer-Verlag, Berlin.
Hartmann, S. R., and Hahn, E. L. (1962). *Phys. Rev.* **128**, 2042.
Holliday, K., He, X. F., Fisk, P. T. H., and Manson, N. B. (1990). *Opt. Letters* **15**, 983.
Jeffries, C. D. (1963). "Dynamic Nuclear Polarization." Wiley (Interscience), New York.
Kastler, A. (1967). Science **158**, 214.
Kintzer, E. S., Mitsunaga, M., and Brewer, R. G. (1985). *Phys. Rev. B* **31**, 6958.
Kohmoto, T., Fukuda, Y., Tanigawa, M., Mishina, T., and Hashi, T. (1983). *Phys. Rev. B* **28**, 2869.

Kreis R., Suter D., and Ernst, R. R. (1985). *Chem. Phys. Lett.* **118**, 120.
Lange W., and Mlynek, J. (1978). *Phys. Rev. Lett.* **40**, 1373.
Lehmann, J. C. (1964). *J. Phys. (Orsay, Fr.)* **25**, 809.
Lehmitz, H., and Harde, H. (1986). *In* "Methods of Laser Spectroscopy" (Y. Prior, A. Ben-Reuven, and M. Rosenbluh, eds.), p. 101. Plenum, New York.
Lehmitz, H., Kattau, W., and Harde, H. (1986). *In* "Methods of Laser Spectroscopy" (Y. Prior, A. Ben-Reuven, and M. Rosenbluh, eds.), p. 97. Plenum, New York.
Levenson, M. D., and Eesley, G. L. (1979). *Appl. Phys.* **19**, 1.
Levenson. M. D., and Kano, S. S. (1988). "Introduction to Nonlinear Laser Spectroscopy." Academic Press, New York.
Levitt, M. H., Suter, D., and Ernst, R. R. (1986). *J. Chem. Phys.* **84**, 4243.
Lowe, R. M., Gough, D. S., McLean, R. J., and Hannaford, P. (1987). *Phys. Rev. A* **36**, 5490.
Lukac, M., and Hahn, E. L. (1988). *J. Lumin.* **42**, 257.
McLean, R. J., Hannaford, P., and Lowe, R. M. (1990). *Phys. Rev. A* **42**, 6616.
Maudsley, A, A., Wokaun, A., and Ernst, R. R. (1978). *Chem. Phys. Lett.* **55**, 9.
Millar, J. M., Thayer A. M., Bielecki, A., Zax, D. B., and Pines, A. (1985). *J. Chem. Phys.* **83**, 934.
Mishina, T., Tanigawa, M., Fukuda, Y., and Hashi, T. (1987). *Opt. Commun.* **62**, 166.
Mishina, T., Fukuda, Y., and Hashi T. (1988). *Opt. Commun.* **66**, 25.
Mitschke, F., Deserno, R., Lange, W., and Mlynek, J. (1986). *Phys. Rev. A* **33**, 3219.
Mitsunaga, M., Kintzer, E. S., and Brewer, R. G. (1984). *Phys. Rev. Lett.* **52**, 1484.
Mitsunaga, M., Kintzer, E. S., and Brewer, R. G. (1985). *Phys. Rev. B* **31**, 6947.
Mlynek, J., and Lange W. (1979). *Opt. Commun. 30,337,*
Mlynek, J., Drake, K. H., Kersten, G., Fröhlich, D., and Lange W. (1981a). *Opt. Lett.* **6**, 87.
Mlynek, J., Lange, W., Harde, H., and Burggraf, H. (1981b). *Phys. Rev. A* **24**, 1099.
Mlynek, J., Wong, N. C., DeVoe, R. G., Kintzer, E. S., and Brewer, R. G. (1983). *Phys. Rev. Lett.* **50**, 993.
Mlynek, J., Tamm, C., Buhr, E., and Wong, N. C. (1984). *Phys. Rev. Lett.* **53**, 1814.
Mlynek, J., Grimm, R., Buhr, E., and Jordan, V. (1988). *Appl. Phys. B* 45.77.
Morris, G. A., and Freeman, R. (1978). *J. Magn. Reson.* **29**, 433.
Pancharatnam, S. (1966). J. Opt. *Soc. Am.* **56**, 1636.
Pines, A., Gibby, M. G., and Waugh, J. S. (1973). *J. Chem. Phys.* **59**, 569.
Purcell, E. M., Torrey, H. C., and Pound, R. V. (1946). *Phys. Rev. 69.37.*
Rabi, I. I., Zacharias, J. R., Millman, S., and Kusch, P. (1938). *Phys. Rev.* **53**, 318.
Ramsey, N. F. (1980). *Phys. Today* July, p. 25.
Rosatzin, M. (1990). Ph.D. Thesis, ETH Zürich.
Rosatzin, M., Suter, D., and Mlynek J. (1990a). *J. Opt. Soc. Am.* B **7**, 1231.
Rosatzin, M., Suter, D., and Mlynek, I. (1990b). *Phys. Rev. A* **42**, ,839.
Rosatzin, M., Suter, D., and Mlynek, J. (1991). To be published.
Rosker, M. J., Wise, F. W., and Tang, C. L. (1986). *Phys. Rev. Lett.* **57**, 321.
Scheufler, P., Appelt, S., Waldenmaier, M., Menke B., and Mehring, M. (1990). *Opt. Commun.* (in press).
Shelby, R. M., Tropper, A. C., Harley, R. T., and Macfarlane, R. M. (1983). *Opt. Lett.* **8**, 304.
Shen, Y. R. (1984). "The Principles of Nonlinear Optics." Wiley, New York.
Shoemaker, R. L., and Brewer, R. G. (1972). *Phys. Rev. Lett.* **28**, 1430.
Sørensen, S., Hansen, R. S., and Jakobsen, H. J. (1974). *J. Magn. Reson.* **14**. 243.
Suter, D., and Mlynek, J. (1991). *Phys. Rev. A* (in press).
Suter, D., Rosatzin, M., and Mlynek, J. (1990). *Phys. Rev. A* **41**, 1634.
Szabo, A. (1986). *J. Opt. Soc. Am.* B 3, 514.
Szabo, A., Muramoto, T., and Kaarli, R. (1990). *Opt. Lett.* (in press).
Tamm, C., Buhr, E. and Mlynek J. (1986). *Phys. Rev. A* **34**, 1977.

Tanigawa, M., Fukuda, Y., Kohmoto, T., Sakuno, K., and Hashi, T. (1983). *Opt. Lett.* **8**, 620.
Taylor, D: R. (1984). *Opt. Commun.* **52**, 204.
Thomas, J. E., Hemmer, P. R., Ezekiel, S., Leiby, C. C., Picard, R. H., and Willis, C. R. (1982). *Phys. Rev. Lett.* **48**, 867.
Torrey, H. C. (1949). *Phys. Rev.* **76**, 1059.
Van Stryland, E. W., and Shoemaker R. L. (1979). *Phys. Rev. A* **20**, 1376.
Walmsley, I. A., Mitsunaga M., and Tang, C. L. (1988). *Phys. Rev. A* **38**, 4681.
Weissbluth, M. (1978). "Atoms and Molecules." Academic Press, San Diego, California.
Wong, N. C., Kintzer, E. S., Mlynek, J., DeVoe, R. G., and Brewer, R. G. (1983). *Phys. Rev. B* **28**, 4993.
Yannoni, C. S., Kendrick, R. D., and Wang, P.-K. (1987). *Phys. Rev. Lett.* **58**, 345.